

VALIDATION OF FULL-SCALE AND SMALL-SCALE
TRANSMISSION LINE TEST RESULTS ON DYNAMIC
LOADS WITH NUMERICAL MODELING

KYLE B. TUCKER

VALIDATION OF FULL-SCALE AND SMALL-SCALE
TRANSMISSION LINE TEST RESULTS ON DYNAMIC LOADS
WITH NUMERICAL MODELING

by

© Kyle B. Tucker

A thesis submitted to the
School of Graduate Studies
in partial fulfillment of the
requirements for the degree of
Master of Engineering

Faculty of Engineering
Memorial University of Newfoundland
April, 2007

St. John's

Newfoundland and Labrador

ABSTRACT

This research presents the numerical validation of two different failure test data. These are: (1) suspension insulator failure test and (2) conductor failure test. The first failure scenario deals with the study of the effect of dynamic load on adjacent towers due to a broken suspension insulator; while the second scenario deals with the effect of dynamic load on a tower when the adjacent tower has failed due to conductor rupture. The published data were gathered from full scale as well as scale model tests for model validations. A finite element model of the line was developed using three different element types. Incremental nonlinear dynamic analysis was carried out in the time domain using a commercially available software package.

Using full-scale test data from broken insulator at the suspension point, a numerical model was developed. Upon validation of the numerical model with the test results, a sensitivity study was carried out for various insulator lengths, ice thicknesses and initial tensions to determine the effects of these parameters on the impact loads on the tower cross arm. Results of the study show that the impact loads are less sensitive to the change in insulator length and initial tension but they do vary significantly when the ice loads are increased. The magnitude of the effect of incremental ice thickness has not been quantified in any previous study. A coordination of strength study showed that a suspension insulator failure can increase the conductor tension considerably thus

initiating conductor rupture and therefore, a possible cascade failure in the longitudinal direction.

Using the scale model test data for broken conductor, a numerical model was developed where a number of towers were allowed to fail (one at a time) in a preferred sequence and the peak forces predicted on the surviving tower. This predicted peak force was compared to the experimental results and a reasonable correlation was established. Results show clearly that by allowing a few structures to fail, the longitudinal peak load on the surviving tower can be reduced significantly. This information can then be used in the design of the anti-cascading tower for proper cascade failure containment.

The study results show clearly that the analysis of dynamic load assessment on transmission system is possible and is cost effective using commercially available finite element software.

ACKNOWLEDGEMENTS

The author of this work would like to gratefully acknowledge the following people for their contributions to this project:

My supervisor, Dr. Asim Haldar, for his never failing encouragement and guidance during my pursuit of my Master of Engineering degree, and for his editing assistance and constructive criticism of the document;

My University supervisor, Dr. A.S.J. Swamidas, for keeping me on track when I went astray, and for also providing constructive criticism of the document;

Cathy Murphy, for skilfully reproducing and simplifying the sketches modified from previously published sources; and finally,

My fiancée, Beverly, for her patience and understanding through it all.

TABLE OF CONTENTS

Abstract	i
Acknowledgements	iii
List of Tables	vii
List of Figures	viii
List of Abbreviations and Symbols	xi
Chapter 1 – Introduction	1
1.1 Scope	7
1.2 Thesis Organization	9
Chapter 2 – Literature Review	11
2.1 Full Scale Tests	12
2.2 Scale Model Tests	20
2.3 Analytical Studies	35
2.4 Summary of Previous Work	46
Chapter 3 – Finite Element Modeling Using ADINA	47
3.1 Nodal Coordinate Generation	49
3.1.1 Nodal Coordinate Generation for Level Spans	51
3.1.2 Nodal Coordinate Generation for Non-Level Spans	52
3.2 Model Element Definition	55
3.3 Material Property Definition	55
3.3.1 Material and Geometrical Non-linearity	56
3.4 Loading and Boundary Conditions	57
3.4.1 Mass Proportional Loads	57
3.4.2 Boundary Conditions	58
3.5 Control Parameters	58
3.5.1 Time Step Integration - Wilson Theta Method	58

3.5.2	Lumped Mass Matrix	59
3.5.3	Death Element	59
Chapter 4 – Analysis of Suspension Insulator Failure		60
4.1	Scope of the Broken Insulator Model	62
4.2	Background	63
4.3	Finite Element Model	67
4.4	Methodology	68
4.5	Analysis of Numerical Model Results	69
4.5.1	Verification of Time Increment	69
4.5.2	Broken Insulator Results	70
4.5.3	Sensitivity Analysis – Insulator Length – IIL1	77
4.5.4	Sensitivity Analysis – Initial Conductor Tension – IIL1	78
4.5.5	Sensitivity Analysis – Incremental Ice Thickness – IIL1	79
4.5.6	Coordination of Strength – IIL1	82
Chapter 5 – Analysis of Scale-Model Tower Failure		84
5.1	Numerical Modeling of the Scale Model Tests	84
5.1.1	Small Scale Model Structure	85
5.1.2	Simplified Numerical Model	87
5.2	Finite Element Model	88
5.3	Methodology for Numerical Modeling	90
5.4	Analysis of Model Results	91
5.4.1	Time Step Sensitivity	91
5.4.2	Numerical Model Verification of Scale Model Response	92
5.4.3	Analysis of Transient Dynamic Peak Forces	95
5.4.4	Transient Forces on Remaining Structures	101

Chapter 6 – Summary, Conclusion and Recommendations	105
6.1 Summary and Conclusions	105
6.2 Recommendations for Future Work	107
References	108
Appendix 1 – ADINA Modeling Guide	111
Appendix 2 – EPRI Modeling Data – Model IIL1	177
Appendix 3 – Kempner Modeling Data – Model 2	180

LIST OF TABLES

Table 2.1	Summary of Test Parameters	32
Table 2.2	Model Parameters for Span/Insulator Length and Span/Sag Ratios	33
Table 2.3	Test Series For The Longitudinal Cascade	34
Table 2.4	Summary of Numerical Models Reported by McClure and Tinawi	36
Table 4.1	Conductor Properties	64
Table 4.2	Broken Insulator Tests Summary – EPRI Full Scale Tests	66
Table 4.3	Static Model Analysis and Full-Scale Results (IIL1 and IIL2)	71
Table 4.4	Calibration Correction	73
Table 4.5	Broken Insulator Model Runs – Comparison of Results Between ADINA and EPRI Tests at Tower T4	73
Table 5.1	Model Conductor Sag	85
Table 5.2	Model Insulator Lengths	85
Table 5.3	Comparison of Peak Forces Using Blue and Red Springs	88
Table 5.4	Models Selected For This Study	90
Table 5.5	Peak Transient Forces	98
Table 5.6	Longitudinal Forces With No Tower Failure – Model 2	102

LIST OF FIGURES

Figure 1.1	Typical Self Supported Steel Structure	2
Figure 1.2	Longitudinal Cascade	4
Figure 1.3	Cascade Failure Types	5
Figure 2.1	Line Section Profiles	13
Figure 2.2	Test Structures	14
Figure 2.3	Summary of Peak Forces	16
Figure 2.4	Line Section Used for Full Scale Testing	17
Figure 2.5	Typical Broken Conductor Response Curve	19
Figure 2.6	Full Scale vs. Small Scale Test Comparison	22
Figure 2.7	Insulator String Configuration – I-String and Inverted V-String	23
Figure 2.8	Relationship Between Span/Sag and Span/Insulator Length Ratios	23
Figure 2.9	Summary of Impact Ratio (R_i)	24
Figure 2.10	Influence of Insulator Configuration on Impact Ratio	25
Figure 2.11	Schematic of Test Setup	27
Figure 2.12	Typical Force Time History	28
Figure 2.13	Small Scale Model Structure	30
Figure 2.14	General Model Layout and Tower Failure Sequence	32
Figure 2.15	Average Impact Factor Ratio – All Model Runs	35
Figure 2.16	Numerical Models R-63 and R-83	37
Figure 2.17	Numerical Model F-85	37
Figure 2.18	Numerical Model F-104	38
Figure 2.19	Simple 2D Model	40
Figure 2.20	3D Model – Schematic and Structure Detail (Inset)	40
Figure 2.21	Structure Model Used in Structure Failure Tests	42

Figure 2.22	Time History – Conductor Tension Due To Failed Conductor	45
Figure 3.1	Key Model Nodes	50
Figure 3.2	Sag Node Coordinates for 50m and 250m – Level Span	52
Figure 3.3	Sag Node Coordinates – Unlevel Spans	54
Figure 3.4	Nonlinear Elastic Conductor Properties and Curve	57
Figure 4.1	Broken Suspension Insulator Induced Dynamic Loads	62
Figure 4.2	Test Line Profile Prior to Testing	65
Figure 4.3	Typical Suspension Tower	66
Figure 4.4	One Span In the Six Span Numerical Model – 3D Isometric View	68
Figure 4.5	Time Step Sensitivity	70
Figure 4.6	Full-Scale and Model Peak Force Comparison	75
Figure 4.7	Insulator Swing Angle – T4 – Test IIL1	76
Figure 4.8	Force Time History – Tower T4 Insulator	77
Figure 4.9	Influence of Insulator Length on Peak Insulator and Conductor Forces	78
Figure 4.10	Influence of Initial Conductor Tension on Peak Insulator and Conductor Forces	80
Figure 4.11	Influence of Incremental Ice on Initial and Peak Insulator Forces	81
Figure 4.12	Influence of Incremental Ice on Initial and Peak Conductor Tensions	81
Figure 5.1	Small-Scale Model Structure	86
Figure 5.2	Kempner Model and Simplified Numerical Model Structure	89
Figure 5.3	Numerical Model Section – Three Tower Failure Sequence	91

Figure 5.4	Sensitivity of Time Step Increment – Small-Scale (50Hz Filtered)	93
Figure 5.5	Scale Model and ADINA Model 2 Overlay – Raw Data	93
Figure 5.6	ADINA Model 2 Results – Raw and 50Hz Filtered	94
Figure 5.7	Scale Model and Filtered Numerical Model 2	95
Figure 5.8	Distribution of Error Between Numerical and Small-Scale Model Results	98
Figure 5.9	Peak Transient Forces – Scale Model and ADINA – Span/Sag = 100	99
Figure 5.10	Peak Transient Forces – Scale Model and ADINA – Span/Sag = 50	100
Figure 5.11	Peak Transient Forces – Scale Model and ADINA – Span/Sag = 20	100

LIST OF ABBREVIATIONS AND SYMBOLS

A	Area (m^2)
Δt	Time step increment (s)
E	Young's Modulus (Pa)
ε	Strain
H_c	Horizontal conductor coordinate (sag profile) (m)
H_{S-MAX}	Horizontal coordinate of maximum sag point (sag profile) – unlevel span (m)
kcmil	Conductor area
L	Overall span length (m)
M&E	Mechanical and Electrical insulator strength rating (N)
RTS	Rated Tensile Strength (N)
S_c	Vertical conductor coordinate (sag profile) (m)
S_{MAX}	Maximum conductor sag (sag profile) (m)
σ	Stress (N/m^2)
T	Conductor tension (N)
V	Vertical elevation difference between ends of conductor span (m)
W	Unit weight of conductor (N/m)

Chapter 1

Introduction

In today's age of technology, electrical power has become a necessity of life, not only from basic needs and survival standpoint, but also from a dependence on a wide variety of electronic "luxury" equipment. From medical life support systems to video games, mankind's demand for power has become something that cannot be denied, even for small durations. Power transmission systems are the backbone of the networks that link the power generation sources to the general public and are frequently required to operate at maximum electrical capacity. High voltage transmission lines are constructed from support structures, electrical insulators, and conductors (Figure 1.1), which are basically connected in series, with very little redundancy built in. Failure of any component will result in an outage to customers, and is therefore, not acceptable, especially for long durations.

Overhead lines are normally designed to withstand two types of loads; primary loads arising from direct meteorological exposure, such as ice and wind, and secondary loads, often known as the unbalanced loads due to ice shedding, or the failure of a component. Primary loads are typically specified by a design return period, and are usually applied as maximum ice, maximum wind, and some combination of wind and ice. The design return period is selected by balancing the initial capital cost of building the line against the cost of failure (damage) during its lifetime operation. Also, the importance of the line plays a significant role in selecting the design return period. Radial lines are typically

more critical than parallel lines or lines within a grid as failure of a radial line often causes an extended outage to the customer. With historical meteorological data that is readily available, and barring changes in weather patterns, primary loads are estimated routinely with some quantifiable risk of experiencing the design loads. Today's reliability based design (RBD) techniques are well developed and are suited for design using primary loads. Secondary loads are more random in nature and are much more difficult to quantify.

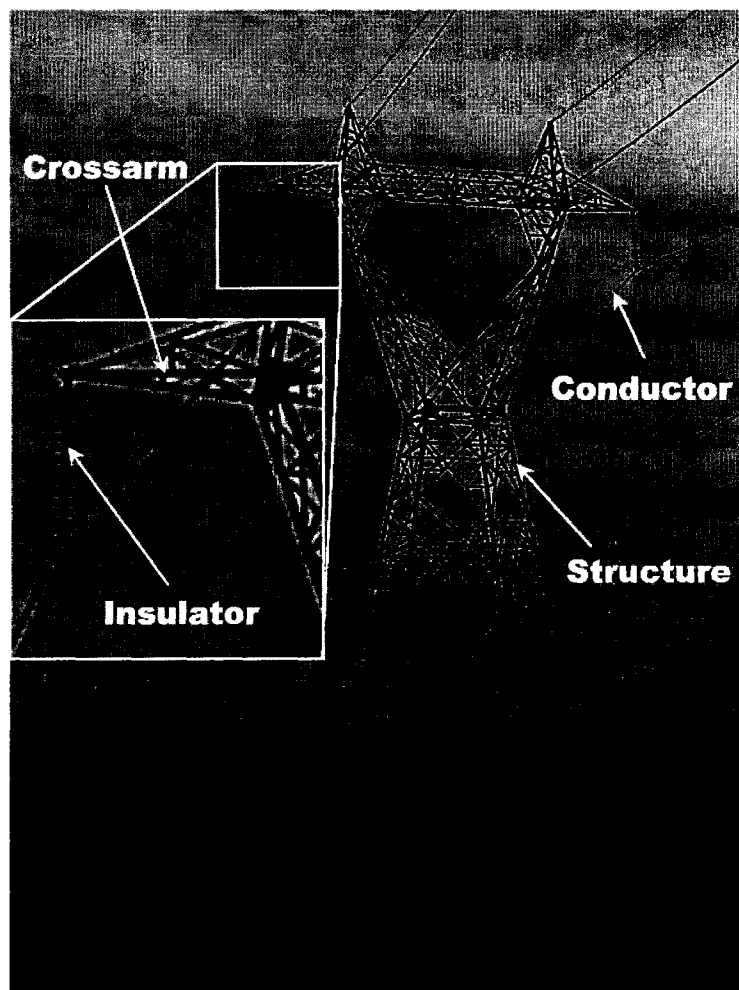


Figure 1.1 – Typical Self Supported Steel Structure

Ice build-up on a transmission line can provide a substantial load on the structure. The structure should be able to maintain its integrity, provided that the static design load is not exceeded. Secondary loads, in conjunction with primary loads, are experienced when, for example, ice shedding occurs in an unequal manner. This provides an unbalanced longitudinal load case that is often random in nature and is more difficult to quantify as it contains a dynamic component, which is followed by a residual static part.

Due to the large amount of stored energy from the heavy loading, failure of mechanical components in the system, such as insulators or deadend hardware, can produce significantly large dynamic loads that are very difficult to quantify or to design for. These dynamic secondary loads, even when the primary loads are less than the design load, can far exceed the structure capacity and can trigger a failure event in the system. A large amount of energy is released and this released energy can cause catastrophic failures that can extend well beyond the location of the initial failure point. This kind of failure, which can exceed tens or even hundreds of structures from the initial failure location, is called a cascade failure. Figure 1.2 shows an example of a longitudinal cascade of a Hydro Quebec 735 kV line during the ice storm of 1998.

The excessive loads imposed by the unbalanced conductor tensions on both sides of the suspension structure can cause the cascade failure, which can extend to a large distance. In one example, 167 structures failed in a longitudinal cascade that extended from coast to coast in Denmark (Frandsen, 1976). This reference also notes a failure of 350

structures in a single event on a 345 kV line in the United States. Transmission structures (suspension/light angle) are capable of withstanding limited longitudinal loading, depending on original design load cases taken into consideration, and are typically not adequate to sustain large dynamic longitudinal loads from failed components. Since the design of all structures to withstand these large dynamic loads is not economically feasible, some means of quantifying the possible loads imposed, and then designing the structures for some acceptable failure level must be understood.



Figure 1.2 – Longitudinal Cascade (Hydro Quebec, 1998)

Three types of cascades are possible in transmission systems; transverse, vertical and longitudinal (Figure 1.3). Vertical cascades are normally caused by failure of phase support (crossarm, insulator) in suspension structures, typically dropping one phase to the ground over numerous structures. Transverse cascades are perpendicular to the line and can be caused by high intensity winds. When a suspension structure fails transversely due to high wind, it imposes a line angle (see Figure 1.3) on the adjacent two structures, and thus creating longitudinal and transverse loads. If the adjacent structures cannot withstand these loads, then failure will propagate causing cascade. The longitudinal cascade is the most common cascade type, and is responsible for events that have damaged or destroyed many kilometres of line and have contributed to significant cost for emergency repairs. They are especially significant considering that failure of a \$50 hardware component can cause hundreds of thousands of dollars worth of damage.

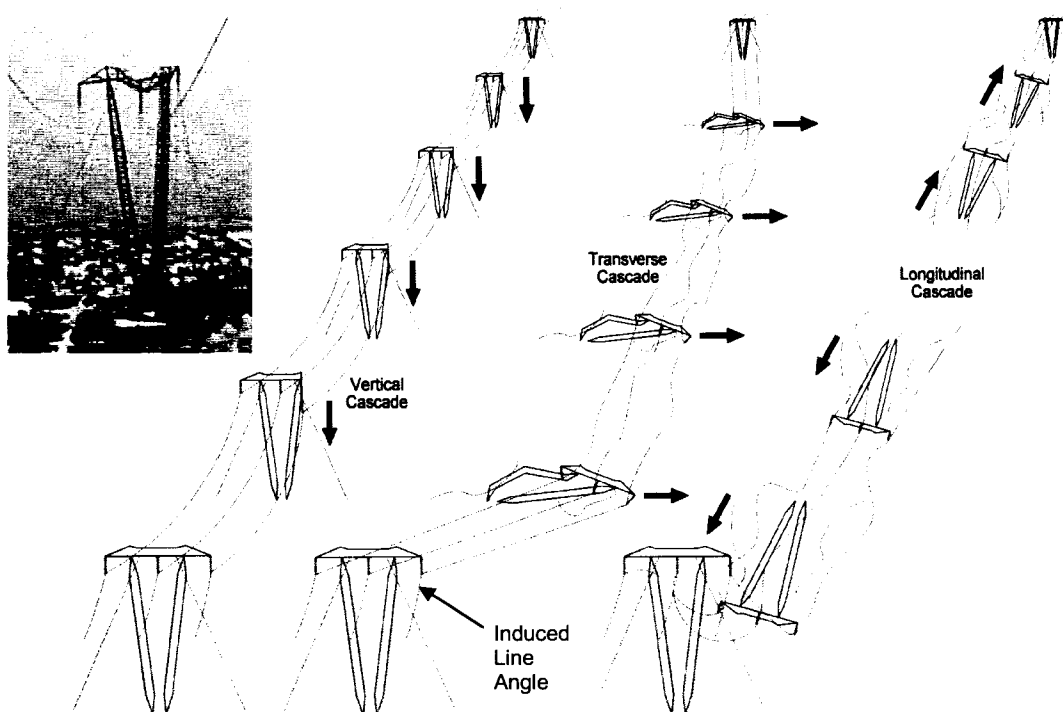


Figure 1.3 – Cascade Failure Types

To reduce the extent of longitudinal cascade, deadends or other special containment structures (anti-cascading tower) with higher longitudinal load capacities can be inserted in the line at regular intervals to limit the distance over which the damage can propagate. Although this is the most effective means used in practice, a better understanding of the dynamic loads experienced during cascade failure would provide designers with the tools required to cost effectively and reliably design the transmission systems and to minimize damage from single component failure. This is especially important when consideration is made for the premature failure of a component below the design load level, which can cause a cascade that could otherwise be prevented or minimized with a proper design methodology.

Current practices in the design of transmission lines for secondary loads are, in general, to provide special containment structures at certain intervals and to design each suspension structure with some limited longitudinal strength. In most cases, the dynamic load effects are not considered and therefore the post failure force distribution is often unknown and remains unquantified. Since the design process under secondary loads using impact factors derived from small-scale and/or full-scale tests only provides a partial solution, there is a strong need to understand the post failure force distribution in a line to ensure that proper strength coordination can be implemented.

1.1 Scope

Transmission line modeling for dynamic load studies has recently been performed using a commercial software package known as ADINA (Automatic Dynamic Incremental Nonlinear Analysis) (ADINA, 2003). Although there may be other commercial software available for the analysis of this type of problem, ADINA has been shown to be a valuable tool in assessing the dynamic impact forces experienced by structures due to failed components (Tucker and Haldar, 2006). ADINA was used during the present research to validate the Electric Power Research Institute (EPRI) full scale test results (Peyrot et al, 1978), and the small-scale model test results (Kempner, 1997), as described in detail in Chapter 4 and Chapter 5 respectively. An understanding of how the ADINA program works will be discussed so that future research can be built on simple models presented in this thesis.

A series of full-scale broken conductor and broken suspension insulator tests were carried out by The University of Wisconsin and EPRI to validate the state of the art at the time in predicting dynamic loads and also to validate a custom made numerical model. The report, Longitudinal Loading Tests on a Transmission Line - EL-905, (Peyrot et al, 1978) provides a very comprehensive set of test data and results, not only limited to their findings, but also complete with all necessary information required for analysis and for development of a numerical model. Since 1978, data from EL-905 report has been analyzed mostly to gain an understanding of longitudinal loading due to broken conductors. A series of test cases studying dynamic load due to broken suspension

insulator was reported in EL-905; however, very little analysis of the results for this scenario were subsequently performed with no significant findings documented. A numerical model will be used to validate the results of the broken insulator test cases. Upon validation of the test results, a sensitivity study will be carried out which will include various conductor tension levels, insulator lengths, and ice loads, and their effects on the peak dynamic loads.

Kempner (1997) performed a series of broken conductor tests on a scale model. Previous studies measured the dynamic loads only on intact towers, for both full-scale structure tests and small-scale model tests, but did not take into account its effects considering structure collapse. Kempner's study was unique because the forces were measured on surviving towers when the proceeding towers have failed. The objective was to assess the dynamic containment load on the first surviving tower due to conductor failure. This data has not been analyzed fully through numerical modeling. Through the use of a numerical model, the results from the scale model tests will be validated and the suitability of using the ADINA software will be assessed.

The primary objectives of the present investigation are to:

1. provide necessary background information for designers/engineers to use dynamic finite element software in modeling transmission line systems;
2. use numerical simulation to validate full-scale test data for broken suspension insulator scenario, and;
3. use numerical simulation to validate small-scale test data on surviving structures for conductor failure scenario.

1.2 Thesis Organization

Chapter 2 provides a literature review of some of the past work that has been documented for analytical, full-scale and small-scale studies. A significant amount of work has been performed to document and to quantify dynamic loading. Much of the published research work, particularly the test results detailed in this chapter, has not been validated using numerical models.

Chapter 3 details the key points of consideration behind the generation of a numerical model using the ADINA finite element software. Published information of numerical model generation for the purpose of quantifying dynamic loads on transmission lines is basically non-existent. A detailed guide to aid in model generation using a simple two-span model with self supported towers can be found in Appendix 1.

Chapter 4 presents validation of the broken insulator test scenario, as performed by EPRI in 1978. The EPRI test data will be used to develop a numerical model to predict dynamic loads due to a broken suspension insulator string. A sensitivity study of modifying insulator length, conductor tension and ice load is also presented to determine the effects of these parameters on the peak dynamic tension of the conductor.

Chapter 5 will validate the results of the scale model tests performed by Kempner (1997). Kempner's study analyzed the effects of failed towers, as well as other variables such as

conductor tension and insulator length. Validation of the scale model test data will broaden the current knowledge of understanding cascade mechanism and therefore a better understanding of design of new lines as well as mitigating existing lines with particular reference to containment loads.

Chapter 6 will summarize the findings of the different models, and recommend future areas of research.

Chapter 2

Literature Review

Electrical transmission systems can take many forms. Lines for the transmission of power at voltages up to 735 kV and higher are constructed to reduce losses in the conductor as remote power sources are frequently located hundreds, if not thousands, of kilometres from the load points. Lower voltage lines are typically constructed of wood or steel pole systems. Higher voltage lines are generally constructed from lattice steel towers, as previously shown in Figure 1.1. The common factor in all transmission line designs is the conductor that connects each tower together. This conductor, strung under tension to prevent ground contact, is the source of the most significant structural loads.

Static meteorological loads on the conductor, as well as on the structure, such as ice or wind are used to determine the capacity of the structure to reliably carry power without structural failure. These loads are relatively straightforward to design for; however, while in service, transmission lines sometimes experience component failure, such as a broken conductor or a broken insulator, for various reasons including overload, operational conditions or vandalism. This failure can produce large dynamic loads that can travel from structure to structure along the conductor having catastrophic consequences. Dynamic forces are significantly higher than the static loads alone. Therefore, a significant amount of research has been done in the past to estimate these loads properly to ensure the reliability of high voltage lines.

2.1 Full Scale Tests

Haro et al (1956), through a series of full-scale tests, recorded the force acting on a structure due to single-phase conductor breakage. The effects of conductor cross-section and initial tension, insulator length and types, and tower types (rigid versus flexible) were studied in their experiments. Conductor overloads due to icing, as well as span length variation, were not considered in these tests.

Through strategic conductor ruptures on two sections of 110 kV and one section of 220 kV transmission lines, forces in conductor, ground wires, guys and on support structures, as well as the support and insulator movements were measured. The section profiles and structure types (all with two overhead ground wires) for these three test groups are shown in Figure 2.1 and Figure 2.2 respectively. Test Group 1 was composed of three spans of self-supported steel H-Frame structures. Tests were performed using four different copper conductors, with cross-sectional areas ranging from 66 mm^2 to 147 mm^2 and initial stresses varying from 7.5 to 21 kgf/mm^2 . While the majority of the tests utilized all three spans, a small percentage of these tests were performed with only one span by anchoring the conductor to the second structure. Test Group 2 was composed of four spans of guyed wood pole/steel cross arm H-Frame structures. Only one conductor type was used (117 mm^2 copper), with initial stresses varying from 9 to 12 kgf/mm^2 . Test Group 3 was composed of eight spans of guyed steel H-Frame structures, with some tests performed on the first four span section (shown in Figure 2.1) using similar anchoring

methods as Test Group 1. One conductor (455 mm^2 ACSR “Condor”) was used with stresses varying from 4.8 to 6.2 kgf/mm^2 . Conductor failure was initiated in all cases using a lock installed close to the insulator string. Insulator string lengths were varied for all tests using 3, 7 or 12 insulators. All remaining phases, as well as the two overhead ground wires, remained unchanged for these tests.

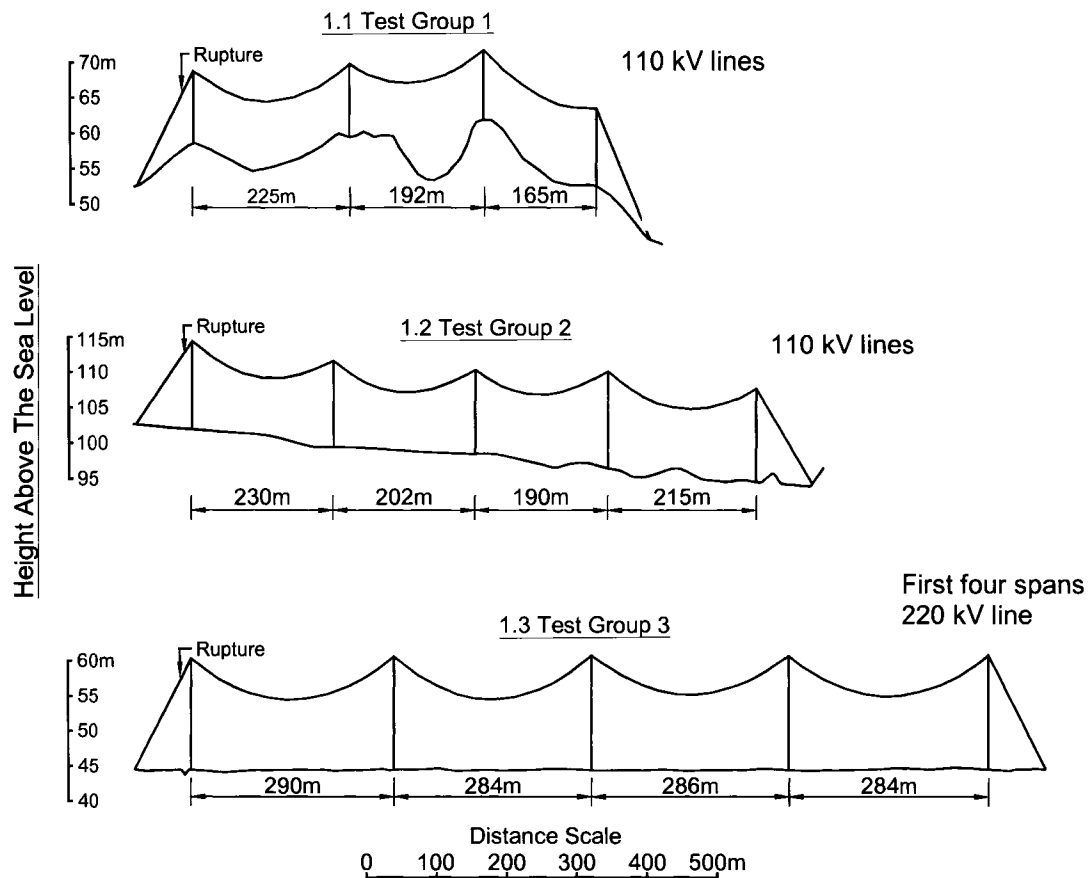


Figure 2.1 – Line Section Profiles (modified from Haro et al, 1956)

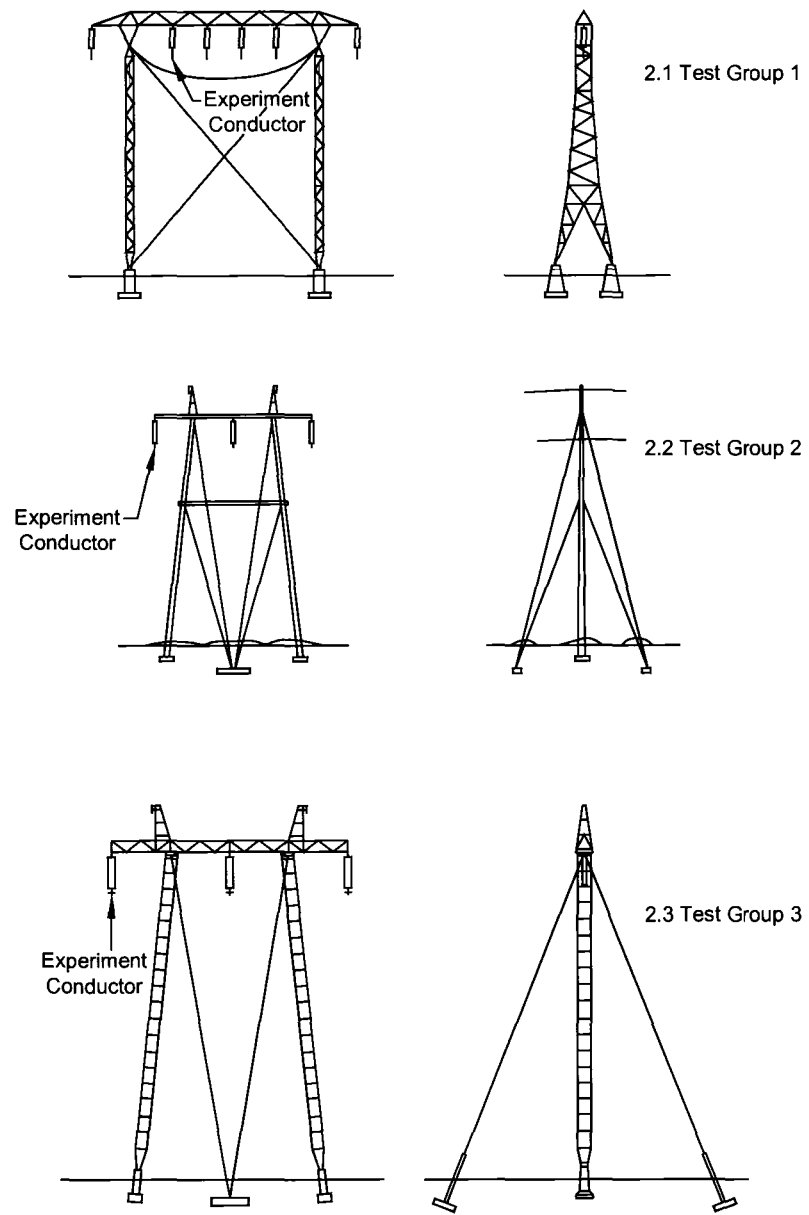


Figure 2.2 – Test Structures (modified from Haro et al, 1956)

After rupture, conductor force time histories showed a significant drop of 90 - 95% of the initial tension, similar to Figure 2.5. This state was maintained for slack time periods ranging from one-tenth to one second, with the time proportional to the length of the insulator string, and inversely proportional to the initial tension. Tension increase after the slack time rose linearly to the peak force, with the incremental rate inversely proportional to the insulator string length, and proportional to the initial tension. After the peak forces were experienced, conductor tension oscillated around the final static tension for one to two minutes before it was damped out.

Haro et al (1956) found that the forces recorded were dynamic in nature. They concluded that the first peak was due to the elastic recovery of conductor tension, and the second peak was from the wave force reflection from the support structure, approximately four seconds after the rupture. Increases in initial tension caused an increase in peak dynamic forces after the conductor breakage; however, the ratio of the peak force to the initial tension decreased with increasing initial tension. A 15% reduction of “peak forces” was realized by using short insulator strings (3 units) over longer strings (7 or 12 units) (Figure 2.3). Flexible support structures (guyed) experienced only $\frac{2}{3}$ of the peak force measured on rigid structures (self supported). Insulator types (individual disks or solid rod) and conductor cross-section had little effect on measured peak forces.

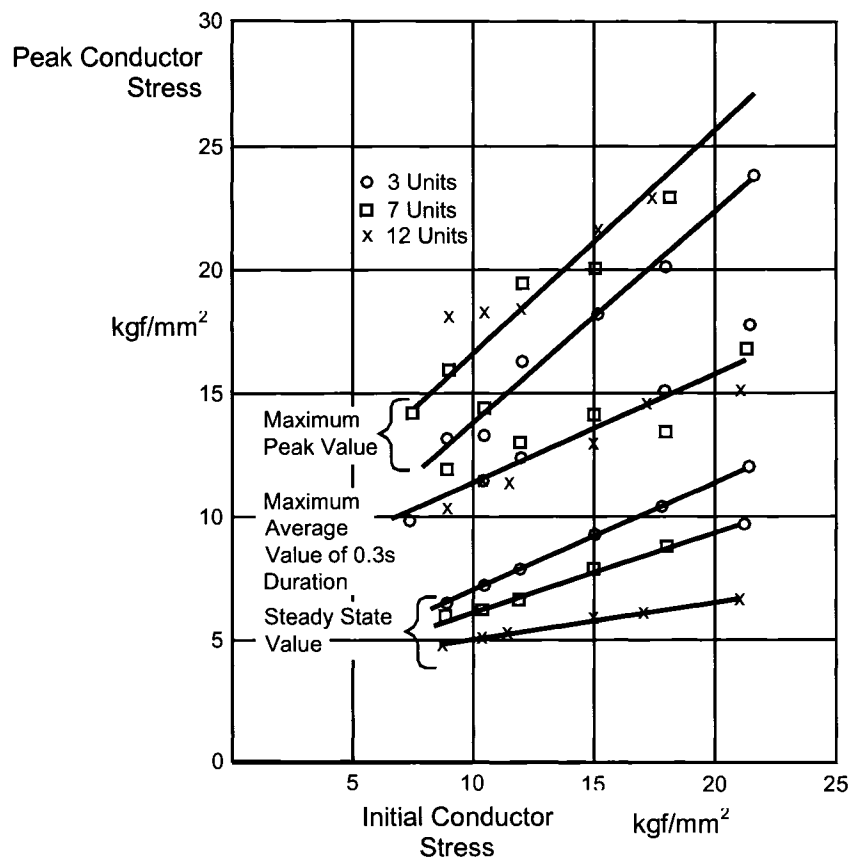


Figure 2.3 – Summary of Peak Forces (modified from Haro et al, 1956)

Peyrot et al (1978) performed full scale testing on an abandoned 138 kV line owned by the Wisconsin Power and Light Company. The line, scheduled to be dismantled, was to provide space for a 345 kV line, but was available for testing without any restrictions on the nature and magnitude of loads that could be applied to it during the investigation. Their objectives in performing these tests were to verify existing load prediction techniques (dynamic and residual) of the time, and to collect data to validate a customized numerical model developed by the researchers, so that further small scale and full scale tests could be avoided.

Although many tests were performed, the test series were broken down to failed conductor and failed suspension insulator tests. In total, 23 tests were performed. These included one test measuring the effects of broken shield wires, and one test where all conductors had failed, in the hope of causing a longitudinal cascade. Six intact spans (Figure 2.4) were included in the testing; with all structures being square based lattice steel towers, each carrying two three-phase circuits, each circuit strung with different conductor types, and two overhead shield wires. The report (EL-905) contained all pertinent information to allow future analysis of the test results.

The broken suspension insulator test was performed by dropping the conductor from the insulator assembly on tower T5, creating a “superspan” that extends from tower T4 to tower T6. The data recorded on tower T4 included conductor and insulator tension, as well as insulator swing angle. The information collected for the broken suspension insulator test is described in greater detail in Chapter 4.

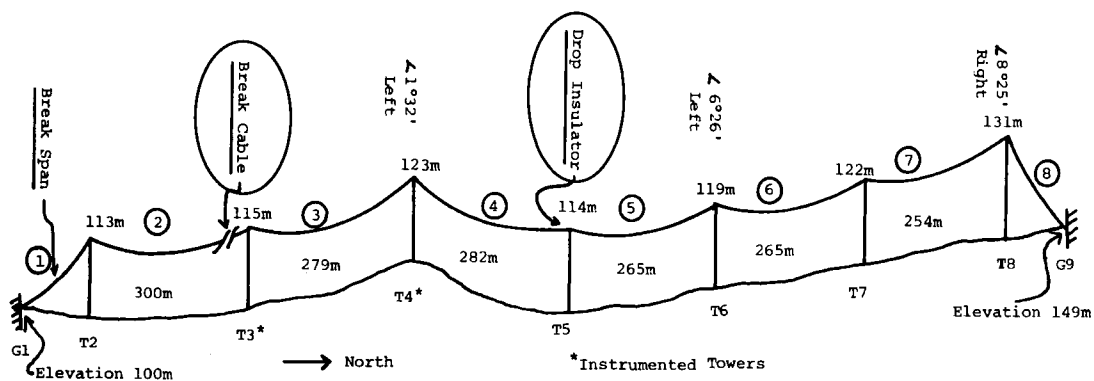


Figure 2.4 – Line Section Used for Full Scale Testing (Peyrot et al, 1978)

The broken conductor test cases comprised the majority of the tests, and were initiated in span 2 (Figure 2.4). In total, 12 broken conductor tests were performed. Combinations of conductor types (397 kcmil ACSR (Aluminum Conductor, Steel Reinforced) and/or 471A copper/bronze), insulator lengths (2.2 m, 3.7 m or 4.3 m) and conductor tensions (12.4 kN to 23.5 kN) were used in these tests. A kcmil is defined as one thousand circular mils, where a circular mil (cmil) is the area of a circle with a diameter of one thousandth (0.001) of an inch. For each test, the force in the insulator on towers T3 and T4 were recorded, as well as the conductor tension in span three next to the break. Other information, such as tension in tower leg members was collected; however, this information was not analyzed in detail in the report.

A significant amount of data for broken conductor test cases was collected and analyzed. Each test produced force time histories similar to Figure 2.5. Immediately after the conductor rupture was initiated, the tension was reduced to almost zero for time periods of up to half of a second, after which a rise time was experienced cumulating in the first peak force. After the first peak, the tension again dropped and subsequently increased to the second peak. After the first two peaks, the tension settled down eventually to a rest state (final tension) after a couple of minutes. This type of force time history has also been recorded in similar broken conductor tests by other researchers. The data was summarized by two impact factors such as IFI (ratio of peak conductor tension to initial conductor tension before break), and IFF (ratio of peak conductor tension to final steady

state conductor tension after break). When compared to tests such as Govers (1970, discussed later), the impact factors were very similar.

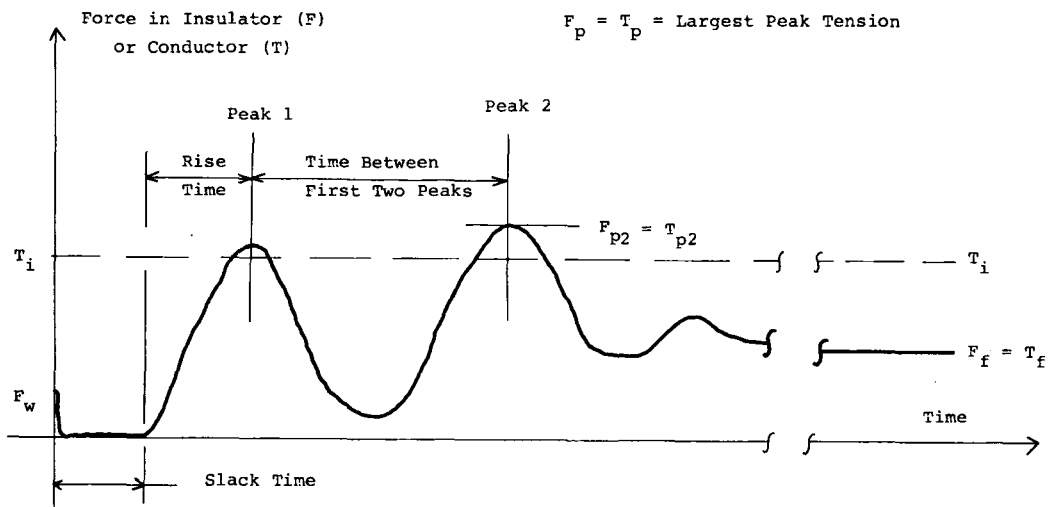


Figure 2.5 – Typical Broken Conductor Response Curve (Peyrot et al, 1978)

The broken suspension insulator test case produced results that were considered by Peyrot et al to be of little significance. This was because the peak force measured was for a bare conductor during freefall, without any of the suspension insulators attached. Peak longitudinal loads on Tower T4 were less than 25% of the initial conductor tension, where as for the broken insulator case, peak forces were in the order of 187%. Peak insulator string tensions of up to 300% were recorded. It was noted that if the conductor was loaded with ice, peak forces could be damaging; however, this was not investigated. It was also noted that longer insulator strings reduced the maximum longitudinal force.

As part of the objectives, a computer program (CABLE5) was developed and was validated to provide an analytical method to estimate broken conductor peak loads. As an extension to this work, Thomas (1981) continued the development of the software (CABLE7). Once verified, a sensitivity study of the contribution to the peak forces attributed to various parameters in broken conductor events was carried out. Thomas concluded that initial conductor tension and number of spans had the largest influence on the peak dynamic forces due to conductor failure. Tower weight and insulator length were determined to have a lesser contribution.

2.2 Scale Model Tests

Govers (1970) studied conductor breakage using many tests on a scale model, and verification tests on a full-scale line to gain insight into dynamic forces. The objective was to see if the basic concepts of design at the time were representative of reality and applied in practice.

Using a section of obsolete line in Amsterdam, full-scale tests were performed to provide a benchmark for a series of scale model tests with comparison of the impact ratio (R_i) shown in Figure 2.6. Note that D represents horizontal displacement of suspension clamp (Figure 2.7). Because of limitations in performing full-scale testing, only a few tests were performed, but the data was verified and the scope extended to a considerable number of small-scale model tests. To re-check the model, a few full-scale tests were

performed again after the scale model tests were completed, using the scale model results as a basis. The tests measured the forces in the insulator string and in the intact conductor span adjacent to the failure span. Model tests were performed for bare conductors, as well as iced conductors by attaching a cable of corresponding weight. Although ice weight could be simulated, the effect of ice shedding could not be determined using this method.

Through the small-scale model tests, the following variables were studied: (1) insulator string length and material; (2) configuration of insulator string (I string and inverted V string) (Figure 2.7); (3) conductor tension and material, as well as; (4) span length and tower rigidity. Data was summarized using three primary ratios; Impact Ratio (R_i), Residual Ratio (R_r) and Tension Overload Factor (R_o). Each ratio is defined as follows:

$$R_i = \frac{F_d}{F_i} = \frac{\text{dynamic transient peak of longitudinal force}}{\text{initial static force of conductor}}$$

$$R_r = \frac{F_r}{F_i} = \frac{\text{residual static force}}{\text{initial static force}}$$

$$R_o = \frac{F_d}{F_r} = \frac{\text{dynamic transient peak of longitudinal force}}{\text{residual static force}}$$

Govers found that the impact ratio was dependent highly on the Span/Sag ratio, and the Span/Insulator length ratio (Figure 2.8). A summary chart is shown in Figure 2.9. In general, increases in Span/Sag ratio and Span/Insulator Length ratio caused a decrease in

the impact ratio; however, Span/Sag ratio had a more significant effect. Modifying the insulator configuration also had an effect on the impact ratio (Figure 2.10). By utilizing an inverted V string configuration, impact ratios were dramatically reduced from the results obtained using I strings due to the reduction in the displacement of the insulator. The remaining factors considered in the tests did not have any significant effect on the results. It was determined, however that impact ratios for conductors with ice loads (simulated) were significantly higher than bare conductors.

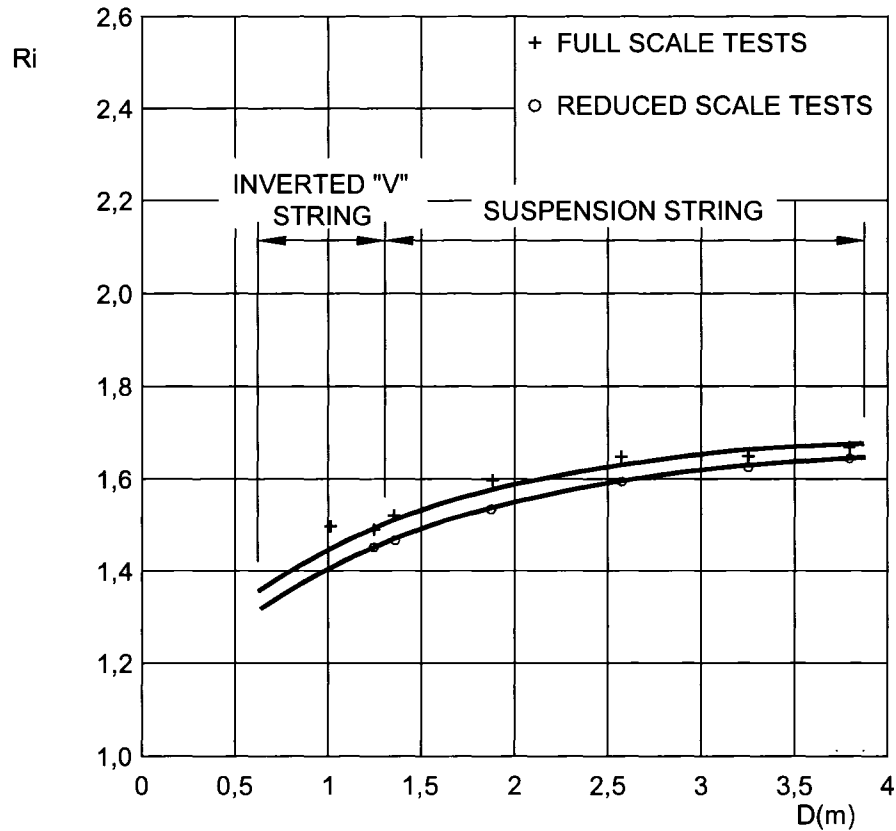


Figure 2.6 – Full-Scale vs. Small-Scale Test Comparison (modified from Govers, 1970)

Govers concluded that sag and insulator length, both with respect to span, and the insulator configuration had the largest influence on the peak dynamic impact forces on the tower. He suggested that if a specific combination of extreme line parameters were used, the design layout should be tested in a reduced scale model in order to gain insight into what impact ratios can be expected in the event of a failure.

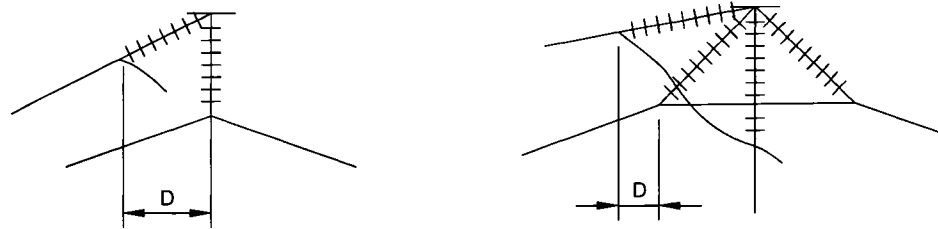


Figure 2.7 – Insulator String Configuration – I String and Inverted V String (modified from Govers, 1970)

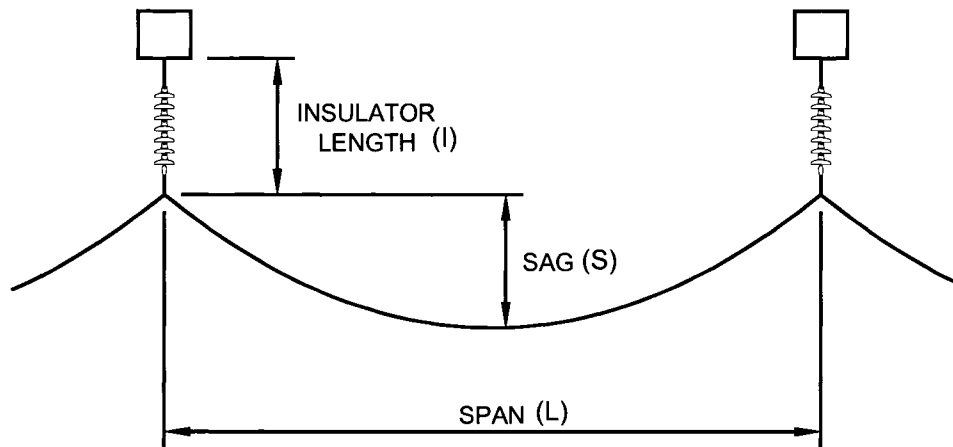


Figure 2.8 – Relationship Between Span/Sag and Span/Insulator Length Ratios

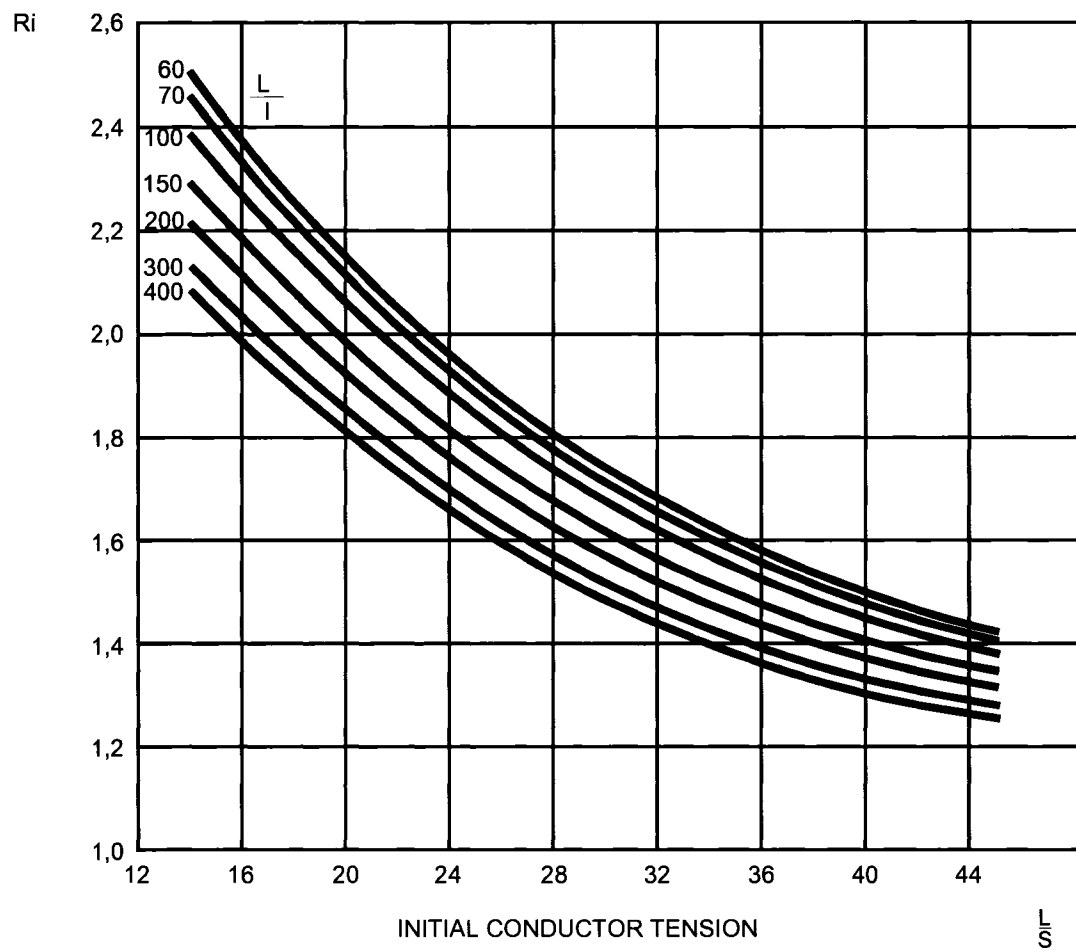


Figure 2.9 – Summary of Impact Ratio (R_i) (modified from Govers – 1970)

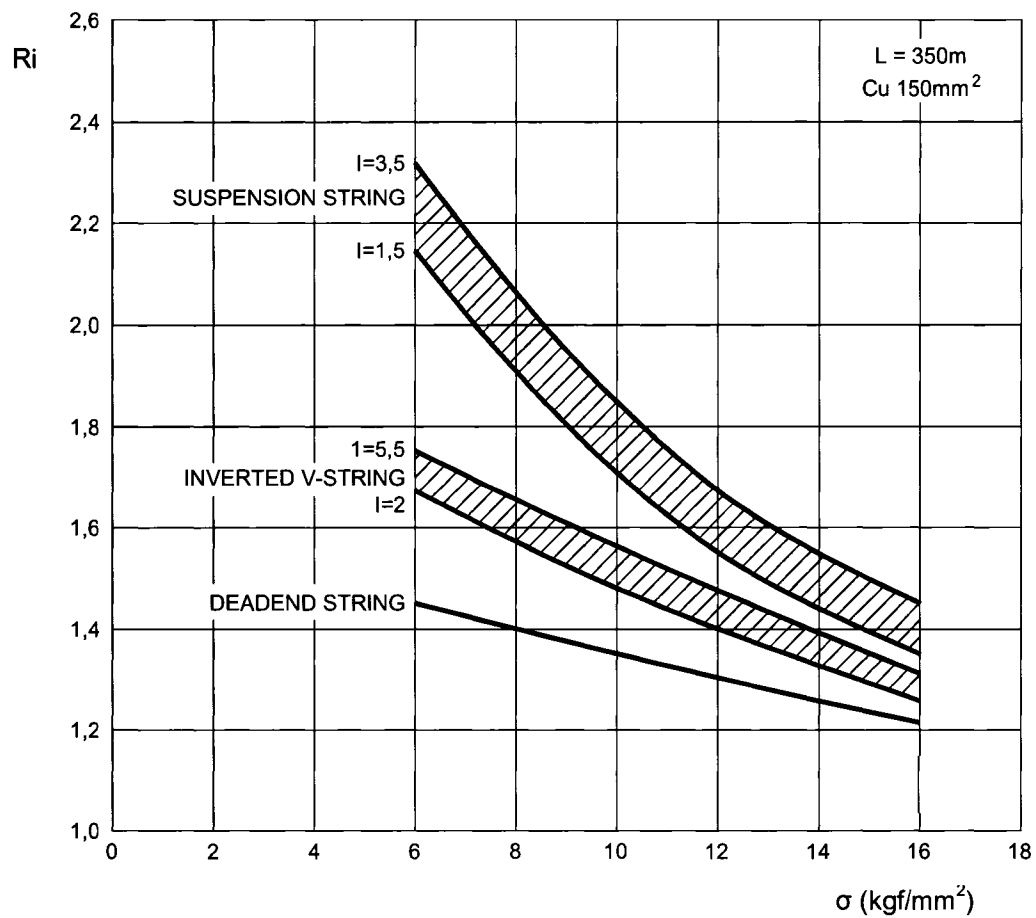


Figure 2.10 – Influence of Insulator Configuration on Impact Ratio (modified from Govers, 1970)

Mozer et al (1981) studied a scale model section of the line to investigate the static and dynamic longitudinal forces produced by broken conductors, broken shield wires and ice shedding. The results were compared with analytical methods developed to predict peak dynamic as well as residual static loads caused by the wire disturbances. Structural flexibility was also considered.

Three spans 9.75 m in length were constructed using two suspension structures, with the last deadend simulated by anchoring the wire (simulated conductor) to the lab wall (Figure 2.11). Wire tension was maintained using weights and pulleys on the first deadend structure. Tension was measured through the sag of the wire, and by plucking the wire and recording the wave propagation time. Two simulated conductors were used: (1) A beaded chain (lamp chain) and; (2) a copper wire outfitted with lead shot weights to provide for proper mass characteristics. Strain gages on the cross arm and on the base of the first structure measured the forces and ground line moment. Linear Variable Differential Transformers (LVDTs) measured the linear movement in each tangent structure shown in Figure 2.11. Using this setup, three sets of properties: stiffness and mass of the structure, tensions in conductor and shield wire, and the length of the insulator and shield wire link, were varied to measure the effects of these parameters on peak conductor forces.

For each conductor test, a short length of string was inserted into the first span, just before the first suspension structure. The string was cut to simulate conductor rupture, and high-speed chart recorders documented the time history of the responses from the strain gages and LVDTs. Two trials were performed for each test to verify the repeatability of the results.

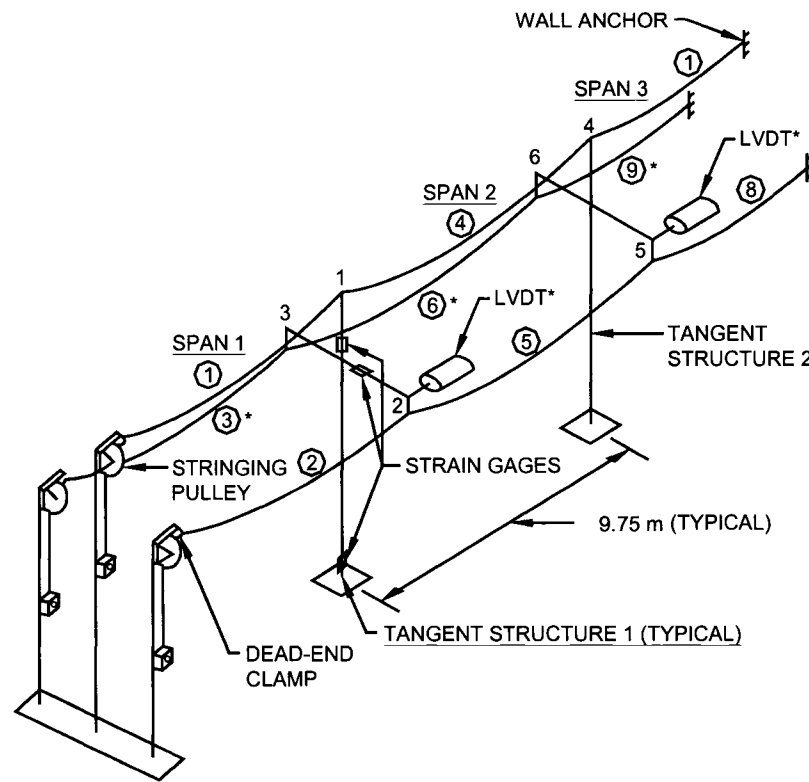


Figure 2.11 – Schematic of Test Setup (modified from Mozer et al, 1981)

The time histories showed that the transient response due to conductor rupture is very rapid, with maximum peak in less than 0.25 seconds after the string was cut. Similar to the two previous test results described in section 1.1, sudden loss of tension was experienced immediately after the conductor failure. Two peaks were measured (Figure 2.12); the first peak (approximately 0.1 seconds after failure) was concluded to be the sudden elastic recovery of the strain in the remaining intact conductor, and the second peak (approximately 0.25 seconds) was from the increase in tension due to the conductor dropping to a lower position, having the insulator string length now added as part of the conductor length. This conclusion was different than Haro's assumption that the second

peak was due to wave reflection from the dead end. High speed cameras showed that the return of the travelling wave reflected from the support occurred after the first two peak forces. It was suspected that the damping and deformation of the beaded chain also had a significant effect on the dynamic response.

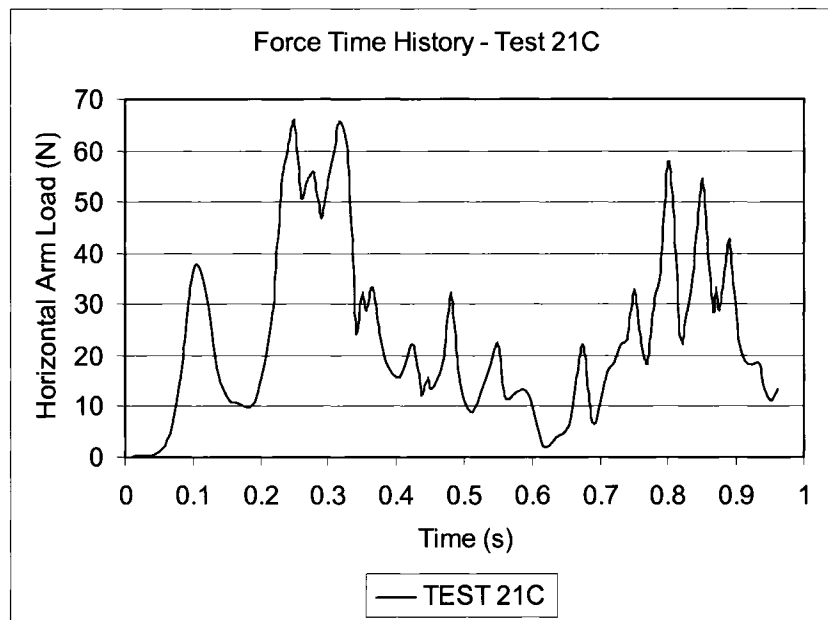


Figure 2.12 – Typical Force Time History (Mozer et al, 1981)

As a result of this scale-model work, it was concluded that dynamic loads and structure responses are quite large. It was suggested that it may not be feasible to design tangent structures to sustain these loads without yielding; however, a minimum level of longitudinal strength for tangent structures may limit failure to only a few structures. It was recommended that further studies to relate longitudinal loads and security of the line to resist cascade failure be performed. The studies should utilize analytical and experimental investigations, and examine line performance with different levels of

longitudinal strength, complete collapse of deadend structure or the complete separation of all wires.

Kempner (1997) modified Govers model to include tower failure. The modified study was performed using small scale models due to the prohibitive cost of performing full scale testing. The study was performed primarily to understand the influence of the tower failures on the longitudinal load in a simulated cascade situation. The longitudinal cascade was analyzed, assessing the influence of: (1) tower type; (2) conductor type; (3) span length; (4) conductor sag (initial tension); (5) insulator length, and; (6) conductor failure location (within the span).

The model by Kempner was constructed at Portland State University at a 1:23 scale (Figure 2.13). Two small scale models were created; the first one was composed of three spans representing actual span lengths of 275 m and was used to verify the repeatability of the results, and a second model consisting of five spans, with each span length being the same as the three span model.

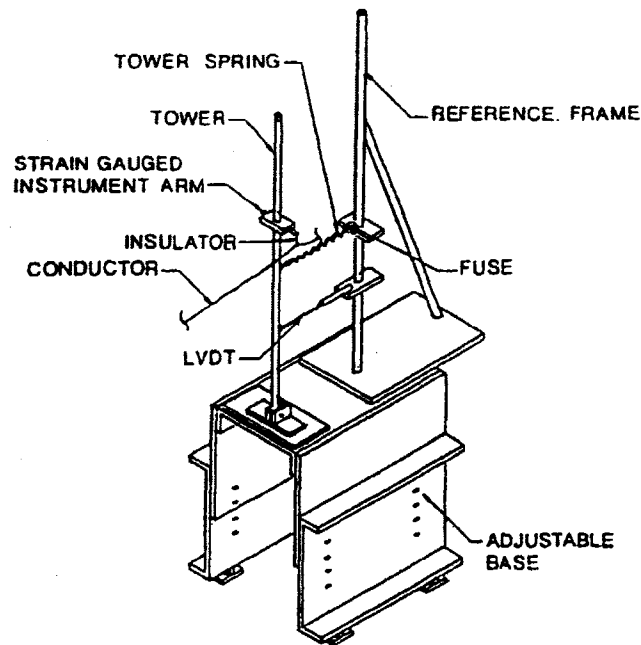


Figure 2.13 – Small Scale Model Structure (Kempner, 1997)

Two conductor types were used in the study; a beaded chain similar to Govers (1970), and a stainless steel wire fitted with lead shot weights. Two different tower springs were used to modify the stiffness of the structure to represent flexible, pole type (blue spring) and rigid, self supported lattice type (red spring) structures.

As per Figure 2.14, Kempner performed a series of scale model tests to study the effect of tower failure. Tower failure was accomplished by burning the tower fuse (see Figure 2.13), a 0.2 mm wire, which would separate the tower from the support within 0.0019 seconds. A summary of the tests performed is provided in Table 2.1, with the sequence summarized as follows:

Model Run 1

- a) Conductor ruptured in span to the right of tower 1 (Figure 2.14)
- b) Data logged at tower 1, in particular force and tower displacement. This data becomes the control results to which all analysis results are related
- c) Using results from Model Run 1, failure time for tower 1 is recorded to be used for Model Run 2 based on a percentage of the peak displacement

Model Run 2

- a) Model is reset back to original condition
- b) Conductor ruptured in span to the right of tower 1
- c) At the appropriate time as per the results of Model Run 1, tower 1 fails by burning off the fuse as shown in Figure 2.13
- d) Data is logged at tower 2, again recording force and displacement
- e) Using results from Model Run 2, failure time for tower 2 is recorded to be used for Model Run 3 based on a percentage of the peak displacement

Model Run 3

- a) Model is reset back to original condition
- b) Conductor ruptured in span to the right of tower 1
- c) At the appropriate time as per the results of Model Run 1 and Model Run 2, tower 1 and tower 2 both fail at their respective times by burning off their fuses
- d) Data is logged at tower 3, again recording force and displacement
- e) Using results from Model Run 3, failure time for tower 3 is recorded to be used for Model Run 4 based on a percentage of the peak displacement

Model Run 4

- a) Model is reset back to original condition
- b) Conductor ruptured in span to the right of tower 1
- c) At the appropriate time as per the results of Model Runs 1, 2 and 3, tower 1, 2 and 3 all fail at their respective times by burning off their fuses
- d) Data is logged at tower 4, again recording force and displacement

By following this sequence for each combination as shown in Table 2.1, a significant amount of data was collected on the cascade event.

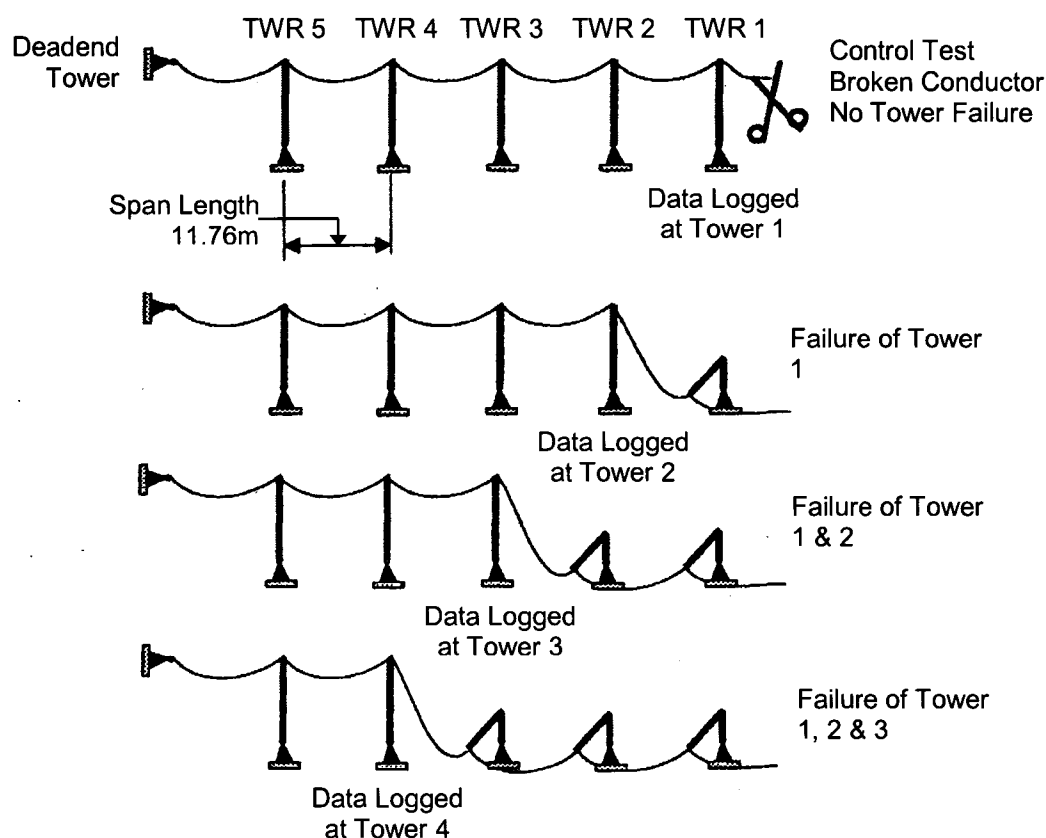


Figure 2.14 – General Model Layout and Tower Failure Sequence (modified from Kempner, 1997)

Table 2.1 – Summary of Test Parameters (modified from Kempner, 1997)

Span/Ins Ratio	Tower Spring	Span/Sag Ratio									
		20		30		50		70		100	
100	Red	SS	BC	SS	BC	SS	BC	SS	BC	SS	BC
100	Blue	SS	BC	SS	BC	SS	BC	SS	BC	SS	BC
200	Red	SS	BC			SS	BC			SS	BC
200	Blue	SS	BC	SS	BC	SS	BC	SS	BC	SS	BC
400	Red	SS	BC			SS	BC			SS	BC
400	Blue	SS	BC	SS	BC	SS	BC	SS	BC	SS	BC

Span/Insulator Length ratios ranged from 100 to 400 through the variation of the length of the insulator wire in the model. Span/Sag ratios covered a range of 20 to 100 and were

varied by changing the initial tension of the conductor. Span/Insulator Length and Span/Sag ratios are provided in Table 2.2. Red tower springs (high stiffness) represented self supported lattice towers, and blue springs (low stiffness) represented unguyed pole structures (wood). Stainless steel conductor (SS) and beaded chain conductor (BC) were both represented to measure the effects of various conductor types. Gaps in Table 2.1 for the red spring and Span/Sag ratios of 30 and 70 were to reduce the number of model runs and subsequent analysis required.

Table 2.2 – Model Parameters for Span/Insulator Length and Span/Sag Ratios (modified from Kempner, 1997)

<i>Represented Span Length = 275m</i>		<i>Model Span Length = 11.8m</i>	
<i>Span/Sag Ratio</i>	<i>Model Sag (mm)</i>	<i>Span/Insulator Length Ratio</i>	<i>Insulator Length (mm)</i>
<i>100</i>	117.6		
<i>70</i>	167.9	<i>400</i>	29.5
<i>50</i>	235.2	<i>200</i>	58.9
<i>30</i>	391.9	<i>100</i>	117.6
<i>20</i>	588.0	<i>Note: Scale Model Factor 23.3</i>	

Each of these model runs was conducted in a series to analyze the effect of tower capacity (represented by percent of maximum displacement) on the cascade failure. The test series is provided in Table 2.3. Low displacement (LD) was calculated as failure at 25% of the maximum displacement from the previous model run. High displacement (HD) was calculated in the same way, but at 75% of the maximum displacement. This was to measure the effect that displacement of the structure prior to failure would have on the results.

Table 2.3 – Test Series For The Longitudinal Cascade (modified from Kempner, 1997)

<i>Model Run</i>	<i>Tower 1*</i>	<i>Tower 2*</i>	<i>Tower 3*</i>	<i>Tower 4</i>	<i>Failure Code*</i>
<i>1</i>	Control test – no failures				C
<i>2</i>	Fail, LD	No Fail	No Fail	No Fail	L
<i>3</i>	Fail, HD	No Fail	No Fail	No Fail	H
<i>4</i>	Fail, LD	Fail, LD	No Fail	No Fail	LL
<i>5</i>	Fail, HD	Fail, HD	No Fail	No Fail	HH
<i>6</i>	Fail, LD	Fail, LD	Fail, LD	No Fail	LLL
<i>7</i>	Fail, HD	Fail, HD	Fail, HD	No Fail	HHH
<i>8</i>	Fail, LD	Fail, LD	Fail, HD	No Fail	LLH
<i>9</i>	Fail, HD	Fail, HD	Fail, LD	No Fail	HHL

* C = Control, L = low, H = high, D = displacement

For each model run, the time history response of the horizontal force due to conductor breakage was recorded and the peak transient dynamic load was documented. The impact factor calculated provided the ratio of the peak load of any given tower that has not failed (survived) to the peak load of the first tower during the first (control) model run. A summary of the results is provided in Figure 2.15. As can be seen, as the cascade progresses, peak transient dynamic loads on subsequent towers is reduced, based on the number of towers that have failed. Therefore, eventually a tower capable of surviving the dynamic force will contain the cascade failure. The effect of proximity of the deadend was not included in the study.

Kempner's work shows that scale model tests are capable of providing an understanding of the cascade phenomenon. To advance the work, analysis of towers of: (1) unequal elevation; (2) structural strengths; (3) numbers of spans, and; (4) individual span lengths could be proposed; however, this would greatly increase the amount of work, and

analysis required. Also, the failure mechanism of a lattice tower may have an influence on the results.

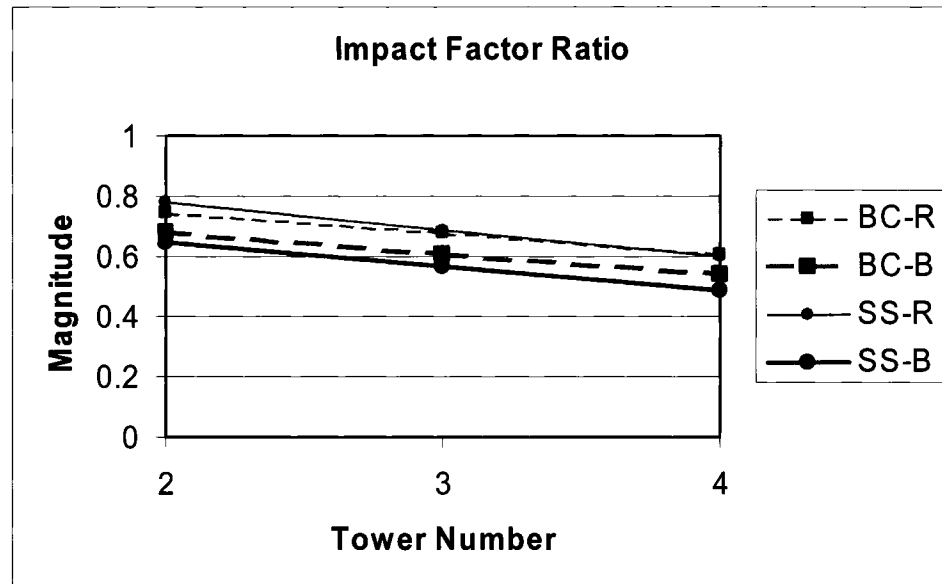


Figure 2.15 – Average Impact Factor Ratios – All Model Runs (modified from Kempner, 1997)

2.3 Analytical Studies

McClure and Tinawi, (1987) developed a numerical model in ADINA to replicate the small scale model test results due to broken conductor scenario studied by Mozer (1981). The study objective was to evaluate current design criteria used by the industry for exceptional longitudinal transient dynamic loads, and was limited only to analysis of the broken conductor scenario. This was also an attempt to verify that the ADINA software was able to accurately capture the scale model test results, as this was the first use of ADINA to predict dynamic loads due to broken conductor on transmission lines.

Four models were selected to be part of McClure and Tinawi's report. Each model progressed from the very simple model, using broad assumptions, to the more accurate model, taking into account the structural flexibility and the torsional rigidity, using one conductor and one overhead ground wire. The four different numerical models are presented in Table 2.4, and are shown in Figures 2.16 to 2.18.

Table 2.4 – Summary of Numerical Models Reported by McClure and Tinawi (1987)

<i>Model Number</i>	<i>Support type</i>	<i>Cable Elements</i>	<i>Insulator Elements</i>	<i>Structure Elements</i>
R-63	Fixed	10 – 3 node cable elements all spans	2 node truss element	None
R-83	Fixed	Same as R-63 except 20 – 3 node cable elements in Span 2	2 node truss element	None
F-85	Flexible	10 – 3 node cable elements	2 node truss element	None
F-104	Flexible	10 – 3 node cable elements	2 node truss element	6 space frame elements

Numerical model R-63 (Figure 2.16) is a very basic model using three conductor spans, and fixed supports. With this model, response of the conductor due to breakage in Span 1 can be calculated; however, the influence of structure stiffness is not taken into account due to pinned connection at the support. Model R-83 is basically the same except that Span #2 has twice the number of nodes as Model R63.

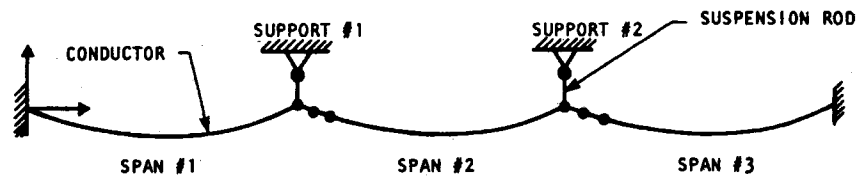


Figure 2.16 – Numerical Models R-63 and R-83 (McClure and Tinawi, 1987)

Numerical model F-85 (Figure 2.17), has the added feature of having flexible supports, simulated by springs. This model, in a simplistic way, now measures the influence caused by the tower stiffness, but still is based on the assumption that the tower can be modeled simply using a translational spring representing the lateral stiffness.



Figure 2.17 – Numerical Model F-85 (McClure and Tinawi, 1987)

Model F-104 (Figure 2.18) presents the line with self supported structures, and both conductor and overhead ground wire. Support structures are modeled using frame members. This numerical model was created to more accurately represent the scale model tests, and was used to capture Mozer's results.

For the two rigid support models, (R-65 and R-83), the peak transient dynamic forces on the support due to conductor breakage were in the order of 50% higher than that reported

by Mozer. This shows that even with a simple model, and ignoring the effects of structure flexibility, the results can be captured; however, more accurate results would be required for analysis. Results from the models F85 and F104 show significant improvement and the forces computed were within 20% when compared to the scale model results. This is due to the fact that the numerical model represented the scale model in a realistic manner by including the structure stiffness and, in the case of F104, the overhead ground wire. For all models, it was reported that aerodynamic damping on tensioned cables in still air is insignificant, and therefore it was neglected.

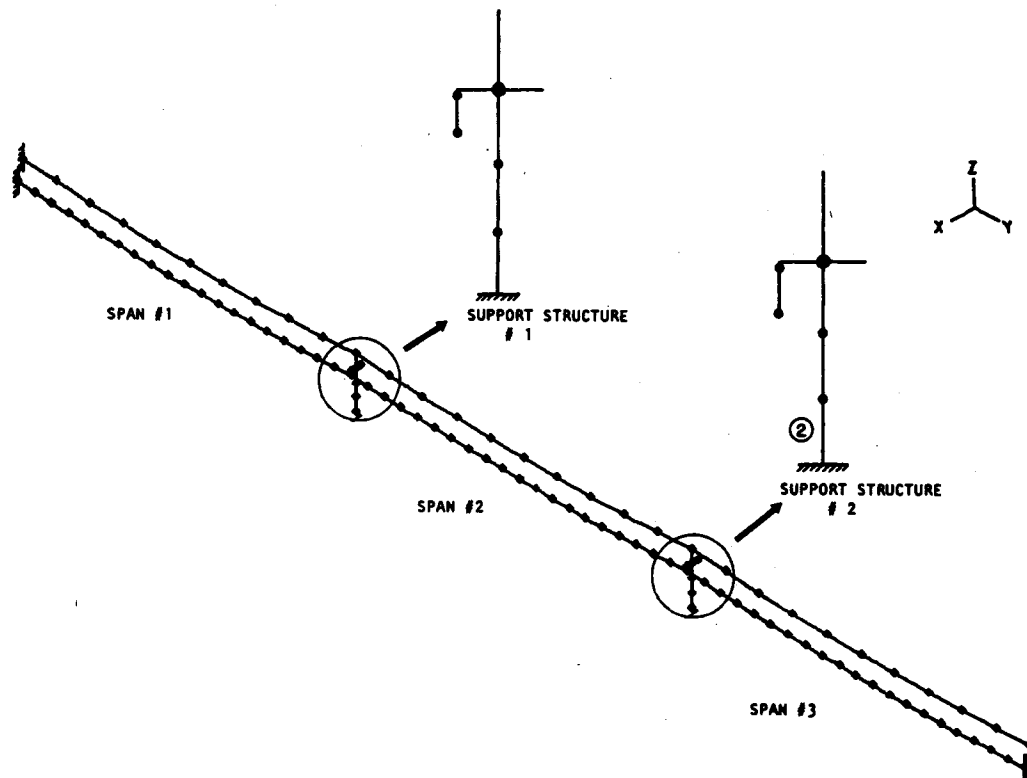


Figure 2.18 – Numerical Model F-104 (McClure and Tinawi, 1987)

From this study, it was verified that the numerical model was able to capture the results of scale model tests performed by Mozer. Dynamic response for simple models with no structure response factored in was significantly higher than the actual model results; however, more realistic models were quite accurate. Through this analysis, the feasibility of performing numerical transient dynamic modeling was proven possible and accurate, using commercially available software.

LaPointe (2003) performed dynamic non-linear analysis to further study and to determine the response of a transmission system due to broken insulators and broken conductors. The primary goal was to predict dynamic behaviour of a line section using simplified models in ADINA.

Two general models were created. A two-dimensional model was used to study the dynamic response due to: (1) conductor rupture, both with and without structure failure; (2) insulator string failure, and; (3) the effect of the number of spans. In this model (Figure 2.19), it was assumed that insulator strings and conductor deadends were fixed to rigid supports, thereby neglecting the effect structure flexibility has on the given failure modes studied. For the three-dimensional model, all six conductor phases, plus an additional shield wire on the top of the structure, were modeled. A simplified schematic of the 3D model line is shown in Figure 2.20 with details of the structure shown in the inset of the same figure. This model was used to study the effects of a two phase failure (C3 & C5 – Figure 2.20 Inset), taking into account the structural flexibility. Conductor

loadings varied from 0 mm, 20 mm and 25 mm radial glaze ice (simplified as *ice*), depending on the model run. In all cases, conductors were modeled using truss elements carrying an initial prestress force to account for the initial tension of the cable.

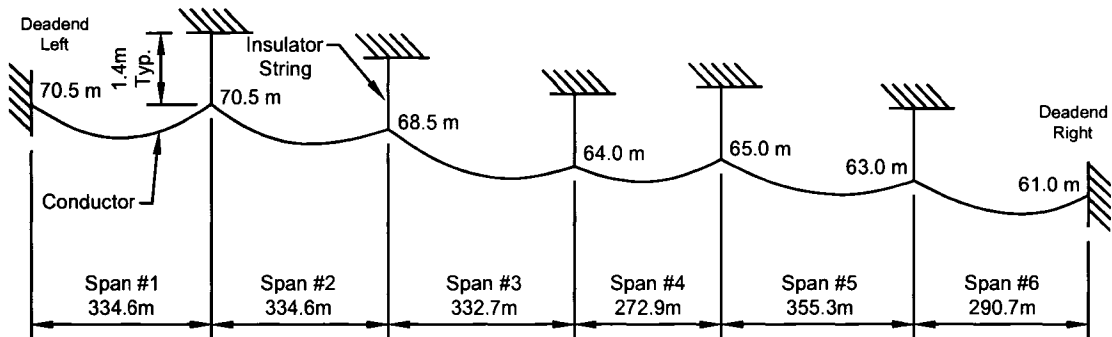


Figure 2.19 – Simple 2D Model (modified from LaPointe, 2003)

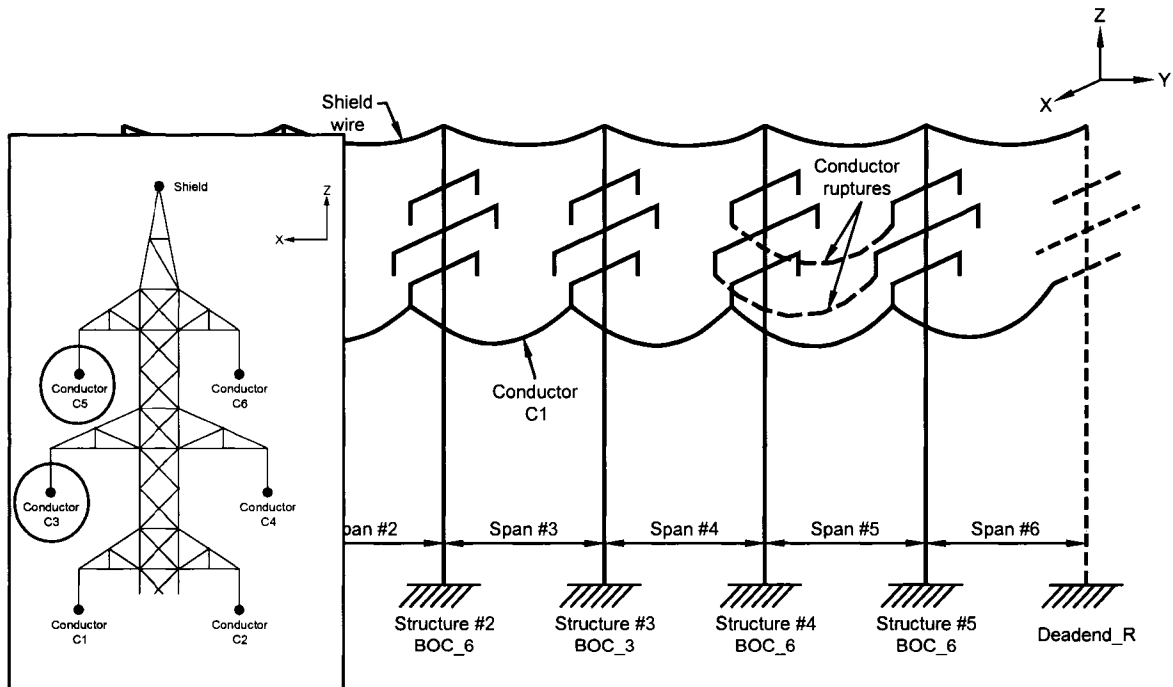


Figure 2.20 – 3D Model – Schematic and Structure Detail (Inset) (modified from LaPointe, 2003)

Four versions of the 2D models were created. The first (2D_CF) studied the effects of a single phase conductor failure in span 5 (Figure 2.19). Non-linear dynamic analysis was performed for this scenario for seven seconds in order to determine the axial forces in the conductor and insulator strings. Also, longitudinal reactions at suspension and deadend structures were recorded and analyzed. As detailed previously, structures were not included in these model runs. Three load cases were considered; bare (no ice), 20 mm ice and 25 mm ice. The second model (2D_SF) studied structure failure after conductor rupture, and the effect on the subsequent structures. Again a single conductor phase was used; however, a simplified typical transmission line structure was simulated with a single beam measuring 0.6 m x 0.1 m x 0.2 m (Figure 2.21). Using an ice load of 25 mm, and an assumed strength for the simplified structure, a plastic hinge at the support of the arm in the ADINA model simulated structure failure. Longitudinal reactions at the deadends and at the unfailed suspension structures were recorded for 3 seconds. The third model (2D_NS) examined the effect of the number of spans on the peak forces on the structure. Using a modified version of the 2D_CF model, 2, 4 and 6 additional spans using the same length as span 1 (Figure 2.19) were added, moving the left deadend farther from the disturbance. This provided the data for the original 4 span model, plus the data for a 6, 8 and 10 span model. For these tests, the load for a 25 mm radial ice thickness was assumed, and maximum longitudinal reactions recorded. The fourth model (2D_ISF) simulated the effect of a suspension insulator string failure. Using a bare conductor load, and a 7 second analysis time, insulator string 5 was removed from the model, creating a new single “superspan” from the original two spans (span 5 and span

6). To measure the result of the disturbance on the system due to the fall of this new single span, insulator string tensions, longitudinal reactions at suspension and deadend structures, and vertical displacements of conductor were estimated.

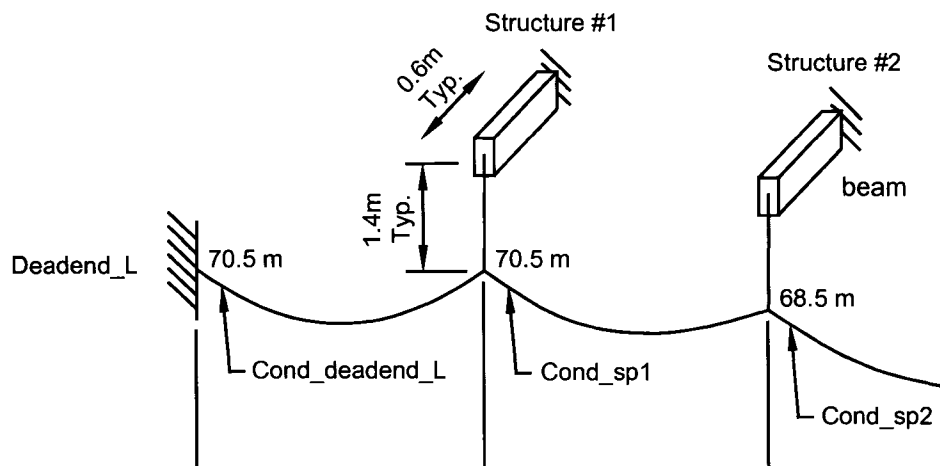


Figure 2.21 – Structure Model Used in Structure Failure Tests (modified from LaPointe, 2003)

Only one three-dimensional model was created. This simplified version of a 120 kV double circuit tower was modeled using beam and truss elements to study the effect of multiple conductor failures. Six conductor phases and a single shield wire were connected in this six span model, with the simultaneous failure of two phases (mid level and top level) on one side of the structure (Figure 2.20 inset). Unlike the 2D models, this model takes into account the effect of structure flexibility on the measured forces. 25 mm ice loads were used for the model run; however, structure failure was not considered. Similar data to the 2D_CF test was recorded for the analysis.

Prior to model analysis, a study on two modeling parameters was performed to determine their respective effects on the results. The first was the effect of the number of elements used to model the conductor. Model analysis using both 30 and 80 elements per span demonstrated that 30 elements were adequate to capture the results. The second parameter was the time increment used for the dynamic analysis. An increment of 0.0015 seconds proved to be adequate based on the analysis.

A time history for the conductor tension due to a failed conductor (2D_CF) is provided in Figure 2.22 for the bare, 20 mm and 25 mm ice loads. This type of result is typical of the results of many of the models. It was noted that two peaks are commonly recorded; however, no explanation as to what caused this response was provided.

For the first of the four 2D models (2D_CF), conductor failure generated forces that can be represented by impact factors, defined as the ratio of the maximum peak conductor tension to the initial conductor tension. These forces act in the longitudinal direction of the line, and transverse force are negligible. The results were compared to previous work performed by Govers (1970), and Kempner (1997), and were shown to be quite similar, but generally higher by up to 68% in some cases. This may be attributed to McClure and Tinawi's findings that neglecting structural flexibility accounted for an over estimation of the forces.

The second of the four 2D models (2D_SF) studied suspension structure failure (longitudinal cascade) under a 25 mm ice load. The study showed that containment of the cascade failure would occur at structure 3. No comparison to actual data was performed; however, it was noted that designing for an acceptable number of failed towers was a valid approach.

The third of the four 2D models (2D_NS) studied the effect of the number of spans adjacent to the broken span, again using the 25 mm ice load. In general, the results showed that the effect of the number of spans is small, except for the influence caused by the return of the stress wave caused by the broken conductor as it reflects from the deadend structure. This stress wave rebound had a different effect depending on the number of spans, and was greatest for the six span model. In general, though, the effect on the towers adjacent to the conductor failure decreases with an increase in the number of spans to the nearest deadend.

The final 2D model (2D_ISF) studied the failure of a suspension insulator string. Since only a general understanding of the rupture phenomenon was pursued, no significant conclusions were drawn; however, it was noted that the variation in conductor tension was gradual, and did not show the dynamic variation as recorded in the broken conductor case.

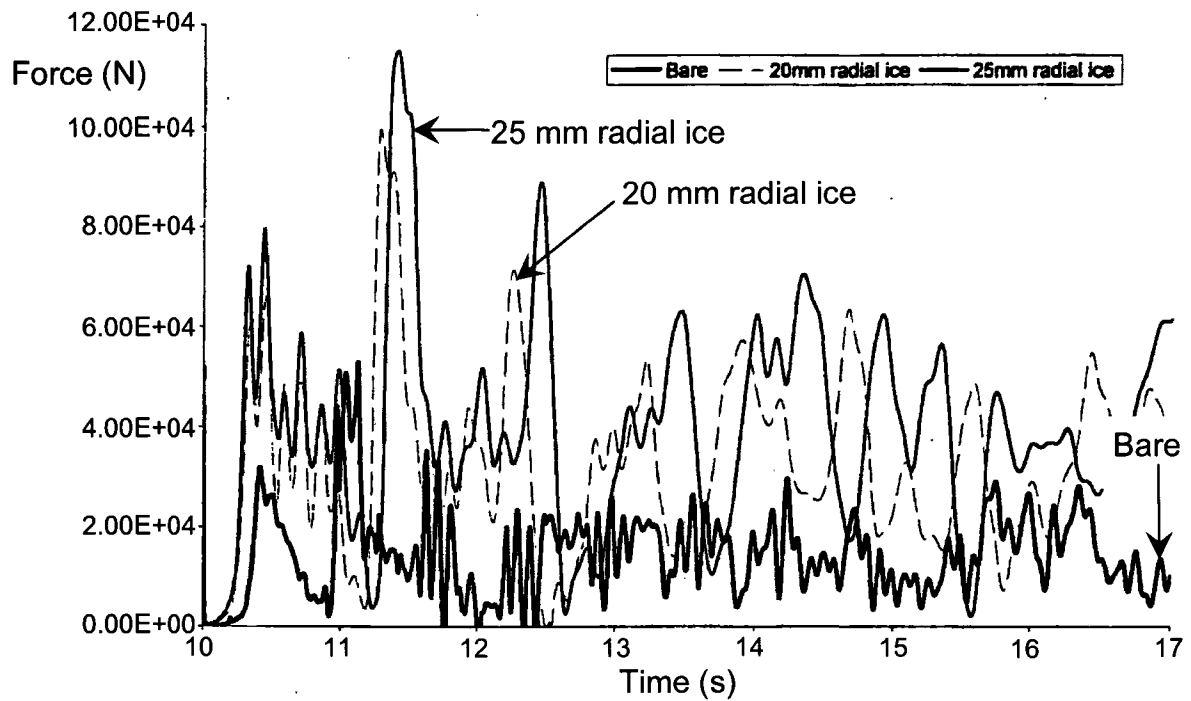


Figure 2.22 – Time History – Conductor Tension due to Failed Conductor (modified from LaPointe, 2003)

The 3D model studied conductor failure on actual structures, taking into account the structural flexibility. Including the flexibility of the structure reduced the peak transient forces exerted on each structure, similar to the results presented by McClure and Tinawi (1987). LaPointe considered this reduction to be an overestimation of the peak forces in the 2D models. This model was considered to be a better representation of the actual response of the system due to a broken conductor; however, the simple 2D models are also useful for providing an initial estimate (upper bound) to the longitudinal loads.

Ostendorp (1997) used previous analytical and experimental results to develop the CASE method. The CASE method estimates the magnitude of longitudinal loads using data for

the energy dissipating characteristics of the line, the load case (maximum ice, cold temperature, etc.), the failure mode (broken conductor, broken insulator, etc.), and the maximum number of structures permitted to fail prior to cascade containment. Peak unbalanced longitudinal loads are calculated for each structure away from the failure event. To evaluate cascade failure potential, the method is initially performed for the first structure. If the first structure does not fail, cascade failure is unlikely. If the first structure does fail, the evaluation is continued for each subsequent structure until no further failure occurs. Using this method for new construction, and an appropriate acceptable structure failure limit, the maximum peak load on the structure that contains the cascade can be estimated, and the structure designed appropriately.

2.4 Summary of Previous Work

Many researchers have investigated the dynamics of component failure and its effect on transmission line systems. Through full scale tests, small scale tests and analytical studies, a significant amount of knowledge has been gained considering the dynamic forces imposed on structures due to failed components. Analytical methods are becoming useful tools in studying the dynamic loads on towers; however, they have not yet been fully explored to study various types of line failure problems under dynamic conditions.

Chapter 3

Finite Element Modeling Using ADINA

Understanding of dynamic forces induced in transmission structures due to failed components can be accomplished in three ways: (1) full-scale experimental testing, (2) small-scale experimental testing, and (3) numerical modeling. Full-scale experimental testing is expensive and can only be economically performed when an opportunity to experiment on an abandoned line is obtained. Small-scale testing is not as costly; however, it is time consuming and limited in study scope. Numerical modeling offers the advantage of cost effective study of dynamic forces using any combination of parameters, such as modification of conductor tension, structural rigidity, terrain effects, etc. One software package that has been used for successful numerical modeling of transmission line dynamic forces is ADINA (McClure, 1987, LaPointe, 2003).

Study of transmission systems means an understanding of cable type problems. Cable problems are not easily solved manually as they are highly non-linear, both in geometry and in material properties. In response to load changes, large geometrical changes occur; however, they are not necessarily accompanied by large stress variation. Geometrical changes are also non-linear, regardless of the linearity of load application or material.

ADINA is a general purpose finite element analysis program, developed with a goal to analyze many different types of boundary value problems under one software package.

This flexibility has its advantages for groups wanting to use it for design; however, this general nature also makes the software difficult to master. The steep learning curve means that new users will have difficulty acquiring enough knowledge of the program to easily and accurately analyze cable type problems. The advantage is that once the program is understood, it can be used in a multitude of ways to solve more complex problems.

For successful model generation, many steps must be taken to include details of all required data. Consistent units must be used; otherwise results will be in error. Using SI units as an example, lengths are in metres, forces are in Newtons, masses are in kilograms, and times are in seconds (ADINA, 2003). In general, the model generation process can be summarized as follows:

- Nodal coordinate generation
- Model element definition
- Material property definition
- Loading and boundary conditions
- Control parameters

The 900 node version of ADINA was used due to cost constraint. It was envisaged that a simple model should be tried first for validation before a more detailed three-dimensional modeling of the full test line is done. For the model generated in this chapter, and further detailed in Appendix 1, structures are modeled using beam elements, and insulators are modeled using truss elements. The conductor is modeled with truss elements carrying an initial strain due to initial cable tension. The location of the suspended cable (individual truss element nodes) can be calculated based on a simple parabolic equation. In cable

problems such as suspended conductors, small strain changes cause large displacements. Therefore, the strain, as calculated in section 3.2 to provide for the initial conductor tension, must be accurate.

Finer details on the step-by-step generation of a simple level span model and analysis for conductor/structure interaction are included in Appendix 1, and should be referred to prior to attempting model generation. This section will provide general background information required to generate the model, without providing in depth functionality of the ADINA software. For further reference, an ADINA modeling guide is scheduled for publication by CEA Technologies (McClure, 2007).

3.1 Nodal Coordinate Generation

ADINA has the capability of importing nodal coordinates from ASCII text files for all model elements. Using this capability, nodal coordinates can be calculated and formatted in a spreadsheet, and can be exported as a text file to ADINA. Locations of key nodes must be determined first and are displayed in Figure 3.1. The first and last nodes for a conductor are defined based on the span length, and the elevation difference between the two structure attachment points within the span. The coordinates for the insulator string are: (1) the lower insulator node coordinate is at the span endpoint, and (2) the top insulator node coordinate is defined by the length of the insulator string. These two nodes are later connected to represent the insulator string. Attachment of the insulator to

the tower is defined with the same top node of the insulator, and the lower node of the tower is at ground line level, a distance equivalent to the tower height.

For a more complex model, as is detailed in Appendix 1, the coordinates are located in three-dimensional space and are plotted (X, Y and Z) in the nodal coordinate spreadsheet, with the Z coordinate oriented vertically. This provides the proper orientation should contact surface generation be required. Contact surfaces would be used if ground contact were to be studied, thereby limiting conductor motion beyond a defined ground level.

Locations of nodes along the conductor profile (Figure 3.1) are calculated using the parabolic sag relationship given in Equation 3.1. Coordinates can be calculated for both level and non-level spans.

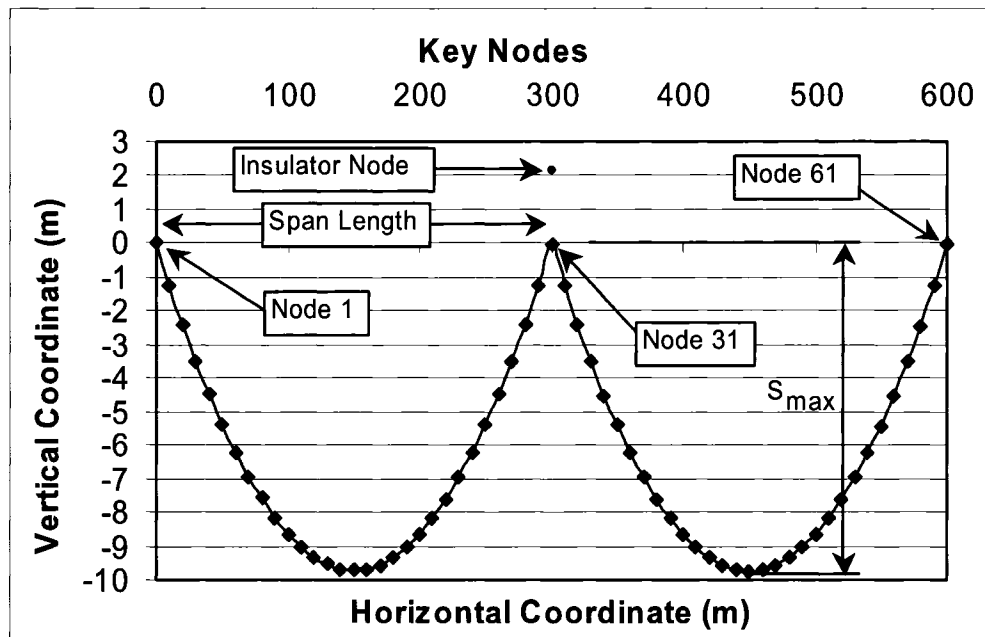


Figure 3.1 – Key Model Nodes

$$S_{MAX} = \frac{WL^2}{8T} \quad (3.1)$$

where:

S_{MAX} = Maximum conductor sag (m)
 W = Unit weight of conductor (N/m)
 L = Overall length of the span (m)
 T = Conductor Tension (N)

3.1.1 Nodal Coordinate Generation For Level Spans

Due to symmetry, generation of nodal coordinates for level spans (ie. the conductor attachment on adjacent structures is at the same elevation) is easier than non-level spans. For level spans, the maximum sag point is located at the mid-point of the span length. Horizontal coordinates of the span are calculated by dividing the horizontal length into 30 equal elements, which are normally sufficient to model the broken conductor case (LaPointe, 2003). Each horizontal coordinate has a corresponding sag coordinate value calculated as follows.

$$S_C = (S_{MAX}) - \left\{ \frac{W(L - (2 \cdot H_C))^2}{8 \cdot T} \right\} \quad (3.2)$$

where:

S_C = Sag node coordinate (y axis)
 H_C = Horizontal coordinate (x-axis)

The term “ $L - (2 \cdot H_C)$ ” in Equation 3.2 provides for a new conductor span reduced by the horizontal distance from the first end node. For a level, 300 m sample span, the new span

for the 50 m and 250 m nodes would be $[300 - 2 \cdot 50 = 200 \text{ m}]$. The second term in Equation 3.2 enclosed by the second bracket $\{ \}$ calculates the sag for this reduced span of the conductor. This value is subtracted from the maximum sag, which provides the projected vertical coordinate (Figure 3.2) of the conductor nodes at 50 m and 250 m. In a spreadsheet, the coordinates of the conductor sag can be easily calculated substituting each horizontal coordinate from the origin to span length into Equation 3.2.

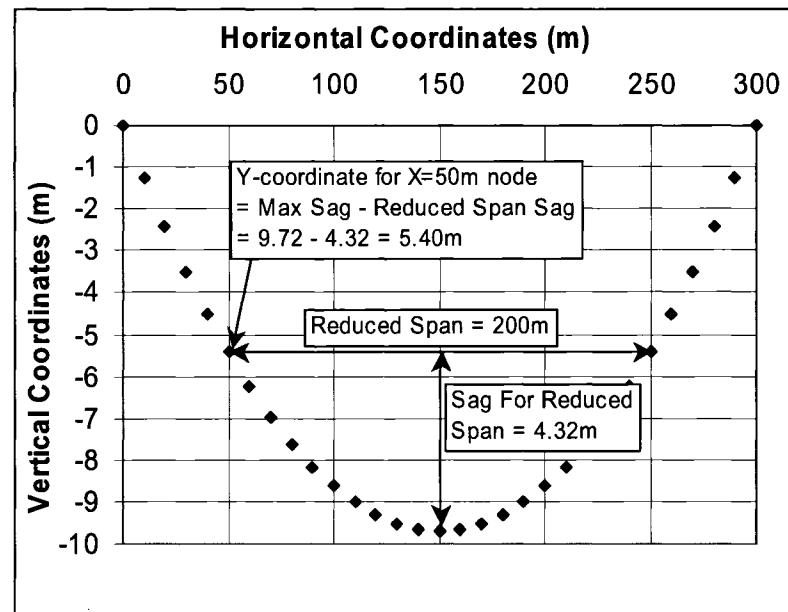


Figure 3.2 – Sag Node Coordinates for 50 m and 250 m – Level Span

3.1.2 Nodal Coordinate Generation For Non-Level Spans

For non-level spans, where the conductor attachment points are at different elevations, the maximum sag point is located to the left or right of the mid-span point, depending on the relative elevation difference (Figure 3.3). All parameters (W , L and T) are the same

as for the level span. It should be noted that to model a real line segment, one needs to consider the generation of nodal coordinates, not only for non-level spans, but also for spans of different lengths.

Equation 3.3 provides the horizontal coordinate of the maximum sag point. The L, T and W data are utilized, and the difference in elevation (V) is referenced here from the first node of the span to the last node of the span (Figure 3.3). Equation 3.4 provides the horizontal location of the maximum sag point for a 300 m non-level span where the structure at 300 m is, in this case, 3 m higher than the structure at 0 m. This causes the maximum sag node to be positioned approximately 11.5 m to the left of the mid span location (Figure 3.3).

$$H_{S-MAX} = \frac{L}{2} - \frac{\frac{V}{T}}{W \bullet L} \quad (3.3)$$

$$H_{S-MAX} = \frac{300m}{2} - \frac{\frac{3m}{18491N}}{15.9667 \frac{N}{m} \bullet 300m} = 138.419m \quad (3.4)$$

where:

V = vertical elevation difference between ends of conductor span

H_{S-MAX} = Horizontal coordinate of maximum sag point

With the maximum sag location determined, Equation 3.2 can be used for each side of the maximum sag point, where it is assumed that there are two level spans calculated as

follows: (1) the span length for the shorter side is, in this case, 276.8 m ($138.4 \text{ m} \times 2$), and; (2) the longer side is 323.2 m ($(300 \text{ m} - 138.4 \text{ m}) \times 2$). The horizontal coordinate for each section on both sides of the maximum sag node is calculated by dividing each section into 15 equal elements. Using Equation 3.2, the sag can be generated at each node point using the relevant half of the sag profile. Figure 3.3 was produced based on this calculation. If the elevation difference is significant, the shorter side can be broken into fewer elements, while more elements can be added to the longer section to give a better nodal distribution over the entire span. Splits such as 10:20 (elements to left of maximum sag point to elements to right of maximum sag point) can be used instead of a uniform distribution of 15:15, if necessary.

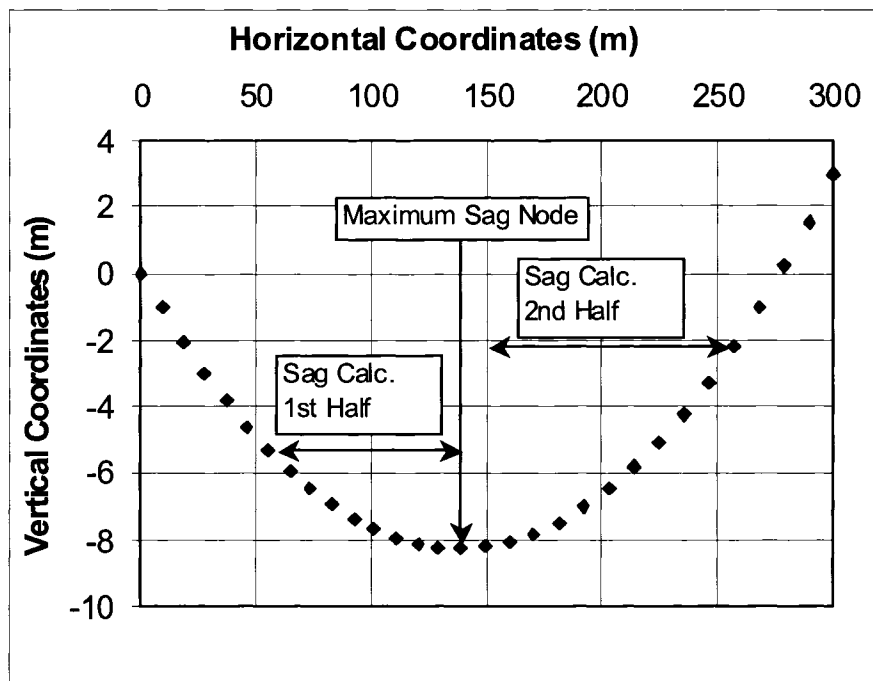


Figure 3.3 – Sag Node Coordinates – Unlevel Span

3.2 Model Element Definition

A line that connects two nodes defines each element in the model. Defining the connectivity of the individual nodes is required to model the elements. Conductor nodes are connected so that each element defined is attached to subsequent elements to form a continuous string. Insulator elements provide the connection of the conductor to the tower. Tower elements support the insulator string from the ground.

Conductor is modeled with truss elements carrying an initial strain due to initial cable tension. Strain is calculated using Equation 3.5. Insulators are also truss elements; however, no initial strain is required. Towers are modeled using beam elements. Contact surfaces are modeled using the geometric lines at the location of the contact plane.

$$Strain(\epsilon) = \frac{\sigma}{E} = \frac{\left(\frac{T}{A}\right)}{E} \quad (3.5)$$

Where:

T = Tension (N)
A = Area (m²)
E = Young's Modulus (Pa)

3.3 Material Property Definition

Model properties are reproduced based on the actual properties provided. Conductor element properties are defined based on the cross-sectional area, Young's Modulus, and

density. The unit weight of the cable is computed internally in the software using the cross-sectional area and the density.

Insulator properties are defined by the density and Young's Modulus for steel, and using a cross-sectional area one can find the weight. Tower flexibility is represented by the calculated cross-section of the cantilever beam.

3.3.1 Material and Geometrical Non-linearity

As conductor is a tension only element, this material should be defined as non-linear elastic in order to correctly represent the stress-strain curve in ADINA. The stress-strain curve is modeled using three values (Figure 3.4), where stress is defined as zero for all strain less than zero (compression), and the stress/strain slope is equivalent to Young's Modulus for all strain greater than zero. For this model definition, it is assumed that the conductor is only at the final stage and is modeled with "final" modulus (elastic).

Geometrical non-linearity in cable analysis allows for calculation of large displacements, although the small strain assumption is made in developing the model.

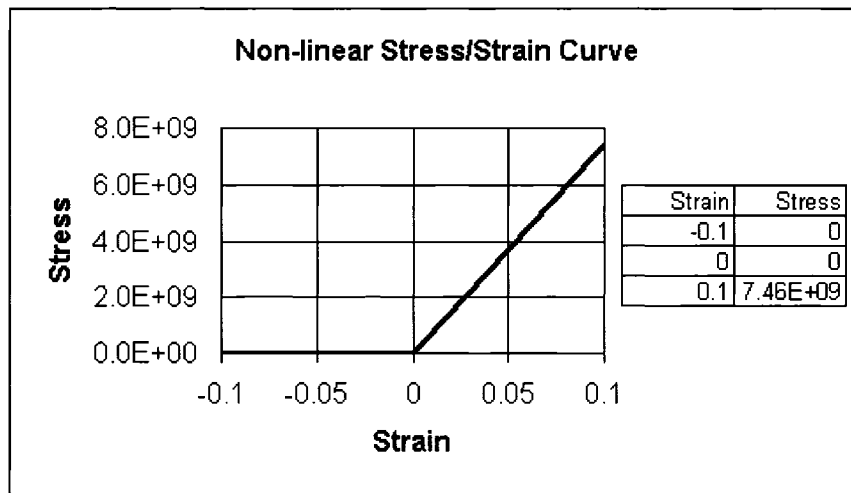


Figure 3.4 – Nonlinear Elastic Conductor Properties and Curve

3.4 Loading and Boundary Conditions

3.4.1 Mass Proportional Loads

Gravity forces for the models studied are all based on mass proportional loading. With this loading method, masses are calculated using the acceleration due to gravity (9.81 m/s^2) and the mass of the elements, calculated from the cross-sectional area per unit length and the density of the material (kg/m^3). This provides for loading in the vertical direction, as specified in the mass proportional definition. This loading method allows for easy modification of the equivalent density in the calculations for ice loading. Calculating the weight of the iced conductor, and using the same cross-sectional area per unit length, a new density can be derived. This new density simulates the weight of the ice-loaded conductor per unit length, regardless of the length of the elements. This is

important as not all elements in the span are of the same length due to the parabolic shape of the catenary curve, and the assumption of the horizontal dimension being divided into equal lengths.

3.4.2 Boundary Conditions

Boundary conditions provide model stability. For towers represented by cantilever beams, movement in all directions and rotations are restricted at the base. For towers simplified as pinned truss elements, movement in the X, Y and Z directions is restricted; however, rotations are allowed. For the towers simulated as truss elements, the structure has to be supported in some way, such as using guys, in order to be stable.

3.5 Control Parameters

3.5.1 Time Step Integration – Wilson Theta Method

For implicit integration, the stiffness matrix is calculated based on the static equilibrium position for the model at time “t”. Displacements are calculated assuming that displacements, velocities and accelerations are constant over time “t + Δt ”, where Δt is the incremental time step selected for the analysis. For the Wilson Theta method (Bathe, 1996), it is assumed that displacements, velocities and accelerations are constant over a time “t + $\theta\Delta t$ ”, where Theta (θ) is a factor which increases the range of coverage of the linearity of the three parameters (displacement, velocity and acceleration) in the dynamic

equation of motion. For unconditional stability, $\theta=1.37$ is required (Bathe, 1996). The default of $\theta=1.4$ in the ADINA software was not changed.

3.5.2 Lumped Mass Matrix

Lapointe (2003) reported that lumped mass matrix was found to be preferable compared to consistent mass matrix as the results obtained showed fewer spurious oscillations.

3.5.3 Death Element

To model the rupture problem for dynamic analysis in ADINA, the “death element” option can be used. If this option is used the corresponding element group automatically becomes nonlinear. The non-linearity condition is required in order to model the element properties such as stiffness matrix, mass matrix and load vector in an incremental form to ensure that the condition is updated at each time step. The death element option will allow the user not to add the associated element mass matrix, stiffness matrix and load vectors to the system matrices for all solution times greater than the time of the death element t_{death} . For example if the user wants to make the element inactive at and after time t_d , then $t_{death} = t_d - \varepsilon$ where $\varepsilon = \frac{\Delta t}{1000}$ and Δt is the time step between the previous solution time and t_d . For details refer to ADINA manual (ADINA, 2003, tmg-a_80.pdf, Section 10.4, pages 593-602).

Chapter 4

Analysis of Suspension Insulator Failure

This chapter will examine the suitability of using numerical modeling in predicting dynamic overloading due to broken insulator failure at the suspension point. The model results will be validated through comparison with the published full-scale test data (Peyrot et al, 1978).

The objectives in the original EPRI tests (Peyrot et al, 1978) were to:

- Collect data on peak dynamic and residual static loads on full-scale transmission towers subjected to sudden loss of line components.
- Determine tower response and its dynamic amplification factor
- Verify and complement analytical and model studies previously performed

A variety of instruments were used to capture the transient dynamic response of the line under broken suspension insulator and broken conductor conditions. From the study, a formula based on energy balance principles was developed to predict impact load factors. The accuracy of the equations, when compared to the tests, was demonstrated to be within $\pm 20\%$; the result was considered to be very good, considering the complexity of the problem. For the broken insulator tests, it was stated that “loads due to dropped insulator support are far less critical than those of a broken conductor” (Peyrot, 1980). Therefore, no significant analysis was performed on the broken insulator tests. Although this quote may be true for every day conditions, it is believed that loss of an insulator

string at a suspension location under ice load can also be critical and can cause a vertical and/or longitudinal cascade failure unless the adjacent towers next to the failure zone are designed to withstand the overload. This will be discussed later.

The dynamic load due to broken insulator in a suspension string is widely regarded to be insignificant, under every day conditions. The broken insulator scenario is conceptualized in Figure 4.1. After the insulator string is removed from the centre structure during a failure, the conductor falls beyond the final conductor location shown, and rebounds up to a point above the final conductor location due to the elastic nature of the wire. This oscillation will continue until damped out by internal friction in a short while. A validation of this failure mode, along with sensitivity of varying parameters, such as addition of ice, has yet to be performed. Lapointe (2003) performed one numerical model run using a 25 mm ice load, and showed that the addition of ice significantly increased the dynamic load; however, this result was not compared to actual test data.

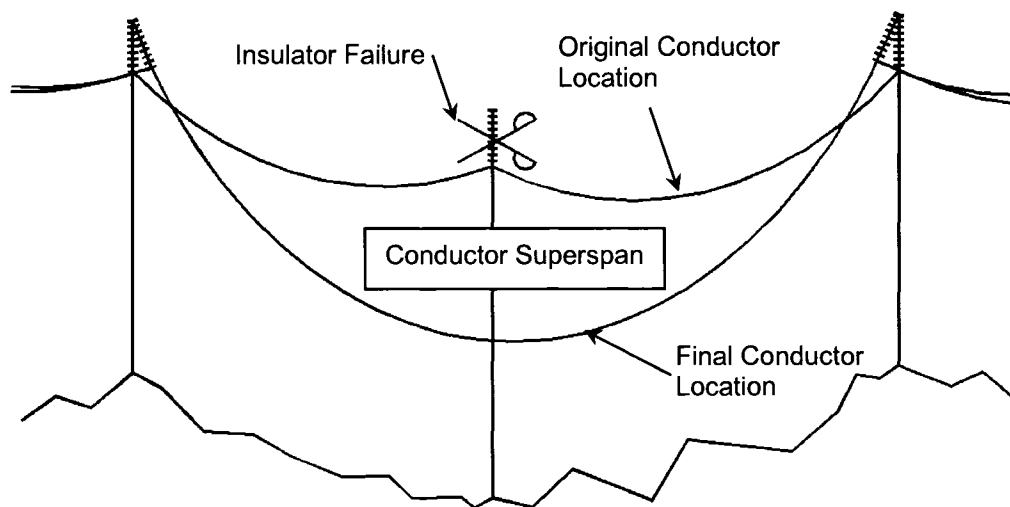


Figure 4.1 – Broken Suspension Insulator Induced Dynamic Loads

4.1 Scope of the Broken Insulator Model

The validation of the numerical model in ADINA will be demonstrated by comparing the measured peak force data obtained from the full-scale broken suspension insulator test with that obtained from the numerical model. A conductor “superspan” (Figure 4.1) is developed after suspension insulator failure, and is defined here as the combined two spans between structure T4-T5 (span 4) and T5-T6 (span 5) as one span (T4-T6) after the failure of the insulator at structure T5. Figure 4.2 presents the specific spans and the location of the “drop insulator” on tower T5. During this freefall, it is assumed that damping due to internal friction will have little effect on the impact loads.

Upon validation of the numerical model, a sensitivity study is carried out to determine the effects of various parameters on the dynamic impact loads. These parameters are: (1) insulator length, (2) initial tension, and (3) ice thickness. Finally, an example is provided to coordinate the strength of two components such as conductor and insulator using the predicted dynamic loads and their respective strength values.

4.2 Background

In 1978, The University of Wisconsin and the Electric Power Research Institute (EPRI) carried out a series of full-scale broken conductor and broken insulator tests. These tests were performed to advance the state of the art at the time, to verify the containment load prediction techniques in line design, and to validate customized in-house numerical models as alternatives to laboratory scale model or full-scale testing. A very comprehensive set of test data and results complete with all necessary information required for numerical modeling and subsequent analysis was provided (Peyrot et al, 1978).

A numerical model of a broken suspension insulator based on the EPRI tests was attempted (Li and Bhuyan, 2003); however, to the best of the author's knowledge, no attempt has been made to compare and validate the full EPRI test results of suspension insulator failure with particular reference to dynamic vertical impact loads considering the sensitivity of various parameters such as insulator length, initial tension, and ice

thickness. Consequently, an understanding of the magnitude of dynamic loads on towers due to broken suspension insulator failure is, at present, limited.

The line profile shown in Figure 4.2 consists of 6 complete spans of varying tower elevations and span lengths. The line is composed of double circuit towers as shown in Figure 4.3. For the broken insulator tests, the six suspension insulator strings on tower 5 (T5) were broken. The right side of the tower carried three phases of 471A Anaconda Copper Bronze conductor, and the left side carried three phases of 397 kcmil ACSR. As well as studying these two different conductors, two different lengths of insulator strings and various initial tensions were investigated. Insulator forces for the broken insulator tests were only measured on tower 4 (T4*). A summary of the conductor properties and test results is provided in Table 4.1 and 4.2 respectively. All six tests performed were numerically modeled and used in the validation process.

Table 4.1 – Conductor Properties (Peyrot et al, 1978)

	<i>397 kcmil ACSR</i>	<i>471A Anaconda Copper/Bronze</i>
<i>Unit Weight (N/m)</i>	7.98	12.71
<i>Modulus of Elasticity (N/mm²)</i>	69627	102970
<i>Rated Strength (N)</i>	72500	68548
<i>Section Area (mm²)</i>	234	193

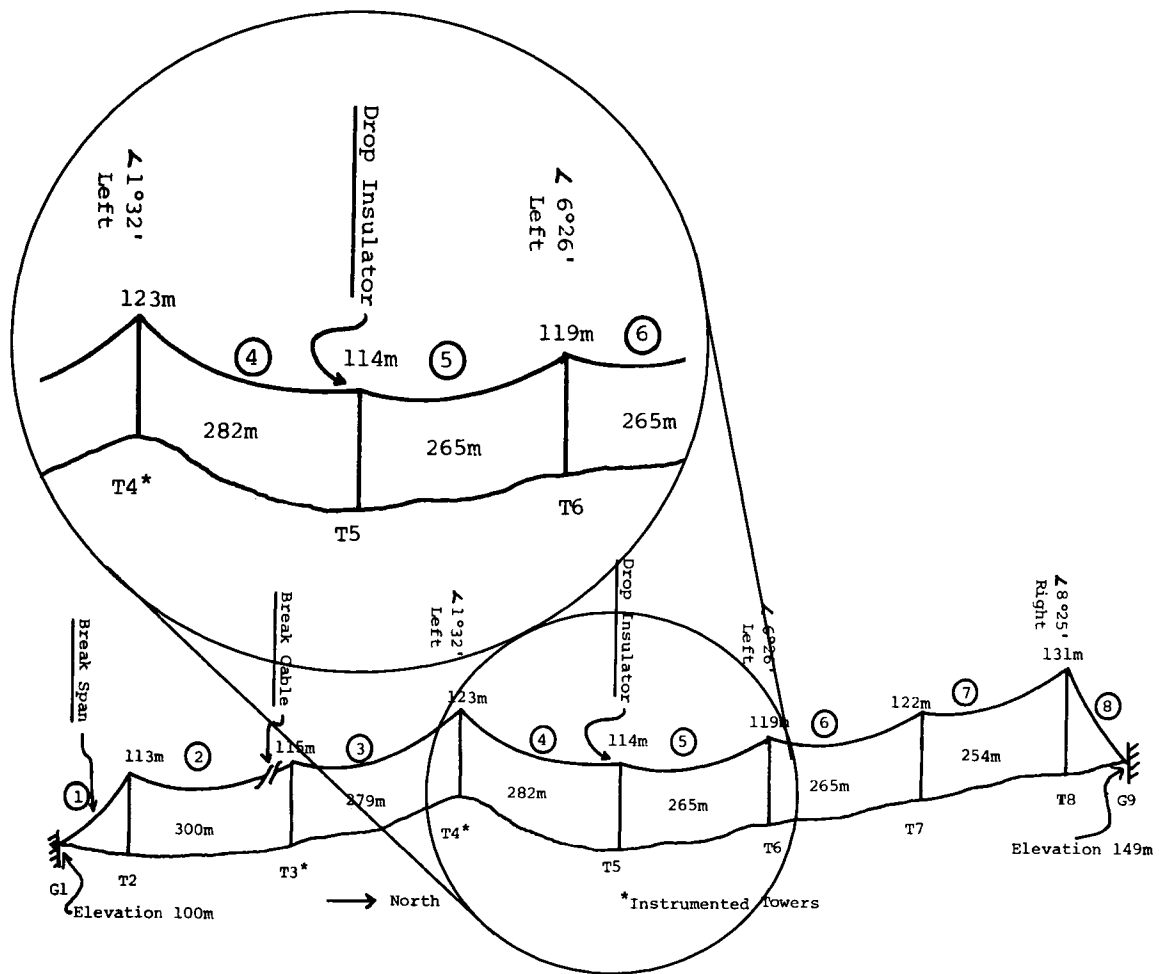


Figure 4.2 – Test Line Profile Prior to Testing (Peyrot et al, 1978)

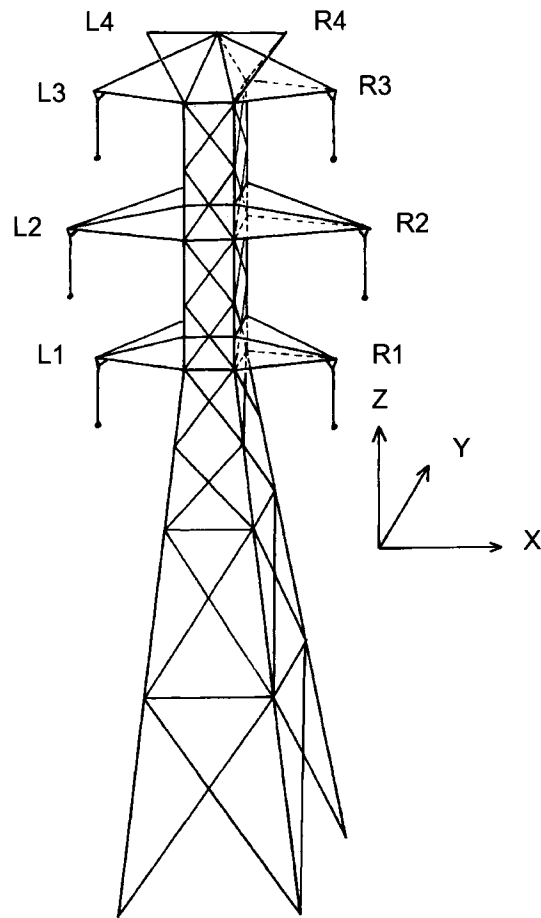


Figure 4.3 – Typical Suspension Tower (modified from Peyrot et al, 1978)

Table 4.2 – Broken Insulator Test Summary – EPRI Full-Scale Tests (Peyrot et al, 1978)

<i>Test #</i>	<i>Insulator Length (m)</i>	<i>Initial Conductor Tension (N)</i>	<i>Initial Insulator Force, (N)*</i>	<i>Peak Insulator Force, (N)*</i>	<i>Final Insulator Force, (N)*</i>
IIR2	2.2	19103	4874	8698	6208
IIL1	2.2	12435	3069	6011	4531
IIL2	2.2	17770	3069	4825	3952
IVR1	4.3	15995	4874	8983	6345
IVL1	4.3	14220	3069	4825	3648
IVL2	4.3	16524	3069	4825	3952

*Recorded at Tower T4

4.3 Finite Element Model

The transmission line was modeled using the ADINA software. The three major components such as conductor, tower and the insulator string assembly were considered in the structural modeling. The conductor was modeled using a three-dimensional truss element with initial prestress which includes the initial tension of the conductor. The insulator string assembly was also modeled as a truss element without any initial prestress. The structures were modeled using beam elements with equivalent areas and stiffness properties obtained from the force deformation data at appropriate locations presented in the test report. The ratio of the tower stiffness to arm stiffness was similar to that of the test data through the sizing of the tower and arm members. For simplicity, it was assumed that the moment of inertia of the structure was constant over its length.

A total number of 180 3-D truss elements were used to model one conductor phase for six spans (30 elements per span) while one truss element was used to model each insulator string assembly. Towers were modeled with one beam element for the cross arm, and a second beam element for each tower body (Figure 4.4). Material nonlinearity of the cable was represented using the appropriate stress-strain curve of the conductor. Geometric nonlinearity was considered by invoking the option in ADINA to use large displacement and small strain analysis. The time step integration was carried out using the Wilson-Theta method (ADINA, 2003) with $\theta=1.4$. The mass proportional loading was used to model the self-weight of the conductor and a lumped mass matrix was used

in the dynamic analysis. All details required to create this model can be found in Appendix 2.

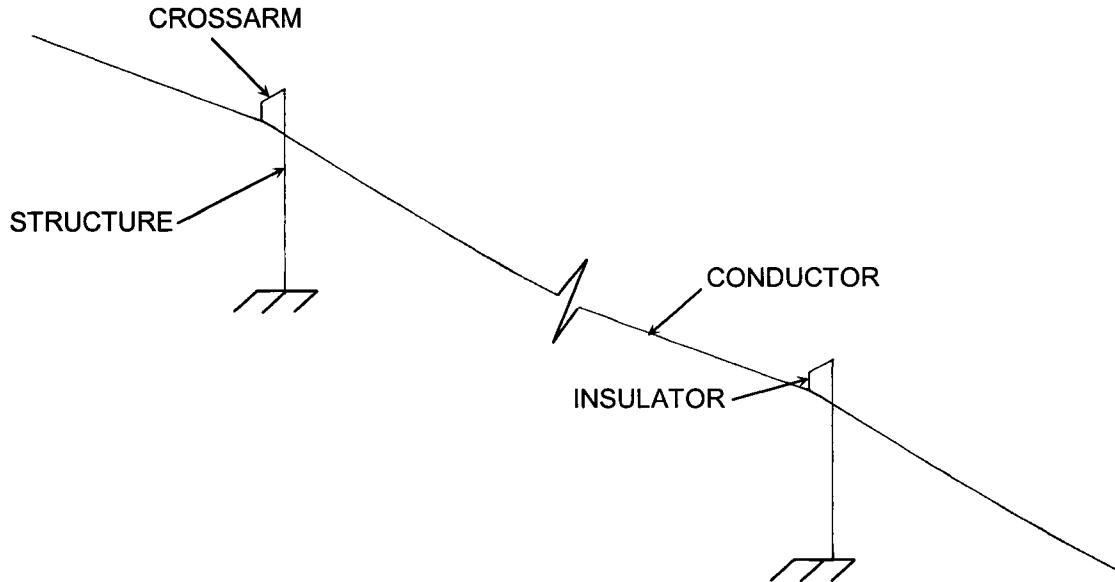


Figure 4.4 – One Span In the Six Span Numerical Model – 3D Isometric View

4.4 Methodology

Since the sag and tension relationship of a transmission cable is highly nonlinear, a number of steps need to be followed before a dynamic analysis can be carried out. These steps are:

1. Define the initial equilibrium position of the cable to determine the nodal coordinates, element connectivity, etc. To do this, the initial sag profile is modeled using a parabolic approximation, which uses initial tension, span and weight. A span in the final model was shown previously in Figure 4.4;

2. A static analysis is first carried out with bare weight to capture the initial equilibrium position of the cable system (six span profile), which in return provides the tension as well as the weight at each suspension insulator point. This information is verified with the actual profile shown in Figure 4.2 and conductor weight and tension as in Table 4.2, and;
3. Once the equilibrium position is determined, a “death element” is introduced to initiate the trigger mechanism (failure of the suspension string assembly) and the dynamic analysis is performed for four seconds. Initially, large time durations were used to estimate the dynamic response; however, after studying various responses, it was found that a duration of four seconds will adequately cover the area of interest in all cases.

After the analysis is completed, the output files are created containing various information on time histories such as nodal translational and rotational displacements, element forces, etc.

4.5 Analysis of Numerical Model Results

4.5.1 Verification of Time Increment

Prior to conducting the model runs, a verification of the time increment selected was performed based on the work performed by LaPointe (2003). To satisfy convergence criteria of an implicit integration, small time increments are required to ensure that numerical stability is guaranteed. A sensitivity analysis of varying time increment from 0.001 to 0.004 seconds was performed to ensure that the results do not vary significantly given the time step chosen. Figure 4.5 presents the analysis results with the maximum peak transient forces shown to be within 1% of each other for the different time step

increments. Smaller increments showed the same results, as shown in a later test of a different model in Figure 5.4. Given the similarity of the time increment sensitivity study results to the full scale test results as detailed later, it is assumed that the tower forces have converged to the correct numerical values.

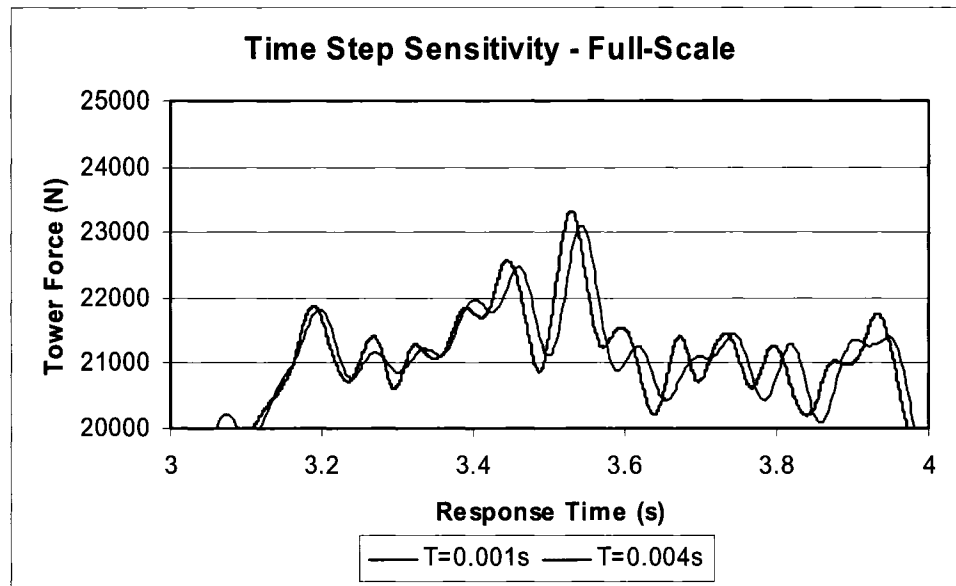


Figure 4.5 – Time Step Sensitivity

4.5.2 Broken Insulator Results

Initial conductor tensions were provided in the test report and were used to develop each of the six numerical models prior to the initiation of the insulator string failure at tower 5. Table 4.3 provides: (1) the initial conductor weight based on manual calculation of two of the tests; (2) the static portion of the numerical model runs, and; (3) the corresponding results from the full-scale tests for IIL1 and IIL2 respectively. The difference between

the manual calculation and the predicted value from the numerical model can be attributed to the fact that the manual calculation did not consider the weight of the insulator rod, which was considered in the numerical model. As in the EPRI tests, this rod was a replacement of the standard insulator string for test purposes and had minimal weight.

Table 4.3 – Static Model Analysis And Full-Scale Results (IIL1 and IIL2)

<i>Condition</i>	<i>Manual Calculations</i>	<i>ADINA Model</i>	<i>Full-Scale Test</i>
<i>IIL1</i>			
<i>Initial Conductor Tension (N)</i>	12435	12464 (0.2%)*	12435 (0%)*
<i>Initial Conductor Weight, T4 (N)</i>	2991	3050 (2.0%)*	3069 (2.6%)*
<i>IIL2</i>			
<i>Initial Conductor Tension (N)</i>	17770	17770 (0%)*	17770 (0%)*
<i>Initial Conductor Weight, T4 (N)</i>	3305	3373 (2.1%)*	3069 (-7.1%)*

* % error between computed and measured values

The discrepancy between the conductor weight from the numerical model run and the full-scale test data was considerable for IIL2 and could not be explained using the information reported by Peyrot et al (1978). Since the tension for IIL2 is considerably higher compared to IIL1, one would expect a larger conductor weight for the given geometry (Figure 4.2). Consequently, the full-scale test result value given for the initial conductor weight for IIL2 by the EPRI report (Peyrot et al, 1978) seems to be underestimated.

In view of this discrepancy, Mr. Robert Kluge of American Transmission Company (ATC), one of the researchers who performed the EPRI tests, was contacted. It was understood from this conversation that during testing, an initial conductor weight was calculated and later this value was used to “initialize” the load cells for other conductor weights, even though there was a change in tension levels (Kluge, 2004) and corresponding change in conductor weight. This was based on the assumption that the subsequent peak load measured by the strain gages was linearly proportional to the initialized load. Based on the discussion, the initial conductor weight values in the EPRI test report should have a “calibration correction” to adjust for this initial offset. The “calibration correction” is defined here as the difference between the actual conductor weights calculated by the ADINA model and the measured insulator force given in Table 4.2 (column 4). All EPRI test results recorded at tower T4 are modified with the “calibration correction” and using the initial insulator force as the base case. This calibration correction is presented in Table 4.4. The corrected EPRI test results are presented in Table 4.5 within brackets, with each result modified by the calibration correction factor shown in Table 4.4. The number not enclosed in brackets (Table 4.5) is the actual result of the ADINA numerical model runs. For example, for test IIL2, the peak insulator force as calculated in the numerical model is 6011 N. The unadjusted EPRI force, as per Table 4.2, is 4825 N. Using the calibration correction factor of +304 N from Table 4.4, the adjusted force is 5129 N. This adjusted force is recorded in brackets in Table 4.5. Numbers highlighted in bold (Table 4.5) are the test cases verified by hand calculations and shown in Table 4.3.

Table 4.4 – Calibration Correction

	<i>Initial Insulator Force</i>		<i>Calibration Correction Factor</i>
	<i>ADINA</i>	<i>EPRI</i>	
<i>IIR2</i>	4786	4874	-88
<i>IIL1</i>	3050	3069	-19
<i>IIL2</i>	3373	3069	+304
<i>IVR1</i>	4658	4874	-216
<i>IVL1</i>	3128	3069	-59
<i>IVL2</i>	3354	3069	+285

As can be seen in Table 4.5, discrepancies are still evident in the results. These errors may be attributed to the simplification of the structure from a lattice steel tower to a single cantilever beam (with constant moment of inertia) for each of the tower and cross arm. Also, natural variations and errors in original experiments may contribute to the differences, as the full-scale test were performed only once for each case.

Table 4.5 – Broken Insulator Model Runs - Comparison of Results Between ADINA and EPRI Tests (Adjusted EPRI Results in Brackets) at Tower T4

<i>Test #</i>	<i>Insulator Length (m)</i>	<i>Initial Conductor Tension (N)</i>	<i>Initial Insulator Force (N)*</i>	<i>Peak Insulator Force (N)*</i>	<i>Final Insulator Force (N)*</i>	<i>Insulator Swing Angle T4 (°)</i>
<i>IIR2</i>	2.2	19103	4786 (4786)	11160 (8610)	6276 (6119)	27 [27]
<i>IIL1</i>	2.2	12464	3050 (3050)	6757 (5992)	3981 (4511)	25 [25]
<i>IIL2</i>	2.2	17770	3373 (3373)	6011 (5129)	4119 (4256)	13 [16]
<i>IVR1</i>	4.3	16014	4658 (4658)	11052 (8767)	6168 (6129)	20 [14]
<i>IVL1</i>	4.3	14229	3128 (3128)	6345 (4884)	4050 (3727)	10 [11]
<i>IVL2</i>	4.3	16524	3354 (3354)	6149 (5109)	4119 (4236)	8 [8]

* Adjusted EPRI Test Results in brackets are based on the data in Table 4-2 and include the “calibration correction” (Table 4.4). All forces recorded at Tower T4.

A few minutes after each full scale broken suspension insulator test, the conductor motion settled down to a new position (rest position), with a superspan between towers T4 and T6. This at rest position is similar to when the numerical model is executed under static analysis only. Since only the static analysis was used, dynamic loads were not calculated. Using the static numerical model, removal of the suspension insulator on tower T5 provided the final insulator force on tower T4 suspending span 3 and the superspan, and is given in Table 4.5 under Final Insulator Force. Insulator swing angles are also provided in Table 4.5, with the EPRI results enclosed in []. These results were not adjusted in any way. In most cases, model and full-scale results are very close, with only a few model runs having minor differences.

As shown in Figure 4.6, the ADINA model results were consistently conservative in predicting the peak insulator force with a mean bias of 1.22 and a coefficient of variation of model error as 6%. The correlation value R^2 is 0.9776. These conservative results could be partially attributed to the effect of neglecting the damping; however, this further verifies that a numerical model can capture the results of the full-scale tests with reasonable accuracy. Therefore, the model was considered to be accurate enough for subsequent runs to measure the sensitivity of varying initial conductor tensions and insulator lengths, as well as the addition of incremental ice.

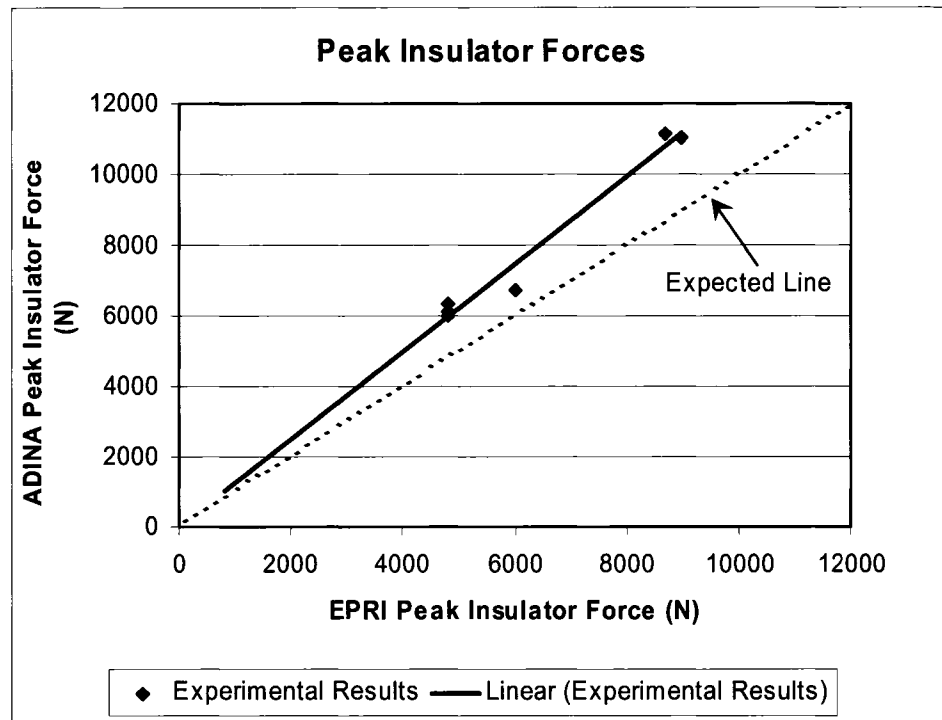


Figure 4.6 – Full-Scale and Model Peak Force Comparison

Figure 4.7 presents the time history plot of the insulator swing angle for Test IIL1. The maximum angle depicted in this figure is virtually identical to the one reported from the test (Table 4.5). The time period between the peak swing angles is the period of conductor oscillation. This oscillation is due to the tension increase from the falling conductor and the elastic recoil pulling the conductor back up. This oscillation continues for several minutes before coming to a gradual “at rest” point.

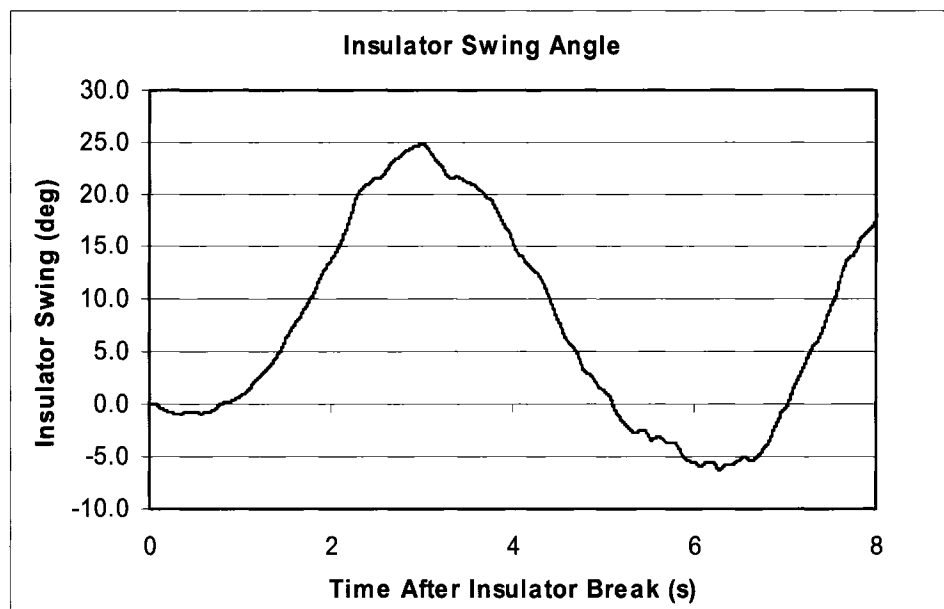


Figure 4.7 – Insulator Swing Angle – T4 – Test IIL1

Figure 4.8 depicts the force time history for the insulator string on tower 4 after the insulator break in test IIL1. This history shows a much less abrupt variation in load than previously shown in broken conductor cases. In this test, it takes 2.3 seconds from failure to the maximum peak force (note that insulator failure occurs at $t=1.0$ seconds). This force is 6757 N, 2.2 times the every day vertical (at rest) insulator force of 3050 N. Also, the angle of swing on the insulator is only 25° at maximum force (Table 4.5), and therefore the peak force is still mostly transferred to the tower in a vertical direction (typically the highest capacity for suspension towers), with only 42% (2838 N based on swing angle and peak force) acting in the longitudinal direction. For the broken conductor case, the insulator string will swing to a virtually horizontal orientation, and transfer most of the peak conductor tension to the tower in the longitudinal direction, typically the weakest direction. Conductor tension is much higher than conductor weight.

In terms of structural stability, this load for the broken insulator case is not very high, and should not be of concern to the integrity of the line. It is because of this reason that the broken suspension insulator case has not received significant analysis to determine the true nature of this failure mode. As will be discussed later (section 4.5.5), ice build-up prior to failure can have a significant influence on this result.

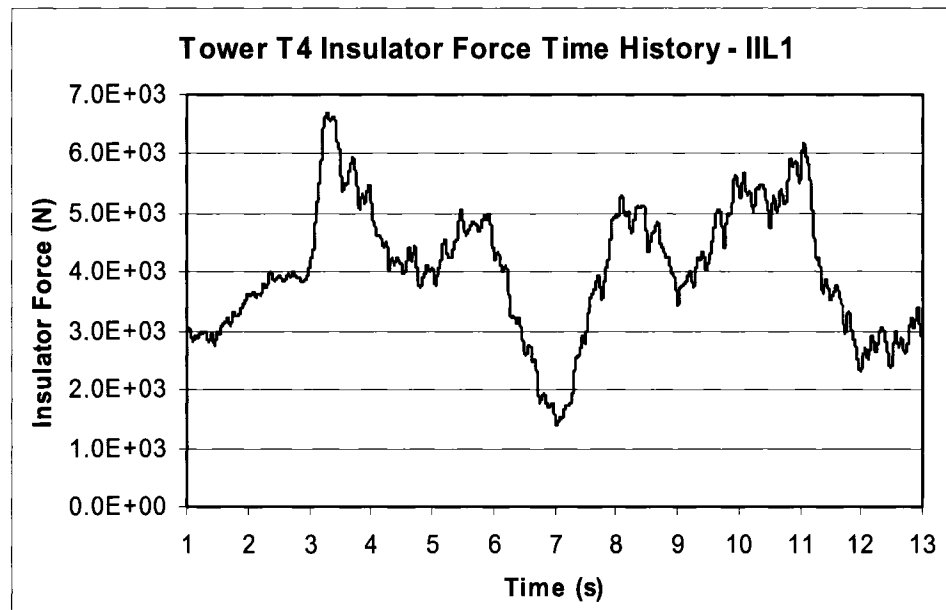


Figure 4.8 – Force Time History – Tower T4 Insulator

4.5.3 Sensitivity Analysis – Insulator Length – IIL1

Using test IIL1 as a base case, the length of the insulator string was varied from 1 m to 4 m in 1 m increments. This increase had no effect on the initial forces as all structures were changed, and the relative position of the conductor over its length remained the same. The 2.2 m standard test was not modified, and replaces the 2 m test. The result of

the sensitivity of changing the length of the insulator is provided in Figure 4.9. As shown, varying the insulator length does not have a very significant influence on the insulator and conductor peak forces. Small force changes are due to the larger swing of the longer insulator string absorbing some of the force by gradually transferring it to adjacent spans. In this case, increasing the insulator length beyond 2.2 m has only a minor effect on the peak forces estimated.

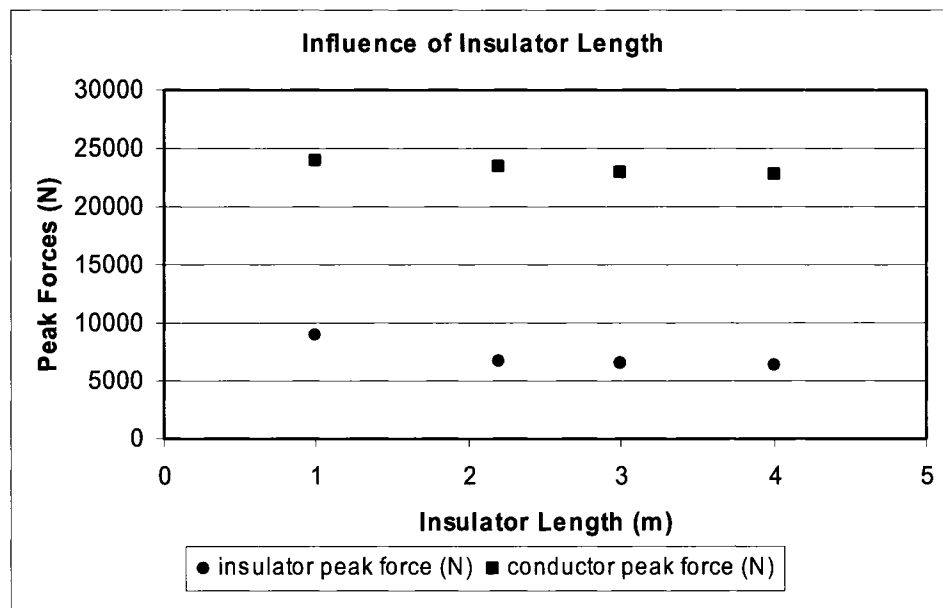


Figure 4.9 – Influence of Insulator Length on Peak Insulator and Conductor Forces

4.5.4 Sensitivity Analysis - Initial Conductor Tension – IIL1

Similar to the sensitivity analysis performed on the length of the insulator string, the effect of the initial tension was also examined. Again, the IIL1 test was used as a base model, including the default 2.2 m insulator string. Four additional model runs were

performed in this analysis, in addition to the default model run with an initial tension of 12454 N (1270 kgf). The four tensions were 9807 N (1000 kgf), 14708 N (1500 kgf), 17162 N (1750 kgf) and 19613 N (2000 kgf), respectively. From these runs, the peak insulator forces and conductor forces were estimated, with the results plotted in Figure 4.10. A 40% increase in the initial tension would increase the peak conductor force by 10%. Increases in tension produce smaller conductor sag. In the configuration shown in Figure 4.2, tower T5 is at a lower elevation than Towers T4 or T6. Therefore, increases in tension would reduce the sag of the individual spans, as well as the superspan created. This sag reduction is directly proportional to the energy released from the falling span of conductor, as a span with a higher initial tension (smaller sag) would not fall as far. Thus the peak transient dynamic forces on the insulator for Tower T4 were reduced, also reducing the relative peak conductor tension increase compared to the initial tension.

4.5.5 Sensitivity Analysis - Incremental Ice Thickness – IIL1

By varying the conductor density in the numerical model, effects of incremental ice loading (thickness) can be studied, and its effects on peak insulator force and conductor tension can be assessed. This part of the study will provide information on the relationship between the static ice load and dynamic peak loads on the conductor and on the insulator string. It is assumed that none of the ice was shed from the line during the failure of the insulator string.

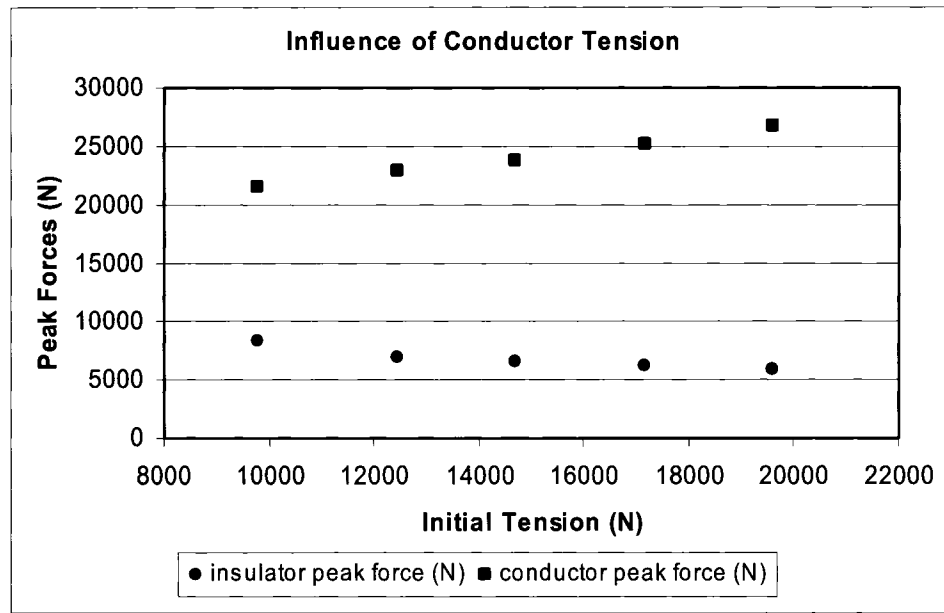


Figure 4.10 – Influence of Initial Conductor Tension on Peak Insulator and Conductor Forces

Again, EPRI test IIL1 was used as the base case. Conductor density in the numerical model was adjusted to reflect the equivalent ice weight up to 50.8 mm radial glaze ice thickness. From these model runs, initial and final conductor tensions, as well as the initial and final insulator loads, were assessed. The results are plotted in Figure 4.11 and Figure 4.12 respectively. As can be seen, an increase in the radial ice thickness from 25.4 mm to 50.8 mm will cause the insulator peak force to be 3.1 times higher. Peak conductor tensions respond similarly with increases in ice thickness. This increase in the peak values, for both insulator forces (Figure 4.11) and conductor tensions (Figure 4.12), is due to the significantly higher energy release from the falling conductor.

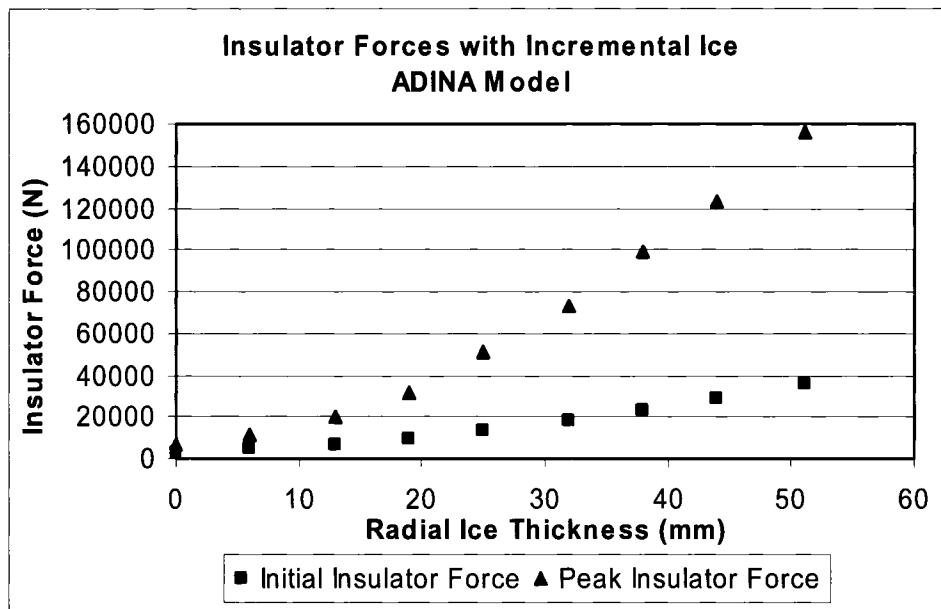


Figure 4.11 – Influence of Incremental Ice on Initial and Peak Insulator Forces

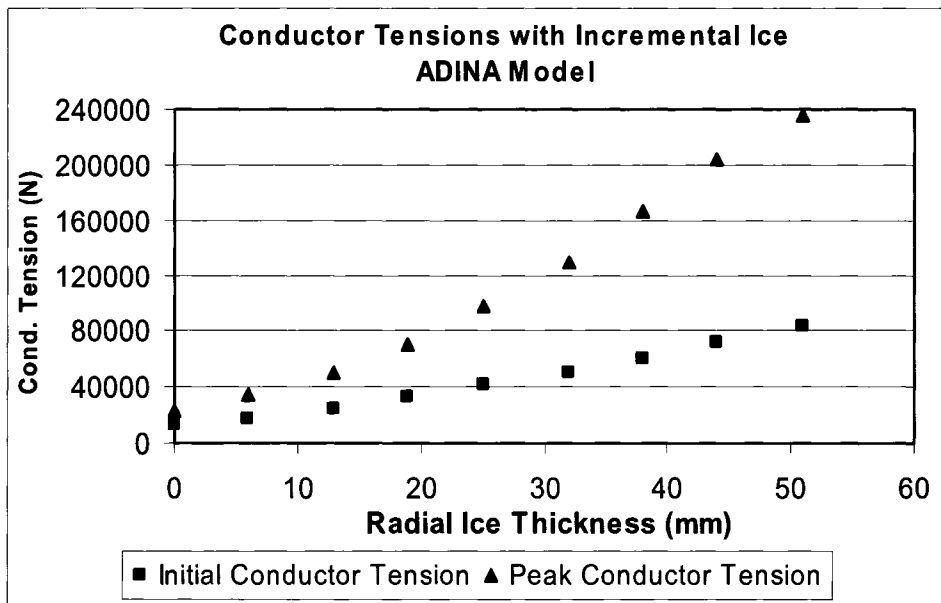


Figure 4.12 – Influence of Incremental Ice on Initial and Peak Conductor Tensions

4.5.6 Coordination of Strength – IIL1

Test IIL1 utilizes the 397 kcmil ACSR conductor and porcelain insulator string. This conductor has a Rated Tensile Strength (RTS) of 72500 N while the strength of the string is assumed to have an M&E (Mechanical and Electrical) rating of 66685 N. M&E ratings stipulate that the insulator should not fail mechanically or electrically prior to reaching their mechanical rated strength. Actual dynamic strength for each of these components is unknown. It is assumed for this illustration that the dynamic strength is approximately 1.5 times the rated static strength. This gives a dynamic strength of approximately 108,000 N for the conductor and 100,000 N for the insulator.

From the plot shown in Figure 4.12, given a premature failure of the suspension insulator string, the conductor can only support a maximum radial ice thickness of approximately 27 mm before reaching the dynamic RTS, while 38 mm of radial glaze ice can be supported by the insulator string on the adjacent structure prior to failure. Therefore, given a premature insulator string failure on Tower T5, with a 27 mm ice load, the conductor will rupture instead of a vertical cascade of broken insulators in subsequent structures. This will cause a longitudinal force on the adjacent tower, which could initiate a longitudinal cascade of structural failure if the tower is not designed for this load. On the contrary, the failure sequence could be reversed if the dynamic impact load of the insulator is lower than that of the conductor.

This conclusion is significant. As noted in the few reports that reviewed the broken insulator scenario (Peyrot et al, 1980, LaPointe, 2003, Li and Bhuyan, 2003), broken insulators under everyday loads provide dynamic impact forces that were considered to be of little concern. Peyrot et al reported that the broken suspension insulator is not regarded as being significant due to the low dynamic nature of the forces, and the overall direction and magnitude of forces imposed on the tower. Under ice, however, dynamic forces will be quite significant with respect to conductor strength. Conductor failure can trigger a cascade failure if one suspension insulator string fails first under ice condition.

This numerical model verification demonstrates one area where numerical model studies can be used to first verify and then expand results to test for scenarios not previously reviewed. Once confidence in the results can be gained, any combination of terrain, line parameters, and load cases can be modeled and studied to ensure that consequences of potential overloads can be understood. Although line design for the full consequences may not be possible, an understanding of the extent of damage may be gained, and measures taken to minimize the loss.

Chapter 5

Analysis of Scale-Model Tower Failure

This chapter presents the validation of a numerical model based on a number of small-scale tests performed by Kempner (1997). The scale model research studied longitudinal loads caused by broken conductors taking into account the effect of failed towers. Some of the primary variables studied included: (1) Span/Sag ratios, varied from 20 to 100, (2) Span/Insulator Length ratios, varied from 100 to 400, (3) conductor type, and (4) structure type representing pole structures and lattice steel towers. A numerical model was developed based on the scale model test data. This numerical model was used as the basis from which a better understanding of the failed tower effect on longitudinal load could be gained. From Kempner's research, it was determined that the most significant factors were the Span/Sag ratio and structure type. Using these conclusions as a base, a limited set of data was selected for the numerical models covering a wide range of parameters.

5.1 Numerical Modeling of the Scale Model Tests

A five span numerical model was developed using Kempner's data. The numerical model conductor was limited to the beaded "lamp" chain data. This conductor model has been used by Govers (1970) with reasonable results, and the differences between the lamp chain and the stainless steel wire results in Kempner's model were minimal. Data

on model conductor sag and model insulator lengths are provided in Tables 5.1 and 5.2 respectively.

Table 5.1 – Model Conductor Sag

<i>Span/Conductor Sag</i>	<i>Model Conductor Sag</i>
100	117.6 mm (4.63 inches)
70	167.9 mm (6.61 inches)
50	235.2 mm (9.26 inches)
30	391.9 mm (15.43 inches)
20	588.0 mm (23.15 inches)

Table 5.2 – Model Insulator Lengths

<i>Span/Insulator Length</i>	<i>Model Insulator Length</i>
400	29.5 mm (1.16 inches)
200	58.9 mm (2.32 inches)
100	117.6 mm (4.63 inches)

5.1.1 Small Scale Model Structures

Towers used for the small-scale models (Figure 5.1) were 915 mm long hollow aluminum tube in a vertical orientation, with a 25 mm outer diameter, and a 1mm wall thickness. Base supports were pinned allowing for longitudinal movement only, pivoting around the pin connection. The cross-arms were 75 mm in length (from centreline) and positioned at a height of 635 mm from the pinned support. Longitudinal structure support was provided for each tower by one set of two different spring types, attached at the 508 mm level, connecting the tower to the reference frame. These springs were designated as

“blue” and “red”, and were sized to model structural flexibility. The “blue” spring had a low stiffness to represent the response of a flexible structure such as wood or tubular steel pole structure, while the “red” spring had a higher stiffness to represent a lattice steel tower. Kempner added a 0.907 kg mass to the blue spring towers, and a 0.15 kg mass to the red spring towers in order to correctly represent the natural frequency of the two structure types. LVDT were utilized to measure linear structure motion during the test. Strain gages on the instrumented arm recorded the forces measured by the broken conductor. A 0.2 mm wire fuse provided the only longitudinal support for the structure between the spring and the reference frame. Structure failure was initiated by electrically burning off this fuse.

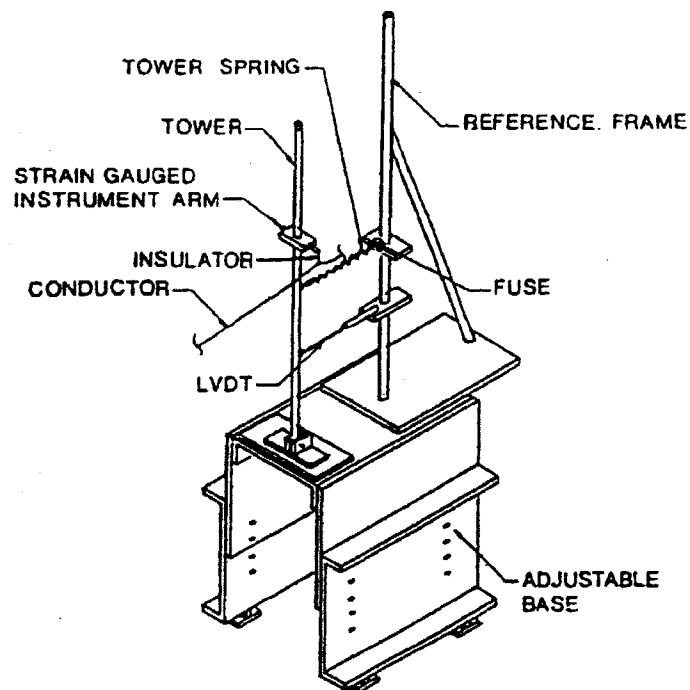


Figure 5.1 – Small Scale Model Structure (Kempner, 1997)

5.1.2 Simplified Numerical Model

Assumptions were made in the development of the numerical model to determine if a simplified version could accurately reproduce the results. Table 5.3 shows the results of Kempner's study, with comparison between the blue spring and red spring peak forces. Based on the maximum peak force of 25.5 N, the conductor attachment point displaces 27.4 mm using the red spring model, and 165.6 mm using the blue spring model, a displacement of more than six times. All results compared in Table 5.3 show that the spring stiffness has little significant influence in the results with higher spring stiffness yielding slightly higher peak forces. Therefore, it was assumed that it would be valid to make modifications to the original design, and subsequent reductions in the displacement due to structure flexibility, to simplify the numerical model without adversely affecting the results. Reducing the structural flexibility would cause a very slight increase in peak force for all models.

With applied forces and boundary conditions at the end nodes, the structure can be modeled using a truss bar instead of a beam element. The following modifications were made to simplify the model, and are displayed in Figure 5.2:

- Remove structure crossarm. Insulator is modeled inline with the structure. Structure twist subsequently neglected.
- Relocate spring from 0.508 m level to the 0.635 m level. Structure bending due to the attachment location of the spring subsequently neglected.

5.2 Finite Element Model

Conductor elements were modeled as three-dimensional truss elements, carrying an initial strain to represent the conductor tension, with 30 elements per span. Structures were modeled as truss elements, pinned at the base, and restrained longitudinally by springs and fuses as shown in Figure 5.2. Out-of-plane (transverse to line direction) movement was restricted in the numerical model as support was provided transverse to the line in the small-scale model by the single degree of freedom pin connection. Insulators, connecting the structure to the conductor, were modeled as truss elements.

Table 5.3 – Comparison of Peak Forces Using Blue and Red Springs (Figure 2.14)

<i>Peak Dynamic Forces – Scale Model Tests</i>				
Span/Sag	Blue Spring Peak Force (N) / Red Spring Peak Force (N)			
	% Agreement			
	T1	T2	T3	T4
100	25.4 / 25.5 99.6%	16.7 / 20.6 81.1%	16.9 / 20.1 84.1%	11.4 / 15.1 75.5%
50	14.4 / 15.0 96.0%	10.1 / 12.5 80.8%	9.7 / 11.2 86.6%	8.5 / 9.8 86.7%
20	8.3 / 7.8 106.4%	5.3 / 5.3 100.0%	5.1 / 6.0 85.0%	5.1 / 6.0 85.0%
Average	100.6%	87.3%	85.2%	82.4%

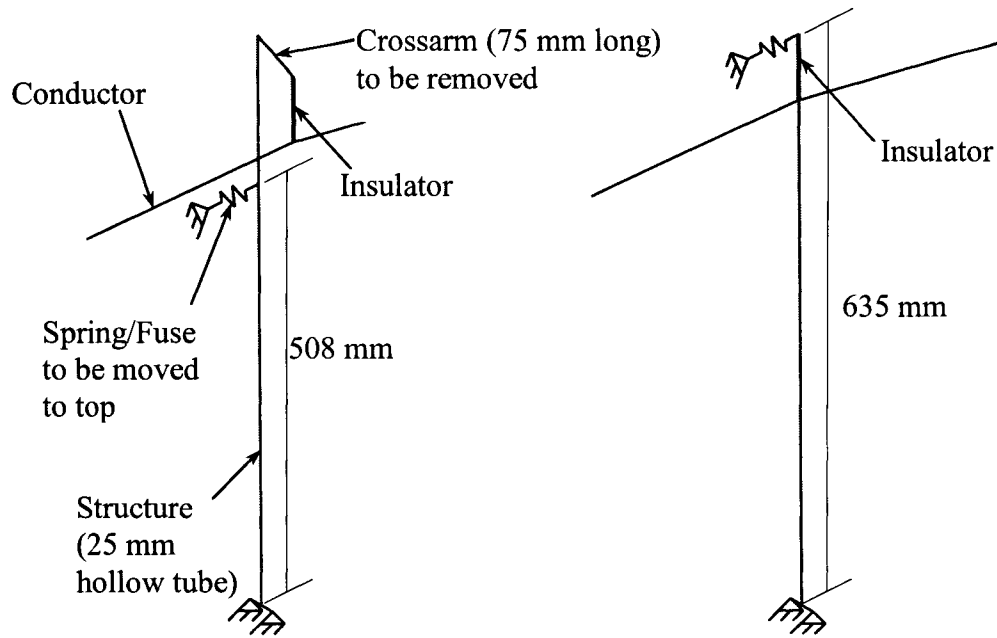


Figure 5.2 – Kempner Model (left) and Simplified Numerical Model Structure (right)

Tower masses, as defined for Red and Blue spring towers, were added as an additional truss element connected at the cross-arm level, and were modified by changing the cross sectional area. Similar to the broken insulator numerical model, conductor damping was not included. Frictionless ground contact using methods detailed in Appendix 1 was initially included in these numerical models; however, it was discovered that peak transient dynamic forces were recorded prior to conductor touching the ground. Therefore, the effect of contact surface was not studied in the analysis because it had no influence on the results. If the cable had contacted the ground in the scale model tests, the friction of the cable on the ground may have had an effect on the measured forces; however, this contact occurred long after the peak forces were realized.

Conductor type (beaded chain), Span/Insulator Length ratio (200), and low displacement prior to failure (25% of maximum displacement) were maintained as constant parameters for benchmarking as these factors had a lesser effect on the model test results (Kempner, 1997). Table 5.4 summarizes the six parameter sets (three span/sag ratios, each modeled with two spring types) selected for this numerical model study. For each parameter set, 4 model runs (control, failure of tower 1, 2 and 3 respectively) as described in Chapter 2 were performed, producing a total of 24 numerical model runs.

Table 5.4 – Models Selected For This Study

<i>Model Number</i>	<i>Cable</i>	<i>Spring</i>	<i>Span/Insulator Length Ratio</i>	<i>Span/Sag Ratio</i>
1	Beaded Chain	Blue	200	100
2	Beaded Chain	Blue	200	50
3	Beaded Chain	Blue	200	20
4	Beaded Chain	Red	200	100
5	Beaded Chain	Red	200	50
6	Beaded Chain	Red	200	20

5.3 Methodology for Numerical Modeling

The methodology for creating and executing the numerical model is the same as in Section 4.4 for the EPRI broken insulator tests. Three Span/Sag ratios were selected to cover the full model range; 20, 50 and 100, and each ratio was executed using either a blue or red spring. A Span/Insulator Length ratio of 200 was selected as an average value, reasonably representative of a 230 kV line. As an example, a typical suspension

insulator length for a 230 kV line would be 2.1 m. With a Span/Insulator length ratio of 200, this would translate to a span length of 420 m, appropriate for this line type.

5.4 Analysis of Model Results

Figure 5.3 shows two spans (out of five for simplicity) in the numerical model, with three failed towers. The relative failed position of each structure can be seen, as tower 1 (left) failed first, with tower 2 (centre) and tower 3 (right) failing in turn. Even with only two spans out of five shown, this three tower cascade situation was the maximum performed by Kempner, with conductor rupture adjacent to the left of the first structure.

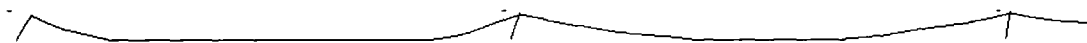


Figure 5.3 – Numerical Model Section - Three Tower Failure Sequence

5.4.1 Time Step Sensitivity

Similar to section 4.5.1, a verification of the significance of varying the time increment (Δt) was carried out for this model, using Δt ranging from 0.00025 seconds up to 0.003 seconds. As shown in Figure 5.4, the selection of time increment within this range has little influence on results. A 50 Hz filter, for reasons described later, was applied to the model results. In the ADINA model, time step increments of greater than 0.003 seconds caused a lack of convergence in the implicit integration, and subsequent model execution

failure. For each of the numerical model runs, a time step increment of 0.001 seconds was selected.

5.4.2 Numerical Model Verification of Scale Model Response

Although all six models were examined in this study, model 2 (detailed in Table 5.4) was selected as an example case for this section. In this model run, the Blue Spring (low stiffness) was used, and Span/Sag ratio was set at 50. The model was executed and the results compared with those of the small-scale test. The transient dynamic forces recorded for tower one, with no structural failure, for both small-scale and numerical models are plotted in Figure 5.5. The heavy line is the small-scale test result, and the light line is the numerical model result, as noted in the figure. The first two peaks forces are higher than all subsequent peak forces, and thus the most important forces felt by the tower. The first peak force (at approximately 0.1 seconds) is verified as due to elastic recovery of the conductor tension as the insulator swings out to transfer strain energy to kinetic energy. The second peak force (from approximately 0.2 to 0.35 seconds) is due to the bottoming out of the conductor span due to freefall as a result of its new slackness, given that the insulator length is now added to the original conductor length.

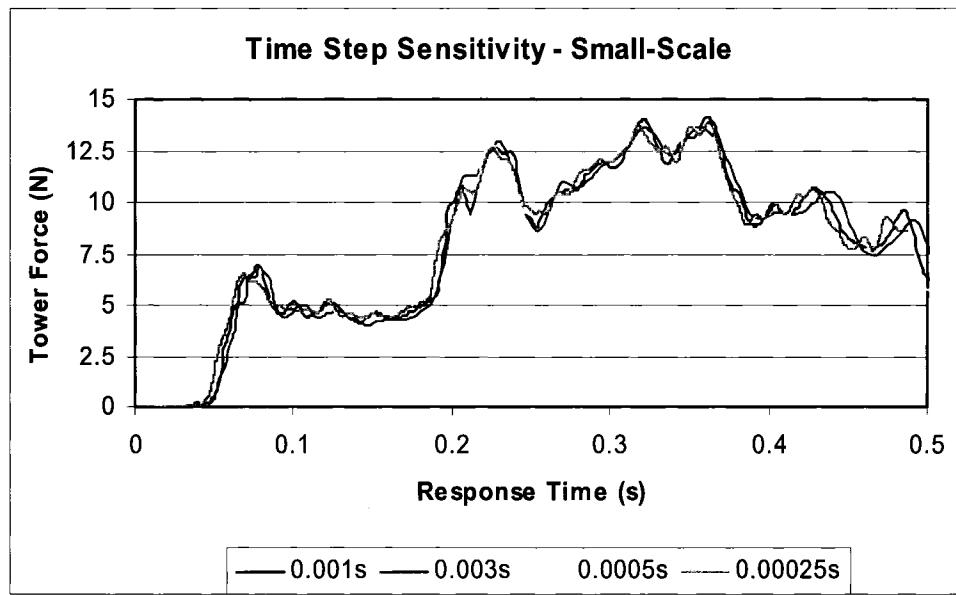


Figure 5.4 – Sensitivity of Time Step Increment – Small Scale (50Hz filtered)

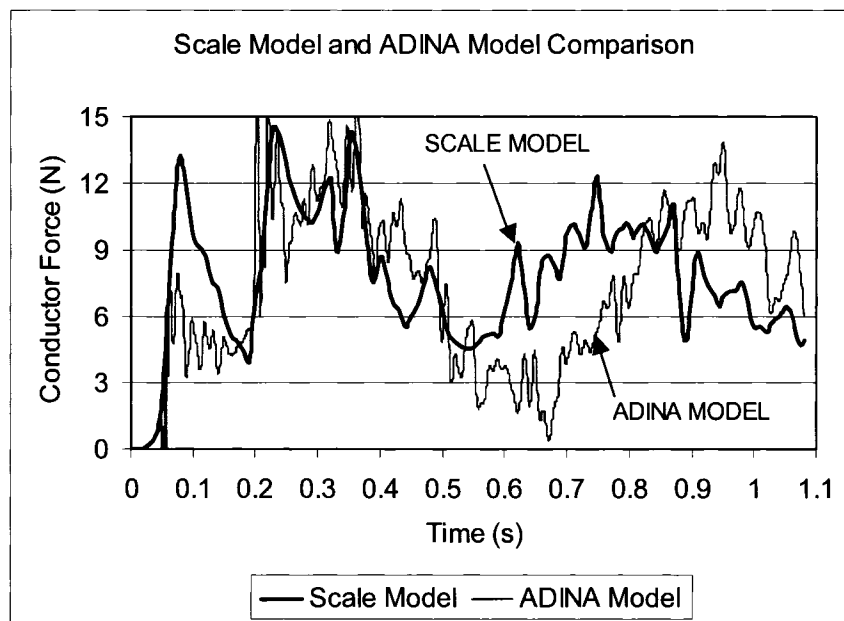


Figure 5.5 – Scale Model (Kempner, 1997) and ADINA Model 2 Overlay - Raw Data

As evidenced by the light line in Figure 5.5, the response is highly influenced by short duration high/low noise like spikes. Peabody (2004) explains this noise as being “due to breaking up the continuous elements in the real structure into discrete pieces in the finite element model”. Kempner also experienced high frequency instrumentation noise, and therefore applied a 50 Hz filter in an effort to remove such spikes from his scale model test results. The result of this filtering is evidenced in Kempner’s force time history plots (Figure 5.5 – dark line). The same filter frequency can be applied to the time history response of numerical model 2. The effect can be seen in Figure 5.6. The filtered response (smooth, dark line) does not carry the spikes of the raw data (light line) but still provides the load response. The 50 Hz filtered numerical model response is similar to the scale model results as shown in Figure 5.7. This filter has been applied to the results of all model runs.

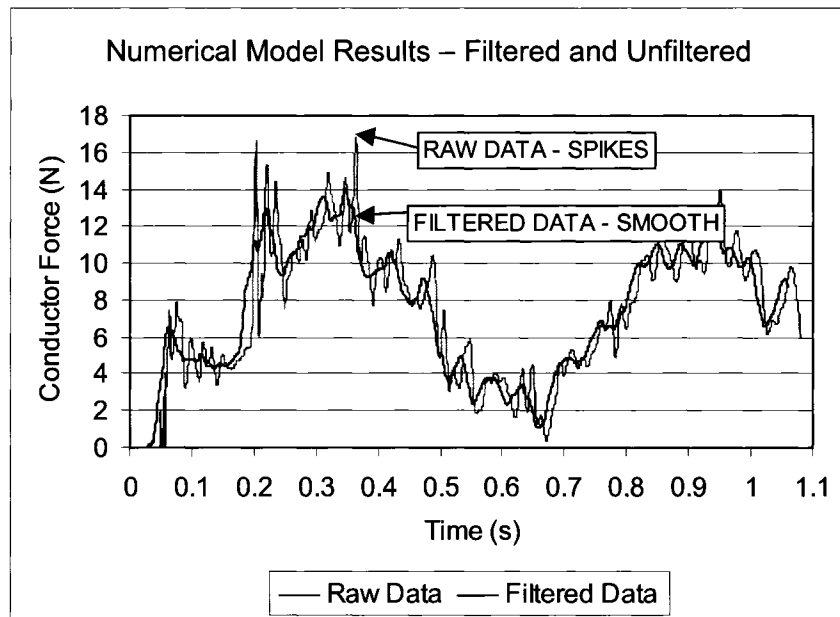


Figure 5.6 – ADINA Model 2 Results – Raw and 50 Hz Filtered

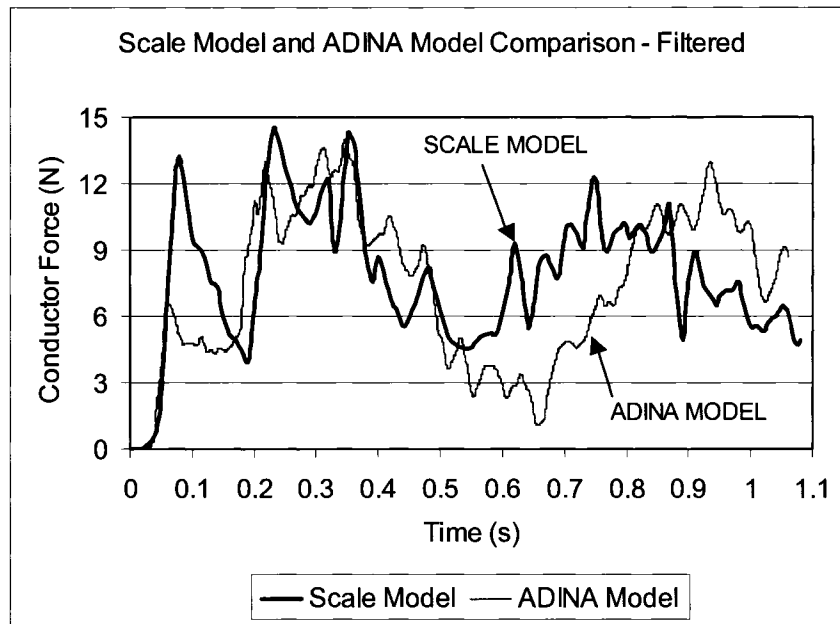


Figure 5.7 – Scale Model (Kempner, 1997) and Filtered Numerical Model 2

5.4.3 Analysis of Transient Dynamic Peak Forces

As is evident in Figure 5.7, the response times for the first and second peaks are very similar between the numerical and scale models. The first peak force in the numerical model at time 0.1 seconds is 40% lower than the small-scale test; however, the second (maximum) peak force at time 0.22 seconds is only 6% lower than the scale model. The numerical model in this case captures the maximum peak load well. Although not shown for all tests, the time responses for the first two peaks are similar to the scale model results; however, accuracy in the peak transient forces varies for each test. The apparent phase lag in later peaks may be due to the exclusion of damping in the model. The numerical results are within 20% of the experimental results in 19 out of 24 numerical

model runs, as shown in Table 5.5. The comparison is good considering that there are inherent variations in the experimental results.

Table 5.5 provides a comparison of the results for peak dynamic loads between the model runs and the scale model tests. Most results show very similar peak transient forces, but a few show significant differences. Overall, the average numerical model results show that the peak transient forces at tower 3 in a two tower failure situation, and tower 4 in a three tower failure situation are quite similar to the scale model results. Tower 1 and tower 2 give, on average, higher forces than the scale-model results. Out of 24 numerical model runs, 11 results have less than $\pm 10\%$ error, and 19 have less than $\pm 20\%$ error. Five runs have greater than $\pm 20\%$ error in peak transient force (highlighted in bold in Table 5.5), with three on the first structure, and two on the second structure. The largest error, +63% (Red spring, Span/Sag Ratio = 20), occurs on a second structure peak force. Four high error results are on the mid and low tension (Span/Sag ratio of 50 and 20 respectively) models using the red spring.

Explanation as to why these five results had significant difference over the scale model results could not be categorically determined as some were higher than the scale model results, and one was lower. Some possibilities are:

- The numerical model does not completely represent the structural stiffness of the scale model, and could possibly create errors. This was ruled out as stiffness, represented by the different springs, did not significantly vary the results, as described in section 5.1.2. Thus, differences of up to 63% would not be caused by structure stiffness;

- As stated previously, failure of the structure up to structure 3 (last failed structure) occurred before the conductor touched the ground, so the friction between ground and cable contact should not have had an effect. It was also assumed that friction in the pinned connection was also insignificant, and would not influence the results; however, this may not have been the case for the small scale models;
- Actual response of the beaded chain may have had an influence on the results in the scale models. Under lower tension (Span/Sag Ratio of 50 and 20), the interaction between the beads and links was not taken into account in the numerical model. The combination of low tension and high dynamic forces in the beaded chain model may have contributed to errors in the scale model study. This was assumed to be the most probable reason for the discrepancy.

Static model verification was performed for each model to verify that it was correct. The only modification to the model for each run for which the results were compared in Table 5.5 was the spring stiffness. Systematic execution of each numerical model reduced possible errors. Results for tower three and four are using the identical structure models as tower one and two, and have eight out of 14 results less than $\pm 10\%$ error, with no values greater than $\pm 20\%$. Figure 5.8 displays a distribution of the model error. As it is evident, much of the numerical model results are less than $\pm 20\%$ different than the scale model results, demonstrating good correlation.

Table 5.5 – Peak Transient Forces (Scale and Numerical)

Peak Dynamic Forces					
		ADINA Peak Transient Force (N) / Scale Model Peak Transient Force (N)			
		% Agreement			
	Span/ Sag	T1	T2	T3	T4
Blue Spring	100	19.4 / 25.4 76.2%	17.1 / 16.7 102.7%	14.5 / 16.9 86.1%	13.7 / 11.4 119.8%
	50	14.0 / 14.4 97.5%	11.7 / 10.1 116.4%	8.7 / 9.7 89.9%	8.4 / 8.5 94.8%
	20	8.1 / 8.3 96.8%	5.5 / 5.3 103.3%	5.1 / 5.1 100.0%	4.5 / 5.1 88.7%
Red Spring	100	29.1 / 25.5 114.1%	21.2 / 20.6 103.0%	19.2 / 20.1 95.4%	17.0 / 15.1 112.6%
	50	23.3 / 15.0 155.5%	16.5 / 12.5 132.9%	11.6 / 11.2 103.6%	8.8 / 9.8 88.7%
	20	11.0 / 7.8 141.1%	8.6 / 5.3 163.0%	6.4 / 6.0 106.7%	5.5 / 6.0 91.9%
Average		113.5%	120.2%	96.9%	100.0%

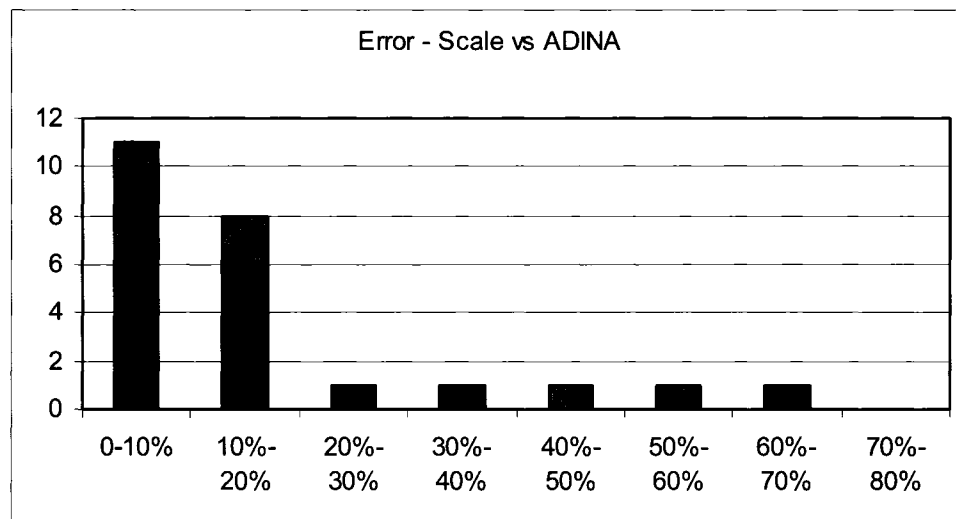


Figure 5.8 – Distribution of Error Between Numerical and Small-Scale Model Results

Figures 5.9, 5.10 and 5.11 provide peak force comparisons for the six model tests from the data contained in Table 5.5, with each separated with respect to Span/Sag ratio. Each plot displays the comparison of the small-scale results (ie “Blue 100/200” represents blue springs, span/sag ratio = 100 and span/insulator length ratio = 200) and the numerical model results (ie “KT Blue 100/200”), both in the same colour. All four tests for a given Span/Sag ratio as indicated in the title are provided in each plot. As previously discussed, the Span/Insulator Length ratio is fixed at 200 for all tests.

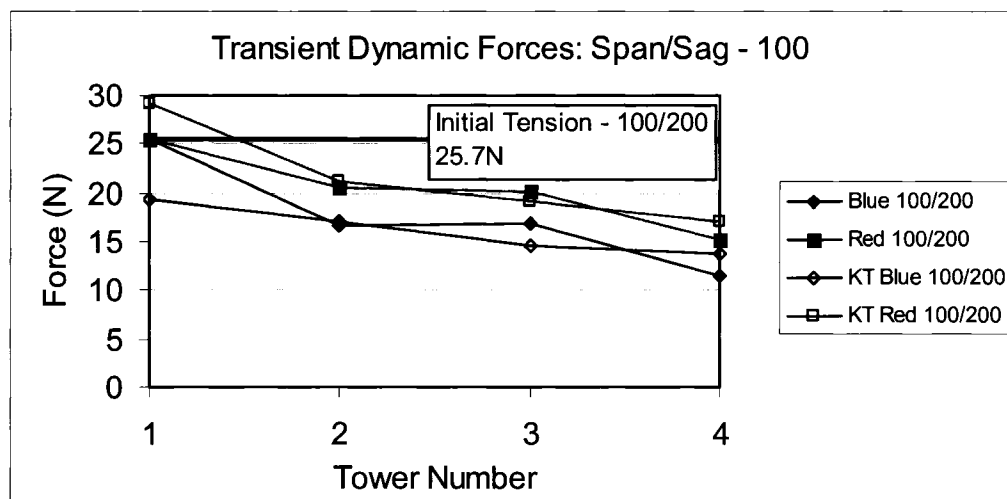


Figure 5.9 – Peak Transient Forces – Scale Model and ADINA – Span/Sag = 100

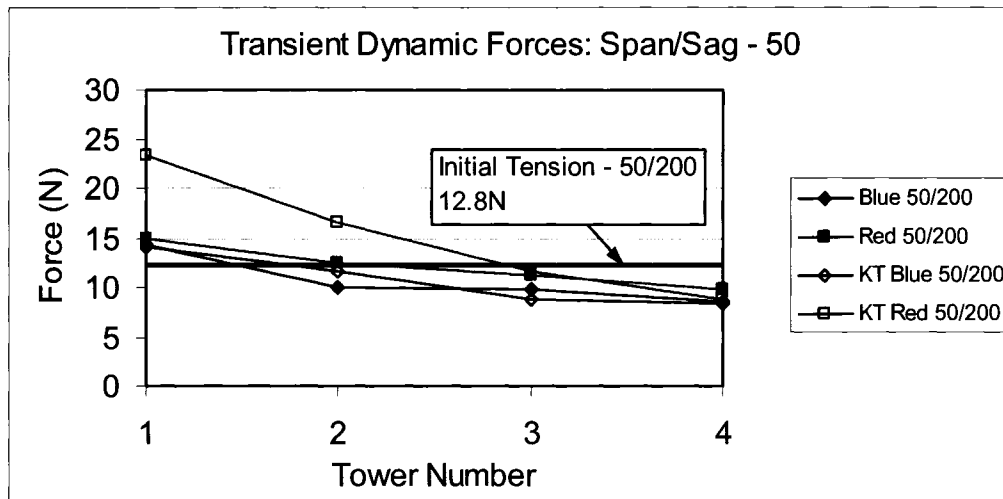


Figure 5.10 – Peak Transient Forces – Scale Model and ADINA – Span/Sag = 50

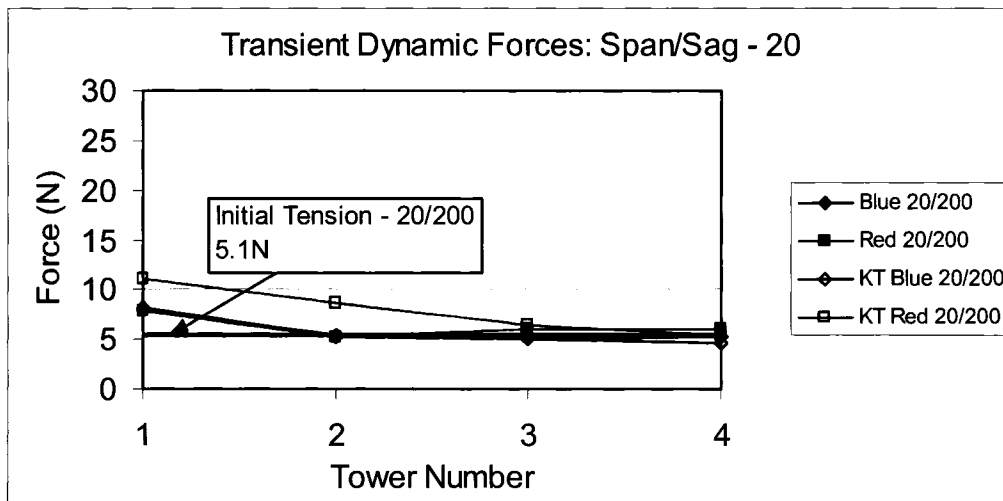


Figure 5.11 – Peak Transient Forces – Scale Model and ADINA – Span/Sag = 20

It can be seen in Figures 5.9 to 5.11 that the trends in the relative forces from one structure to the next are similar. In Figure 5.9, the small-scale results show a large decrease in longitudinal force between tower one and tower two, but very little decrease between tower two and tower three. This trend is also captured in the numerical model

results, shown in the same figure; however, the numerical model results do not have the same extreme variation as the scale model results. In all cases, the numerical model results show a smoother variation across all structures as the tower failure progresses. Since the structures were identical in the numerical model with no variation from materials and construction, it is assumed that the numerical model better captures the relative similarity between the forces from one structure to the next. The results from the scale model tests show a large decrease between tower one and tower two, little decrease between tower two and tower three, and another large decrease between tower three and tower four. No direct explanation could be developed with respect to the response pattern shown in the small-scale models; however, it may be possible that differences in the individual small-scale structures may be the cause.

5.4.4 Transient Forces on Remaining Structures

As shown in Table 5.5, the force imbalance between the intact span and the failed span causes a significant longitudinal load. This longitudinal load without structure failure is not as high as the load on the previous failed structure. For example, for model 2 (blue spring, span/sag ratio = 50), the maximum longitudinal load on tower one is 14.0 N, and after tower one fails, the longitudinal load transferred to tower two is 11.7 N. This imbalance is due to the fact that failure of tower one reduces the tension in the conductor span between tower one and tower two to near zero. Thus, the imbalance due to the tension in the span from tower two to tower three acts on tower two. Had tower one not

failed, the tension in the conductor on both sides of tower two would have had an equalizing effect that would reduce the longitudinal load.

Using the model 2 control test results (first run, no structure failure), the force on tower one, as stated previously, was 14 N. With no failure in tower one, the maximum longitudinal load on tower two, given intact conductor spans on both sides of the tower, is recorded as 6.1 N, significantly less than the tower one load. Table 5.6 provides the maximum longitudinal force on each structure in the five span model given no tower failures. The small forces on subsequent towers show that if tower one is capable of surviving, the remaining towers will not experience the same magnitude of the force had tower one failed. Therefore, it may be concluded that this data shows that the cascade failure of towers is directly caused by the failure of the first tower, and that the survival of tower one may not allow the cascade to initiate, given the right condition.

Table 5.6 – Longitudinal Force With No Tower Failure – Model 2

<i>Tower Number</i>	<i>Maximum Longitudinal Force (N)</i>
<i>1</i>	14.0
<i>2</i>	6.1
<i>3</i>	3.2
<i>4</i>	1.8
<i>5</i>	0.9

This conclusion assumes that tower two can survive the applied 6.1 N force. It is a possibility that each structure is already at its capacity due to existing loads (ie. maximum

ice). Prior to conductor failure, the tension is balanced on both sides of each tower, thus providing no longitudinal load. If it is assumed that tower one is a suspension structure that is designed to survive the longitudinal forces from a conductor failure (anti-cascade tower), it may survive the 14 N force. Unfortunately, due to the suspension insulator string configuration, the slackness in the conductor will still transfer a certain portion (6.1 N) of load to the next tower. The next tower, not designed for the same longitudinal force as the anti-cascade tower, may be at maximum vertical capacity and may not have any reserve capacity left to withstand a small longitudinal load. Thus, the load imbalance of 6.1 N may still cause the tower to fail. This shows that suspension structures designed for significant longitudinal load (anti-cascade) may survive the peak loads, but may still transfer significant forces from the disturbance and not stop the continuance of the cascade failure to subsequent towers.

A failure envelope for the capacity of a structure against vertical, longitudinal and transverse load can be developed. This envelope will show that as the structure load approaches the maximum capacity in any one direction, ability of the structure to sustain forces in the other directions decreases. Therefore, tower two under maximum force in the vertical direction, may not be able to carry any additional longitudinal force, even if the anti-cascading tower (tower one) survives. This shows where full knowledge of the capacity of each structure, and a complete understanding of the magnitude and direction of the dynamic loads, is required to ensure that a cascade failure can be contained.

Numerical modeling under these conditions will provide a better understanding of the transmission line loads and allow different case scenarios to be analyzed.

Chapter 6

Summary, Conclusion and Recommendations

6.1 Summary and Conclusions

This research study investigated the dynamic effects of broken suspension insulator and multiple tower failures on electrical transmission lines using the commercially available finite element software ADINA. A numerical model of a test line was first developed to simulate a broken insulator failure at the suspension point, with the predicted dynamic loads on the adjacent towers compared with those available from the published full-scale test data. A second numerical model, based on small-scale test data, was also validated where the suspension towers were allowed to fail in certain sequence and the predicted impact load on the surviving tower was compared with that available from the test results. The above two models provided a better understanding of the cascade failure of transmission lines. A sensitivity study was carried out to determine the effects of various parameters that may influence the peak loads.

The results from the first numerical model showed that the predicted peak insulator force has a mean bias of 1.22, a model error of 6%, and a correlation value (R^2) of 0.9776. A number of conclusions were drawn based on the results of the sensitivity study. These are:

- Increase in insulator length (standard length of 2.2 m) from one metre to four metres had negligible effect on the estimated peak insulator force.
- Similar observation was also noted when the conductor tension was varied up to two times the lowest tension.
- However, the increase in radial ice thickness from bare to 50.8 mm glaze ice caused the dynamic insulator impact factor (ratio of the peak insulator force to initial insulator force) to increase by a factor of two, and the dynamic conductor impact factor (the ratio of the peak conductor tension to the initial conductor tension) to increase by a factor of 1.5.

A simple coordination of strength analysis between the conductor strength and the insulator strength demonstrated that given a suspension insulator failure under ice condition, there is a likelihood of conductor rupture prior to insulator failure on adjacent structures, thus potentially initiating a cascade failure in the longitudinal direction. The results from the second numerical model showed that the correlation of peak forces induced by conductor failure had good agreement, in general, with those obtained from the model test results. Out of all the numerical model runs executed, 80% of the results were within a $\pm 20\%$ error margin. The remaining 20% were outside this range, where it appeared that the difference might have been contributed by neglecting the interaction between the beads and links of the scale model conductor (beaded chain). The numerical model validated that bending stiffness of a structure has only moderate influence on the peak forces experienced during cascade failure. This is demonstrated by a 20% increase

in the predicted peak force when the bending stiffness is increased by six times. The analysis results showed that on an average, the peak force decreased by 18% on each subsequent tower as the cascade progressed. It was also shown that if a structure does not fail, a significant force could still be transferred to the subsequent structure. This force could be high enough to cause the subsequent structure to fail if it is not designed to withstand this load. The present analysis methodology provides a better way of determining the peak dynamic forces that can be used for tower design.

6.2 Recommendations for Future Work

Studies detailed in Chapter 4 and Chapter 5 validated numerical models based on the actual geometry used during the full-scale test and small-scale model test. Future modeling should consider studying the influence of parameter variations such as: (1) bending and torsional stiffnesses of the structure; (2) model damping; (3) variable span lengths; (4) structure elevation differences, etc. Also the influence of conductor having a ground contact as well as the unbalanced ice shedding problem should be studied. The results from the future work could be used later to develop a design nomograph of the various parameters to estimate the peak dynamic load. Through continued analysis, a complete understanding of the dynamic forces experienced during component failure can be evaluated appropriately and be used to design for more reliable transmission line systems.

References

ADINA (Automatic Dynamic Incremental Nonlinear Analysis), (2003) ADINA R&D, Watertown, MA.

Bathe, K., (1996) “Finite Element Procedures”, Upper Saddle River, NJ., Prentice Hall, 1037 pages.

Frandsen, A. G. and Juhl, P. H., (1976) “Cascade of Tower Collapses, Design Criteria”, Paper No. 22-10, International Conference on Large Electric Systems (CIGRE), Paris, 13 pages.

Govers, A., (1970) “On The Impact of Unidirectional Forces on High Voltage Towers Following Conductor Breakage”, Paper No. 22-03, International Conference on Large Electric Systems, 10 pages.

Halder, Asim, (2002) “CEA ISMIG Technology Watch – Project On Longitudinal Unbalanced Loads”, April.

Haro, L., Magnusson, B. and Ponni, K., (1956) “Investigation of Forces Acting on A Support After Conductor Breakage”, Paper No. 210, International Conference on Large Electric Systems (CIGRE), Paris, 15 pages.

Kempner, L. J., (1997) “Longitudinal Impact Loading on Electrical Transmission Line Towers: A Scale Model Study”, PhD Thesis, System Science: Civil Engineering, Portland State University, Portland, Oregon, 201 pages.

Lapointe, Marc, (2003) “Dynamic Analysis of Power Line Subjected to Longitudinal Loads”, Master of Engineering Thesis, McGill University, Montreal, 105 pages.

Li, H., and Bhuyan, G. S., (2003) “Numerical Simulation for Dynamic Response of Overhead Lines With and Without Load Control Devices – Using ADINA – 900 Node Version”, CEA Technologies, 10 pages.

McClure, G., (2007) “ADINA Modeling Guide and Benchmark Tests for Component Failure Analysis in Overhead Line Sections”, CEA Technologies, Project No. P-3319A, in press for publication.

McClure, G. and Tinawi, R., (1987) “Mathematical Modeling of the Transient Response of Electric Transmission Lines Due to Conductor Breakage”, Computers and Structures, Vol 26, No. ½, pp. 41-56.

Mozer, J. D., Pohlman, J., Fleming, J. F., (1977) “Longitudinal Load Analysis of Transmission Line Systems”, IEEE Transactions on Power Apparatus and Systems, Vol PAS-96, No. 5, September/October, pp. 1657 - 1665.

Mozer, J. D., Wood, W. A. and Haribor, J. A., (1981) “Broken Wire Tests on a Model Transmission Line System”, IEEE Transactions on Power Apparatus and Systems, PAS-100: pp. 938 - 947.

Ostendorp, M., (1997) “Longitudinal Loads and Cascading Potential of Transmission Line Upgrades”, personal communication.

Peabody, Alan Bowe, (2004) “Applying Shock Damping to the Problem of Transmission Line Cascades”, PhD Thesis, McGill University, Montreal, 214 pages

Peyrot, A. H., Kluge, R. O., and Lee, J. W., (1980) “Longitudinal Loads From Broken Conductors and Broken Insulators and Their Effect on Transmission Lines”, IEEE Transactions on Power Apparatus and Systems, Vol. PAS-99, No. 1, Jan./Feb., pp. 222 – 231.

Peyrot, Alain H., Kluge, Robert O., and Lee, Jun W., (1978) “Longitudinal Loading Tests on a Transmission Line”, EL-905, September, 145 pages.

Siddiqui, F., and Fleming, J., (1984) “Broken Wire Analysis of a Transmission Line Systems”, Computers and Structures, Vol 18, No. 6, pp. 1077-1085.

Thomas, M. B., (1981) “Broken Conductor Loads on Transmission Line Structures”, PhD Thesis, University of Wisconsin, Madison, 311 pages.

Thomas, M. B., and Peyrot, A. H., (1982) “Dynamic Response of Ruptured Conductors in Transmission Lines”, IEEE PES, Winter Meeting, pp. 1 - 5.

Tucker, K. B. and Haldar, A., (2006) “Numerical Model Validation and Sensitivity Study of a Transmission Line Insulator Failure Using Full Scale Test Data”, accepted for publication, IEEE Transactions on Power Delivery, 6 pages.

APPENDIX 1

ADINA Modeling Guide

This guide was developed to provide a step-by-step process to create and execute a simple finite element model for dynamic analysis of a transmission line considering insulator and/or conductor breakages. All units are in SI. It is one way to create a conductor model, and includes contact surfaces. More methods may exist, and may prove to be more time efficient; however, this method has proven to be accurate and effective and was used to generate all models in this document. The model created herein is simple in its composition, and can be used as a basis for more complicated models. It is not intended to replace the documentation provided by ADINA with the software package, or to cover more extensive models possible, including towers, but to allow for easy model generation and execution, as specific cases of conductors and the special considerations required are not covered in the ADINA manuals. This guide has been written in great detail so that a new user should be able to take this document and reproduce the results recorded for a simple two-span model. For new models not covered, this document can be used as a step-by-step guide to reduce the possibility of skipping a step in the model creation. These steps will cover:

- Geometry and Materials
- Boundary Conditions and Loads
- Finite Element Mesh
- Contact Surfaces
- Control Parameters (time function, kinematics, etc.)
- Static model execution
- Dynamic model modification and execution
- Analysis of results

Throughout this document, selections from the menu toolbars are enclosed by < >, and windows and selections within windows are enclosed by quotations “ ”. The menu bar is used to open selected windows and perform actions and is displayed as <File – Save As...> for example. In many of the menu items, icons are displayed which coincide with icons on the toolbars. These icons may not reproduce clearly in the document, so referral to the ADINA documentation should be made. Both methods of menu selection (icons or menu bar) perform the same action and are provided where possible. Also, hovering the mouse pointer over a button will display a popup description of the icons function.

Generation of Nodal Coordinates

The first step in model creation is the calculation of the geometry point coordinates used to define the location of each finite element node. For the simple two span model used for this guide, the span length is 300m, sag is 9.71m, conductor tension is 18491N, and the conductor unit weight (using 795 kcmil ACSR Drake as a selected conductor) is 15.97N/m. To model the conductor, the standard conductor sag equation is applied as per Equation A1.

$$S_{MAX} = \frac{WL^2}{8T} \quad \text{Equation A1}$$

where:

S_{MAX} = Maximum conductor sag
 W = Unit weight of conductor (N/m)
 L = Overall length of the span (m)
 T = Conductor Tension (N)

The span is divided into 30 equal elements along the horizontal length of the profile (Figure A1). 30 nodes are adequate for broken conductor analysis (Lapointe, 2003). Each horizontal coordinate has a corresponding sag coordinate value calculated as follows.

$$S_C = (S_{MAX}) - \left\{ \frac{W(L - (2 \cdot H_C))^2}{8 \cdot T} \right\} \quad \text{Equation A2}$$

where:

S_C = Sag node coordinate (y axis)
 H_C = Horizontal coordinate (x-axis)

The portion of the equation “ $L - (2 \cdot H_C)$ ” provides for a new conductor span reduced by the horizontal distance from the first node. For a 300m sample span, the new span for the 50m and 250m nodes (same due to level span symmetry) would be $[300 - 2 \cdot 50 = 200\text{m}]$. The second half of the equation enclosed by $\{ \}$ calculates the sag for this reduced section of conductor, and subtracts this value from the maximum sag, providing the projected vertical coordinate (Figure A1) of the conductor nodes at 50m and 250m. In a spreadsheet, the entire list of 61 sag coordinates for two spans can be easily calculated substituting each horizontal coordinate into Equation A2. Node point 62 (Table A1) is the insulator string, and is 2.12m above node point 31, the insulator/conductor attachment. The ground points, nodes 63-65, are selected as 20m below the conductor level, representing towers that are 22.12m (20m + 2.12m) tall, and are located at 0m,

300m and 600m along the line length. The coordinates, provided in Table A1 can be saved as a text file from the spreadsheet, and imported into ADINA.

Nodal coordinates should be in four columns as shown in the sample Excel spreadsheet displayed in Figure A2. Usage of columns 3 (y) and 4 (z) are required should contact surfaces be required [1]. All nodal coordinates should be included in this file, and saved as a text (.txt) file.

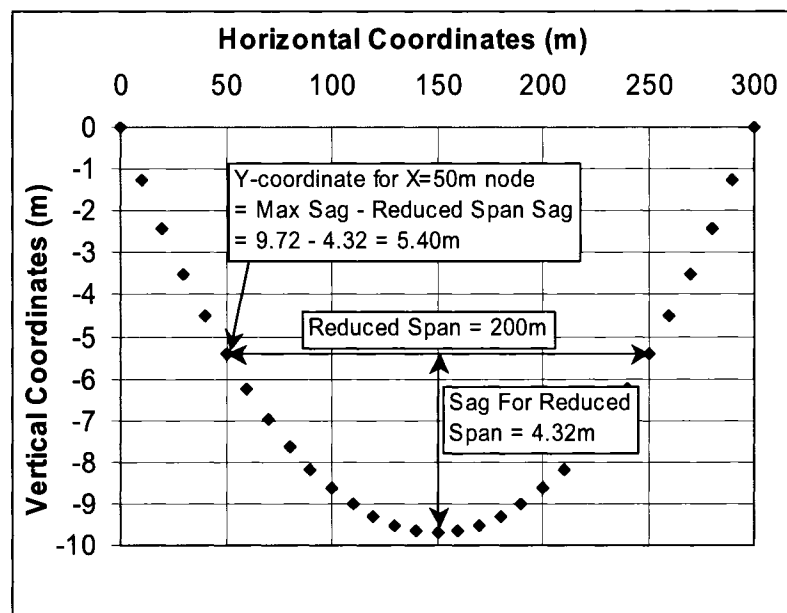


Figure A1 – Sag Node Coordinates for 50m and 250m

Microsoft Excel - Nodes - simple two span model.xls

File Edit View Insert Format Tools Data Window Help

Arial 10 B I U

	A1											
	Node	x	y	z								
2	1	0	0	0								
3	2	0	10	-1.25219								
4	3	0	20	-2.41803								
5	4	0	30	-3.49751								
6	5	0	40	-4.49063								
7	6	0	50	-5.39739								
8	7	0	60	-6.21779								
9	8	0	70	-6.95184								
10	9	0	80	-7.59952								
11	10	0	90	-8.16085								

Figure A2: Excel Spreadsheet with sample model nodes

Table A1 – Nodal Coordinates For Simple Two Span Model

node	x	y	z				
1	0	0	0.0	33	0	320	-2.41803
2	0	10	-1.25219	34	0	330	-3.49750
3	0	20	-2.41803	35	0	340	-4.49062
4	0	30	-3.49750	36	0	350	-5.39738
5	0	40	-4.49062	37	0	360	-6.21779
6	0	50	-5.39738	38	0	370	-6.95183
7	0	60	-6.21779	39	0	380	-7.59952
8	0	70	-6.95183	40	0	390	-8.16085
9	0	80	-7.59952	41	0	400	-8.63582
10	0	90	-8.16085	42	0	410	-9.02443
11	0	100	-8.63582	43	0	420	-9.32668
12	0	110	-9.02443	44	0	430	-9.54258
13	0	120	-9.32668	45	0	440	-9.67212
14	0	130	-9.54258	46	0	450	-9.71530
15	0	140	-9.67212	47	0	460	-9.67212
16	0	150	-9.71530	48	0	470	-9.54258
17	0	160	-9.67212	49	0	480	-9.32668
18	0	170	-9.54258	50	0	490	-9.02443
19	0	180	-9.32668	51	0	500	-8.63582
20	0	190	-9.02443	52	0	510	-8.16085
21	0	200	-8.63582	53	0	520	-7.59952
22	0	210	-8.16085	54	0	530	-6.95183
23	0	220	-7.59952	55	0	540	-6.21779
24	0	230	-6.95183	56	0	550	-5.39738
25	0	240	-6.21779	57	0	560	-4.49062
26	0	250	-5.39738	58	0	570	-3.49750
27	0	260	-4.49062	59	0	580	-2.41803
28	0	270	-3.49750	60	0	590	-1.25219
29	0	280	-2.41803	61	0	600	0.0
30	0	290	-1.25219	62	0	300	2.12
31	0	300	0.0	63	0	0	-20.0
32	0	310	-1.25219	64	0	300	-20.0
				65	0	600	-20.0

Start ADINA-AUI

Start the ADINA-AUI Program. Ensure that the “Program Module” is set on ADINA (white bar on the lower left hand side of the default toolbar sets) and the “Analysis Type” (next white bar to the right) is set on Statics (Figure A3). This initial model will be created for a static analysis; however, with small modifications, it can be subsequently updated for a dynamic model.

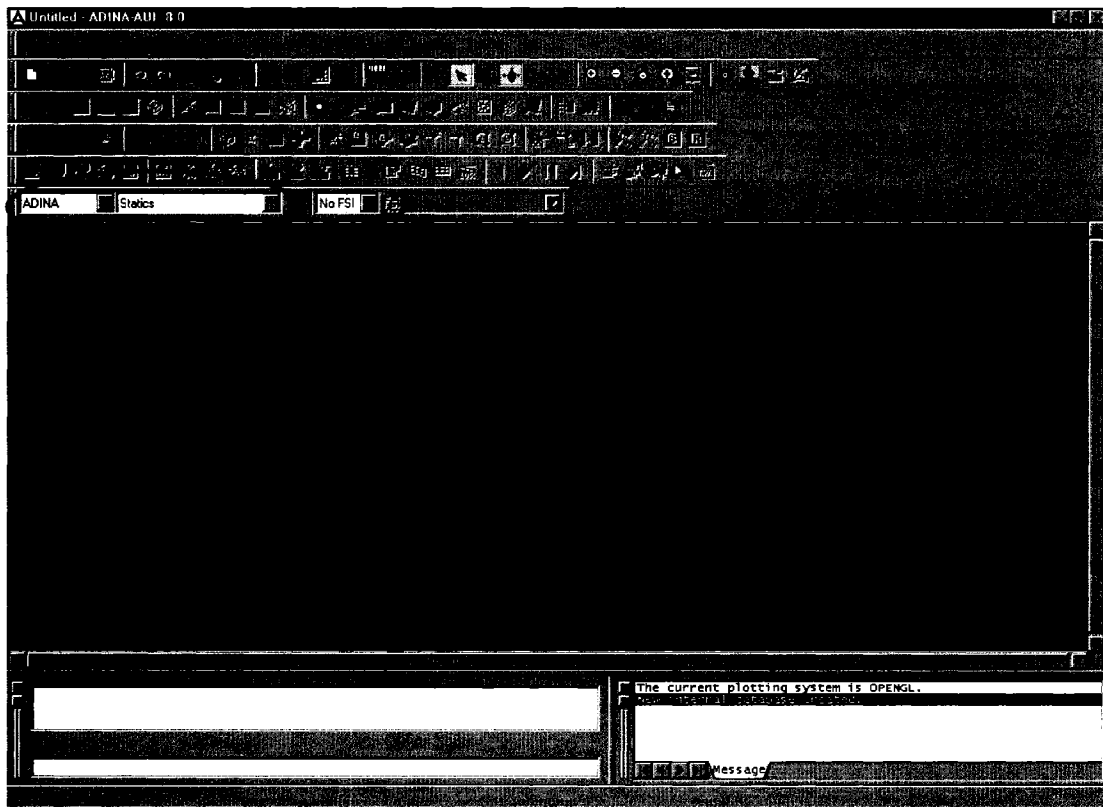



Figure A3 – Adina AUI Opening (Primary) Screen

Before you begin, click  or <File-Save> to provide an initial file name. Spaces and standard restricted characters are not permitted in file names. Also, ADINA can only

handle a limited number of nested directories, so the directory the file is saved in should not be nested too deeply from the root directory. If the directory name is too long, a Microsoft Windows error may occur during file execution. The problem heading should be defined as it will appear on all model output files; however, it is not required. To do this, select <Control-Heading> (Figure A4). A descriptive title should be added and click OK to accept.

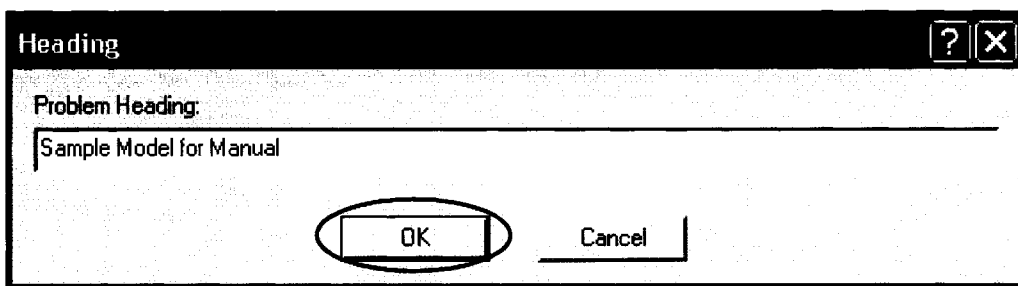



Figure A4 – Problem Heading

Import Nodal Coordinates

Select  or <Geometry-Points...> on the Primary screen. The “Point Coordinates” screen will pop up (Figure A5).

Click the “Import” button. A file “Open” screen will display (Figure A6). Using normal file navigation techniques, find the text file in which the nodal coordinates were saved from the sag node generator Excel file or another text file used to store nodal coordinate information. Select this file and click open.

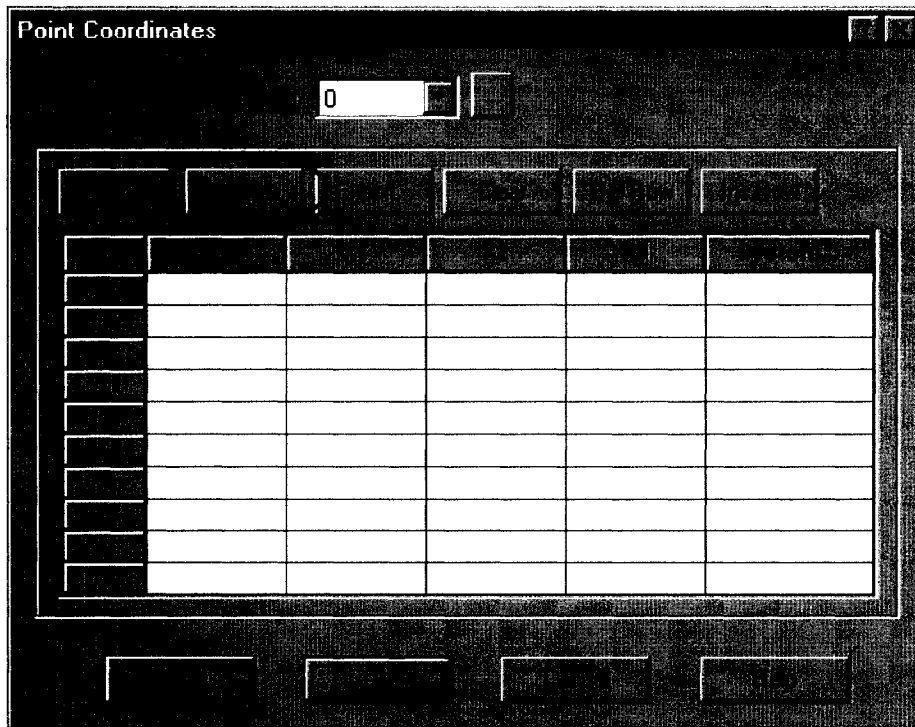


Figure A5 – Point Coordinates Window

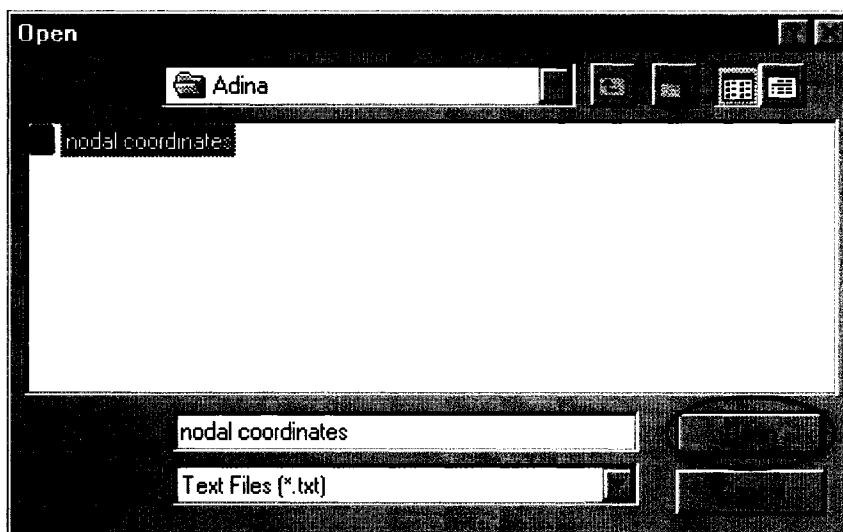
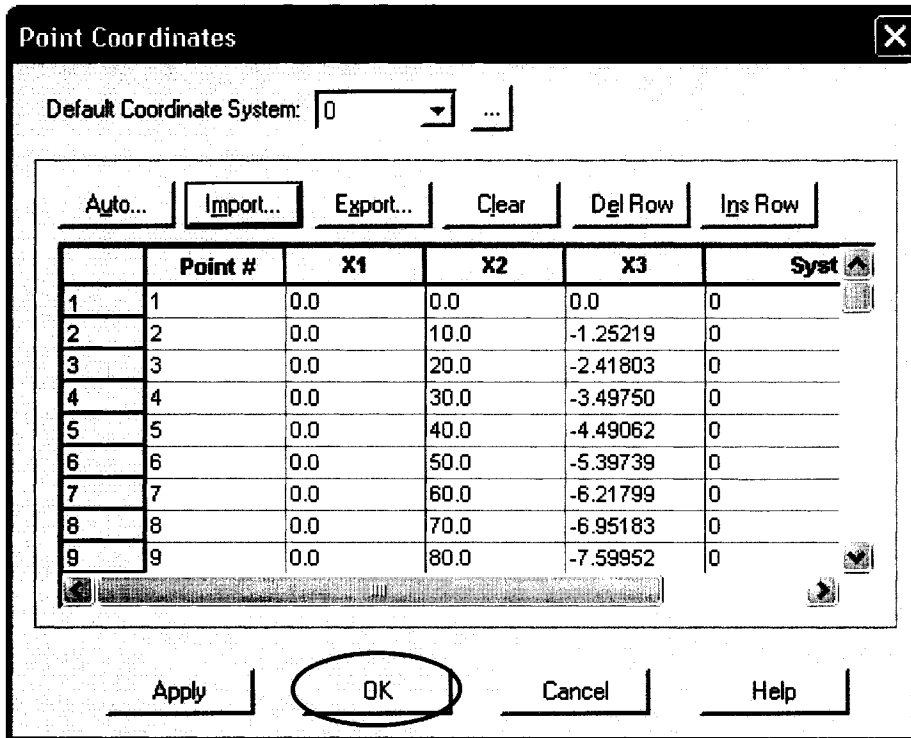


Figure A6 – File Open Window

This will import all coordinates for the numerical model. Check the point coordinates listing (Figure A7) to ensure that all required information is included. As stated


previously, for models using contact surfaces, the Y-Z coordinate axis is required. Therefore, all coordinates are in the X2 (Y) and X3 (Z) columns.



The image shows a software window titled "Point Coordinates" with a close button (X) in the top right corner. At the top, there is a label "Default Coordinate System:" followed by a dropdown menu showing "0" and a button "...". Below this is a row of buttons: "Auto...", "Import..." (highlighted with a black border), "Export...", "Clear", "Del Row", and "Ins Row". The main area contains a table with 6 columns: "Point #", "X1", "X2", "X3", and "Syst". The table has 9 rows of data. Below the table is a horizontal scrollbar. At the bottom of the window are four buttons: "Apply", "OK" (circled with a black oval), "Cancel", and "Help".

	Point #	X1	X2	X3	Syst
1	1	0.0	0.0	0.0	0
2	2	0.0	10.0	-1.25219	0
3	3	0.0	20.0	-2.41803	0
4	4	0.0	30.0	-3.49750	0
5	5	0.0	40.0	-4.49062	0
6	6	0.0	50.0	-5.39739	0
7	7	0.0	60.0	-6.21799	0
8	8	0.0	70.0	-6.95183	0
9	9	0.0	80.0	-7.59952	0

Figure A7 – Point Coordinates Entry Window

If the coordinates are correct, click OK. Otherwise, make any required changes and then click OK. The main screen should appear with all nodes displayed (Figure A8). Remember to periodically save your work! If the screen does not appear as expected, press F5,  or <Display – Redraw> to redraw the view. Default screen background colours are black; however, they have been modified for print clarity using <Edit – Background Color...> to change the background to “white”, and <Edit – Environment Settings...> to change the remainder of the display to the inverse colour. To distinguish

line definitions and element meshes, it is preferred to leave the screen colours as set by default while creating models.

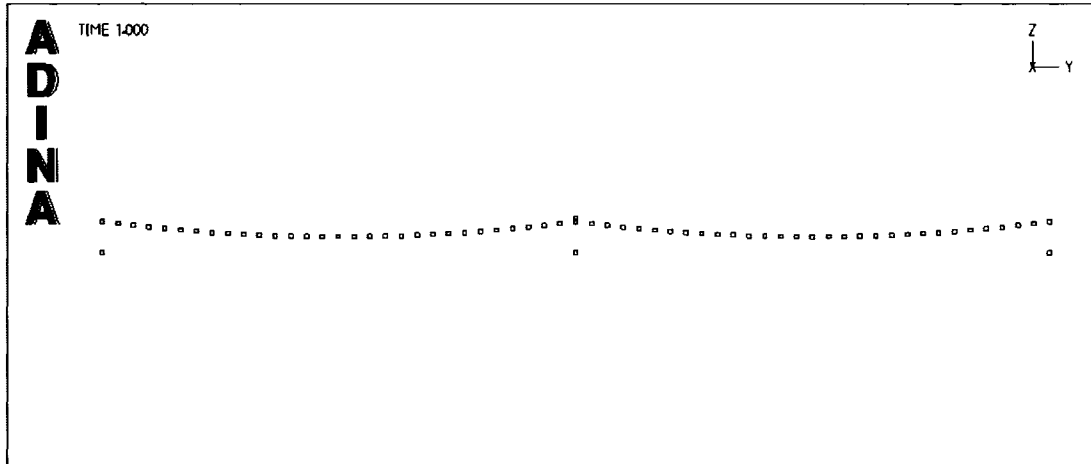



Figure A8 – Adina GUI Displaying Coordinate Points (Graphic Window Only Displayed)

Define Geometry Lines

Select  or <Geometry-Lines-Define> to connect the nodal coordinates. This part of the process is tedious and time consuming as all nodes must be connected in order and in proper sequence. Care must also be taken to ensure that mistakes are not made or the model will not work. This method allows for a death element (discussed later) to be inserted at any location. Also, once generated, the same model can be reused by relocating the same nodes to create different structure elevations or span lengths. Providing the same number of nodes and connectivity of members are used in the new model, coordinates are easily modified.

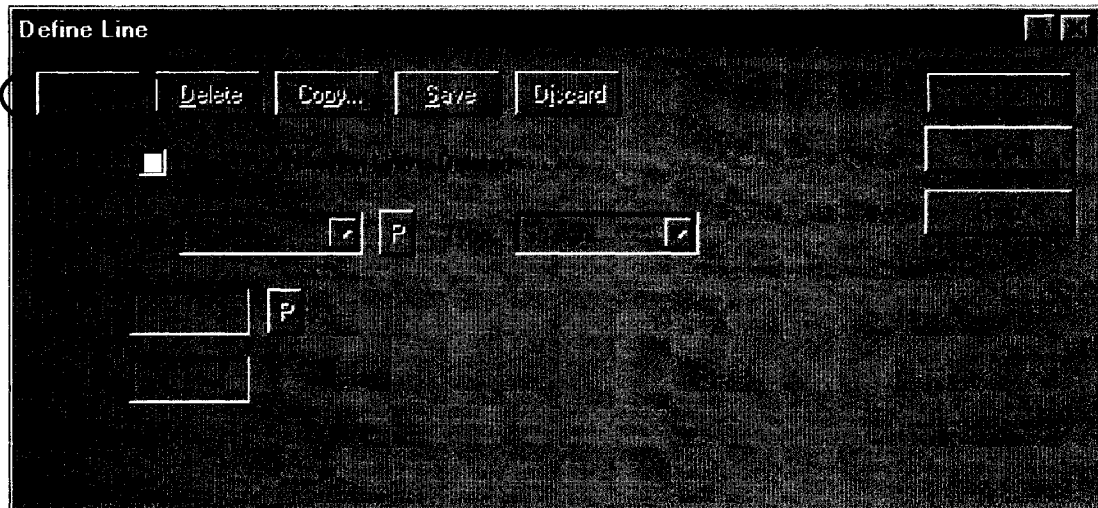


Figure A9 – Define Line Window (*only top half shown*)

Click “Add...” to start the selection process (Figure A9).

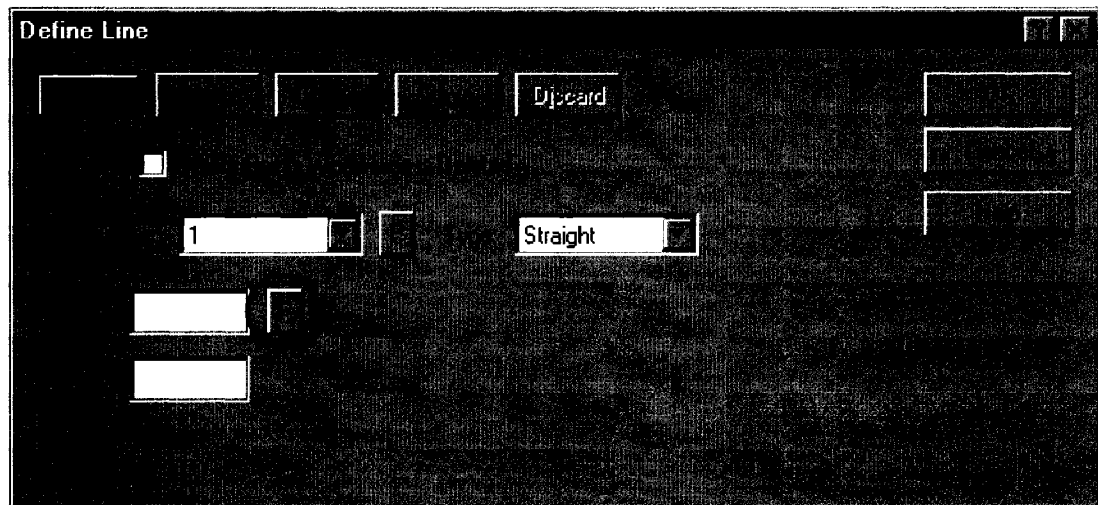


Figure A10 – Define Line Window – New Line 1 Added (*only top half shown*)

The lines are numbered in sequence, starting with line number 1. Click the pick “P” icon to the right of “Point 1” (Figure A10).

This will return you to the main graphic screen from which you can select the first point on the line, in this case the left most node on the conductor (Figure A11).

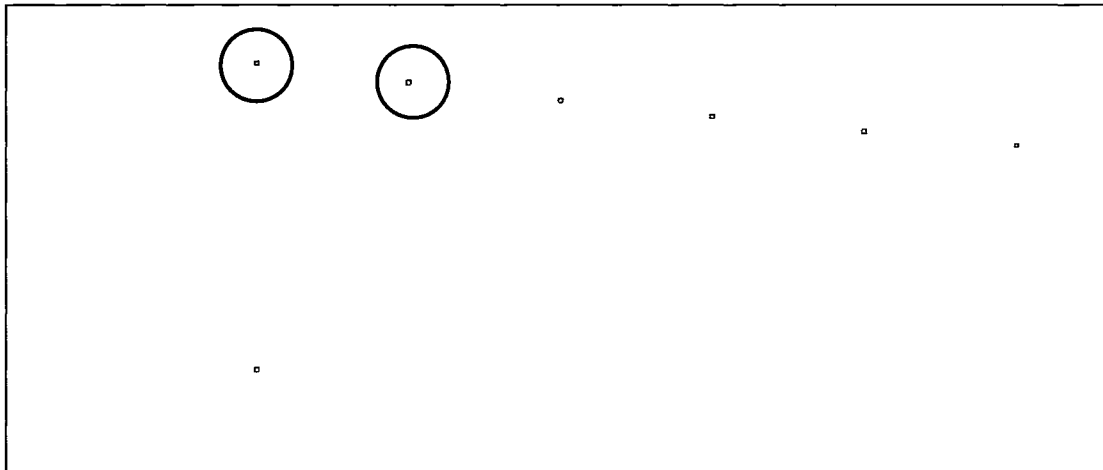



Figure A11: Node Selection (zoomed to first 6 conductor nodes)

This highlights the selected node and turns it white. Select the second node to create the line segment. The selection of the second node reopens the “Define Line” screen, which is now populated with the node numbers for the selected line (Figure A12).

The line will not update on the main screen until OK is selected, or you add another line. OK does not have to be selected until all lines are defined; however, if it is selected, return to  or <Geometry-Lines-Define> to reopen the “Define Line” selection screen. To start another new line segment, click the “Add...” icon again on the Define Line selection screen, and a new line number will display. Continue again with the P icon next to Point 1 to select a new line segment. As each line is completed, they will be displayed on the main screen.

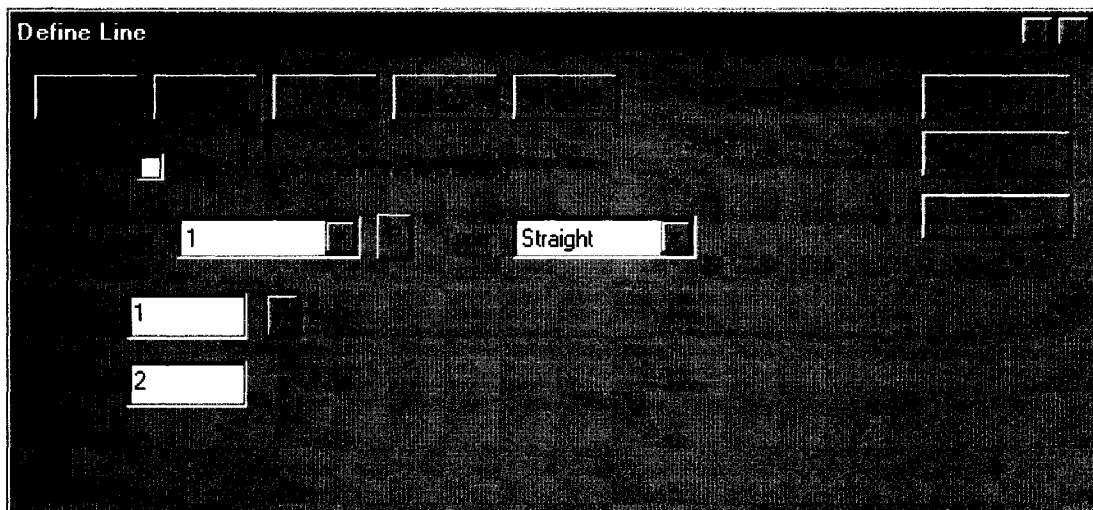



Figure A12 – Define Line Window – Line Points Added (*only top half shown*)

If, during selection of nodal points, the scale is too small, select , the zoom icon, and draw a box around the area of interest by clicking and holding the mouse button on the upper left location of the zoom box window and dragging the window down and to the right to the required size. This cannot be done while selecting node points in the “Define Line” window. Click OK from the “Define Line” screen to close the window and zoom into the area of interest. It is best to only zoom in as little as required, as the scroll bars can be used during point selection, even though the zoom icon cannot. With the zoomed selection available, return to Define Lines.

Define all lines in sequence to make further procedures easier. For the two span, 30 element per span model, define the 60 conductor elements first, from node one to 61, then the insulator element for the centre structure, and finally the ground elements. Note that the ground elements should preferably be defined in the opposite direction of the

conductor selection to make the contact surface, defined later, valid; however, incorrect selection can be corrected later by reversing the contact surface orientation (Figure A37). Therefore, if the conductor lines are selected with the left node first, and then the right node, then the ground must be selected with the right node first, and then the left node. This is required to maintain the opposite directional relationship between the contact surfaces.

With all lines defined, the display should look like Figure A13. In this simple model, towers are not defined.

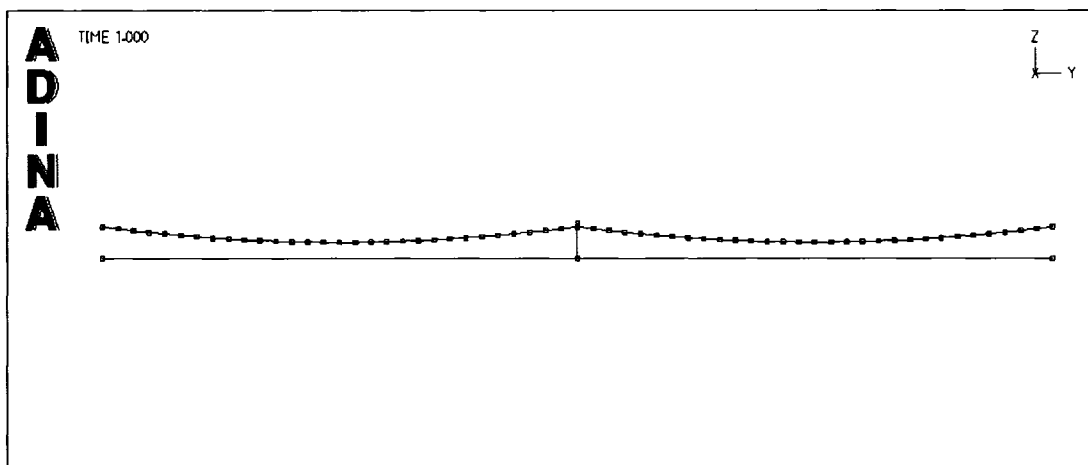




Figure A13 – ADINA AUI – Displaying Geometry Lines

Using the Zoom button , select a region covering half of the first span. Next click on , the “Point Labels” icon, to display the node numbers (Figure A14). Knowing the exact node numbers can be useful in later processes.

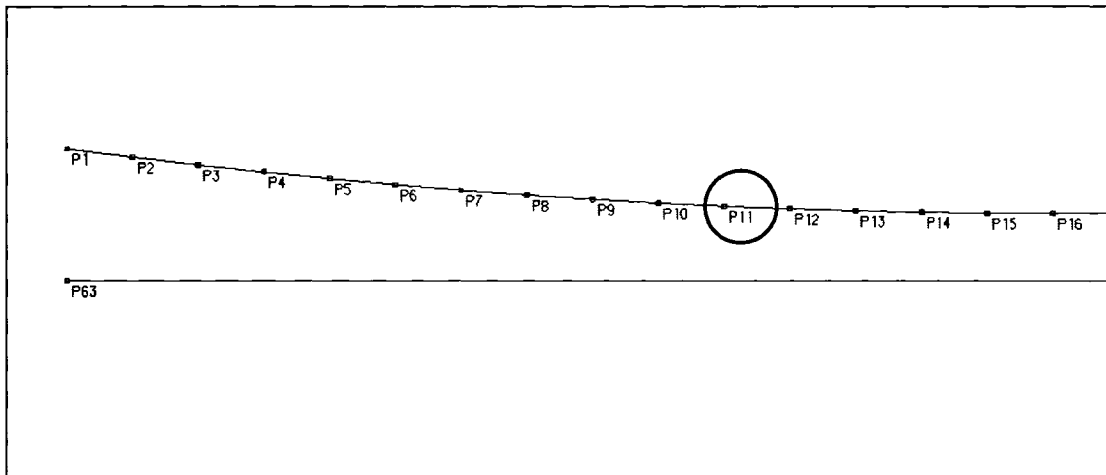




Figure A14 – ADINA GUI – Point Labels Turned On

Turn off the “Point Labels” icon and click , the “Line/Edge Labels” icon to view the geometry line numbers (Figure A15). Note that the directional arrow on the ground segments is opposite to the conductor arrows. This is important for correct contact surfaces defined later. Turn off the line numbers and zoom back out with .

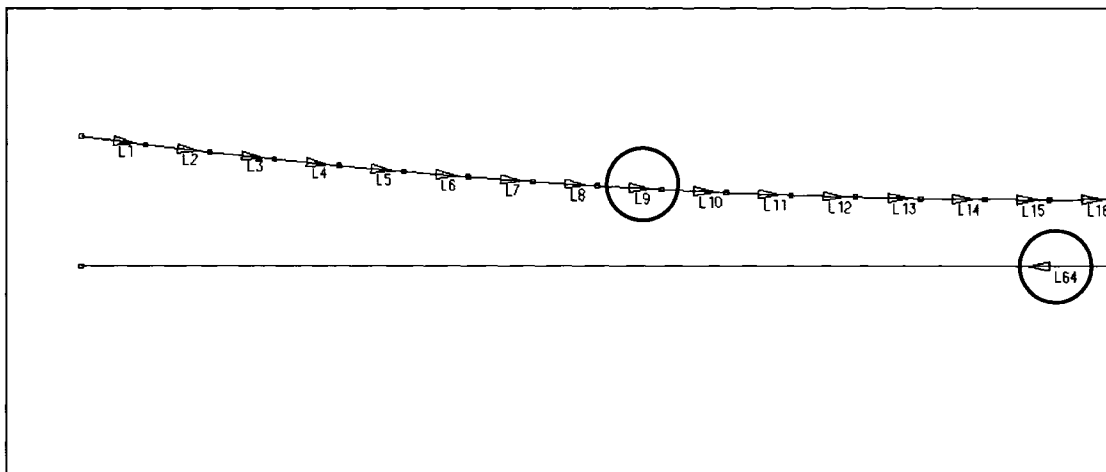



Figure A15 – ADINA GUI – Line Labels Turned On

Material Definition

From the toolbars, click on the “Manage Materials”  icon to display the materials that have been defined for the project. This window (Figure A16) will allow for the creation of any material that will be used in the model.

For the conductor, select “Nonlinear” from the “Elastic” box to open the “Define Nonlinear Elastic Material” window (Figure A17). This menu is used to provide the material definition for the conductor selected for the project. The nonlinear model, through the method of entering a very basic stress strain curve, can be used to restrict the conductor from going into compression. Click “add” to enter a new material, in this case Material Number 1. Using ACSR 795 kcmil Drake as an example, Young’s Modulus is $7.455\text{E}+10$ Pa, and the density is 3465 kg/m^3 . In order to simulate nonlinearity, the stress/strain curve is defined as shown in Figure A17. The density is entered in the appropriate location as well as a description of the material. Other cable elements, such as guy wires, should be entered in this method. The stress and strain values in line 3 provide a Young’s Modulus of $7.455\text{E}10$ Pa. Select OK when finished entering the conductor properties.

Manage Material Definitions [?] [X]

Elastic

Plastic

Thermo

Creep

Creep Variable

Rubber/Foam

Geotechnical

Others

Currently Defined Materials

	Material #	Material Model	Descriptive Name
1			
2			
3			
4			
5			
6			
7			
8			
9			
10			

Figure A16: Manage Materials Definitions

Define Nonlinear Elastic Material

Material Number: Density:

Description:

Stress-Strain Curve

☐ Reference ID

☒ Direct Input

	Strain	Stress
1	-1	0
2	0	0
3	.1	7.455e+009
4		
5		
6		
7		
8		

Figure A17 – Material Definition for 795 Conductor

Select “Isotropic” from the “Elastic” box to enter the insulator and tower properties, which have been simulated as a steel bar and a steel beam respectively. From this menu (Figure A18), clicking add will create a new material number, in this case #2 as the conductor is #1. Enter in the Young’s Modulus, Density and a description of the material as per Figure A18. Additional materials may be added in this way. When complete, select OK to close the “Define Isotropic Linear Elastic Material” window. When finished adding material properties, click “Close”.

Define Isotropic Linear Elastic Material

Add... Delete Copy... Save Discard Put MDB

Material Number: 2 ...

Young's Modulus: 200000000000

Poisson's Ratio: 0

Density: 7850

Coef. of Thermal Expansion: 0

Description: Insulator/Tower Steel

OK Cancel Help

Figure A18 – Material Definition for Steel Members (Insulator/Tower Steel)

Material Geometry Definition – Truss Elements

In the simple model used for this manual, most elements are truss elements, with a beam for the tower model. By going to <Model-Geometry Attributes-Simple Geometry-Truss>, the Assign Truss Properties to Lines menu opens (Figure A20 – at this step, this table is blank) where descriptions of each truss element can be entered. From here, the Line Number is entered, the material number, the cross sectional area, and the initial strain, used for conductor elements. This is also the location where birth and death times are entered into the model (discussed later). For this model, the conductor is modeled with elements 1 to 30 for the first span, and 31 to 60 with the second span. The insulator is element 61. The two line numbers for the ground surface are 62 and 63 and, as they are defined as contact surfaces, are not included in the material definition. The easiest

way to enter in repetitive data is to use the AUTO (Auto Generation) feature (Figure A19). From this feature, the line numbers for a constant material section are entered. The “From Line #” is the first element, in this case 1, and the “To Line #” is the last conductor element, in this case 60. The material number for conductor has previously been defined as 1. The cross sectional area for the 795 conductor is 0.0004684m^2 , and is entered in both the From and To fields. The strain is calculated from the everyday tension as follows:

$$\epsilon = \frac{\sigma}{E} = \frac{\left(\frac{T}{A}\right)}{E} = \frac{\left(\frac{18491\text{N}}{4.68386\text{E}-04\text{m}^2}\right)}{7.45507\text{E}+10\text{Pa}} = 5.2955\text{E}-04 \quad \text{Equation A3}$$

where: ϵ = Strain
 σ = Stress
T = Tension (N)
A = Area (m^2)
E = Young’s Modulus (Pa)

The “Initial Strain” field is just off the displayed screen in Figure A19 and can be accessed using the horizontal scroll bar. The value must be entered in the “From” and “To” rows. All fields not completed will have a default value of “0” entered by the program when “OK” is selected.

Auto Generation

1	1	0.0004684				0.0
60	1	0.0004684				0.0

OK Cancel

Figure A19 – Auto Generation of Conductor Material

Clicking OK gives the following figure, previously seen with no data. All of the conductor elements are now completed. The only other element in this model is the insulator.

Assign Truss Properties to Lines

Del Flow

1	0.0004684	0.0	0.0	0.0	0.00052955	No
1	0.0004684	0.0	0.0	0.0	0.00052955	No
1	0.0004684	0.0	0.0	0.0	0.00052955	No
1	0.0004684	0.0	0.0	0.0	0.00052955	No
1	0.0004684	0.0	0.0	0.0	0.00052955	No
1	0.0004684	0.0	0.0	0.0	0.00052955	No
1	0.0004684	0.0	0.0	0.0	0.00052955	No
1	0.0004684	0.0	0.0	0.0	0.00052955	No
1	0.0004684	0.0	0.0	0.0	0.00052955	No

OK Cancel

Figure A20 – Material Properties for Conductor Members

By scrolling down to the bottom of the Assign Truss Properties to Lines menu, a 61st element can be entered (Figure A21). This element simulates the insulator string by a single truss member. The line number (61) is entered, material number, as defined previously, is number 2, and the section area is assumed to be 0.00064516m². Any cell with no data is again assumed to be zero. Initial strain for the insulator is not required. Click OK when all members are complete. If new truss elements are to be entered at a later date, just go back to this input screen.

Line	Material	Area	Strain	Modulus	Weight	Initial Strain	Initial Modulus
1	0.0004684	0.0	0.0	0.0	0.00052955	No	
1	0.0004684	0.0	0.0	0.0	0.00052955	No	
1	0.0004684	0.0	0.0	0.0	0.00052955	No	
1	0.0004684	0.0	0.0	0.0	0.00052955	No	
1	0.0004684	0.0	0.0	0.0	0.00052955	No	
1	0.0004684	0.0	0.0	0.0	0.00052955	No	
1	0.0004684	0.0	0.0	0.0	0.00052955	No	
1	0.0004684	0.0	0.0	0.0	0.00052955	No	
1	0.0004684	0.0	0.0	0.0	0.00052955	No	
2	0.00064516						

Figure A21 – Material Attributes for Insulator Added

Material Geometry Definition – Beam Elements

For beam elements, the cross section has to be defined. Using the same beam, simulated in the EPRI model, the cross section is 0.632m x 0.632m. To enter this property, select

<Model-Geometry Attributes-Cross-Sections>. Click “Add...” to create a new cross-section (number 1) and enter Width (W) and Height (H) dimensions as per (Figure A22). Click OK to accept the new beam element. Assigning the beam properties to lines is similar to truss property assignment, and is found in <Model-Geometry Attributes-Simple Geometry-Beam>, where data for line, material and cross-section can be entered.

Define Cross Section

Add... Delete Copy... Save Discard OK Cancel Help

Section Number: 1
Type: Rectangular

This cross section can ONLY be used for Hermitian BEAM or ISOBEAM elements.

Dimensions
Width W: 0.632 Height H: 0.632

Torsional Rigidity Factor: 1

Shear Area Factors
s: 0 t: 0


☐ Include Transverse Shear Effects

Offsets from Beam Origin to the Centroid (Used ONLY for Hermitian Beam)
s: 0 t: 0

Diagram: A rectangular cross-section with width W and height H. The horizontal axis is labeled 's' and the vertical axis is labeled 't'.

Figure A22 – Material Cross-Section for Tower

Set Boundary Conditions

Boundary conditions are set using the  icon, or <Model-Boundary Conditions-Apply Fixity>.

Prior to setting the boundary conditions, you have to know what points you want to restrict, and how they should be restricted. By turning on the point labels, described earlier, the points you want to restrict can be easily identified. In this sample model, the deadends are at point 1 and point 61. For all these points, displacement should be restricted; however, rotation should be allowed as these points are pinned connections. Go to the boundary condition input screen and the “Apply Fixity” window opens (Figure A23).

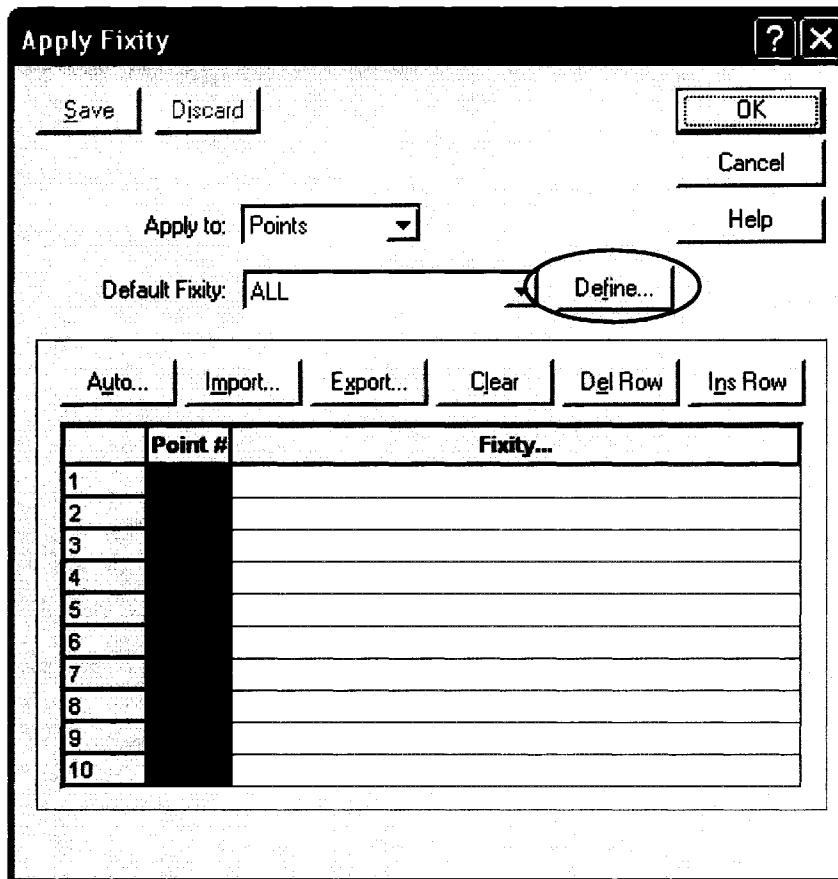


Figure A23 – Fixity Application Window

As pin connections are required (movement restriction, but no restriction on rotation) a new definition should be created. Click on Define to open the Define Fixity dialog box (Figure A24). Click Add to apply a new fixity definition. Enter a name such as PINS and click OK. With the definition named, the Define Fixity box is displayed. For pin connections, the X, Y and Z translation boxes should be selected as shown in Figure A24, with all other boxes left blank. Click OK when done.

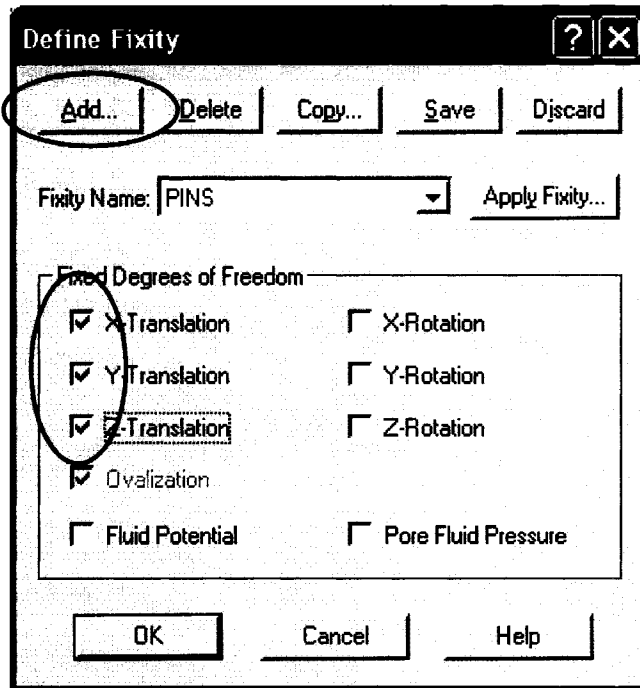


Figure A24 – Fixity Definition Window

With the Applied Fixity window open (Figure A25) for the example model, the pin connection should be placed on nodes 1, 61 (Figure A26 – points denoted as “B”). Enter a 1 in the green “Point #” column in row 1. Click in the white box in the Fixity column next to the cell you just entered and a down arrow selector is displayed to the right of the box. Click this selector and select PINS from the dropdown list. Typing “pins” in the Fixity box will also select the correct fixity definition. The tower is modeled as a cantilever beam, so the base node (#64) should have all degrees of freedom restricted. Therefore, point 64 (centre structure base – Figure A26 – point denoted as “C”) should have a “Fixity” defined as “ALL”. When all points required to have boundary conditions applied are complete, click OK.

Apply Fixity [X]

Save Discard Help OK Cancel


Apply to: Points

Default Fixity: ALL Define...

Auto... Import... Export... Clear Del Row Ins Row

	Point #	Fixity...
1		PINS
2		PINS
3		ALL
4		
5		
6		
7		
8		
9		
10		

Figure A25 – Pin Connections Applied to Nodes

Boundary conditions are shown using the  icon or <Display – Show Boundary Conditions – Default>. This turns on the boundary conditions in the main graphical view screen (Figure A26). As can be seen in the lower right hand side, locations marked with a “B” have X, Y and Z displacement (U_1 , U_2 & U_3) restricted, but X, Y and Z rotation (θ_1 , θ_2 , & θ_3) are allowed, symbolized by a dash and tick respectively. Locations marked with a “C” have all degrees of freedom restricted.

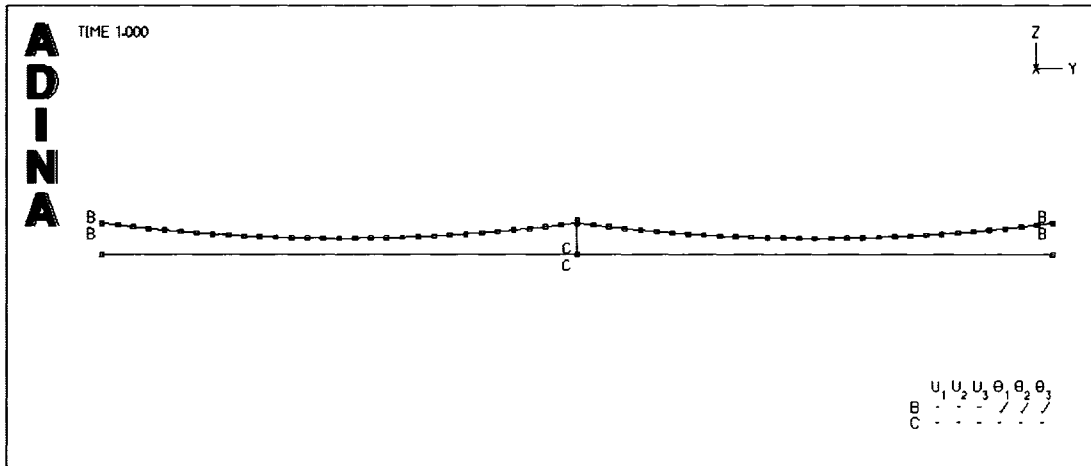



Figure A26 – ADINA AUI Displaying Boundary Conditions

Define Element Groups

The next step is to define what elements are the parts of a group (conductor element group, insulator element group, etc.) so that all elements in that group can be treated as one system. This is the beginning of the meshing process of the model creation. Element groups are defined through , (do not click on the small down arrow, this feature will be defined later) or the <Meshing – Element Groups...> menu item, which opens the Define Element Group dialog box (Figure A27). Click “Add...” to make a new element group 1. The default “Type” is Truss, which is required for conductor elements. The default material is 1, which is the material number previously created for the conductor in the Material Definition section. For conductor elements, the Displacements are set to large. The Numerical Integration order can be left as Default. The Calculated Mass Properties should be set to Yes as the material density was included in the Material Definition section. Finally, Initial Strains should be set to Element Strains Only. This

links back to the initial strains entered into the Material Geometry Definition. The Define Element Group screen for conductor elements should look like Figure A27.

The screenshot shows the 'Define Element Group' dialog box. At the top, there are buttons: 'Add...' (circled), 'Delete', 'Copy...', 'Save', 'Discard', and 'Set'. On the right are 'OK', 'Cancel', and 'Help' buttons. The 'Group Number' is set to 1 and 'Type' is set to 'Truss' (circled). Under 'Element Sub-Type', 'General 3D' is selected. The 'Default Material' is 1. 'Displacements' is set to 'Large'. 'Numerical Integration Order' is 'Default'. 'Calculate Mass Properties' is 'Yes'. 'Initial Strains' is set to 'Element Strains Only'. On the right side, 'All Elements Have Gaps' is unchecked, 'Special Option' is 'None', 'Rebar Label' is 1, and 'Creep Time Offset' is 0.

Figure A27 – Element Group Definition for Conductor

To add the insulator element, click Add to store the conductor element and start a new definition. This will be group 2, and is also Type: Truss. The default Material in this case is 2 as per the Material Definition for insulators. Displacements are large, and the mass properties should be calculated. For insulators, Initial Strains are none. Click Add again to define another group, and change the Type to beam (Figure A28). The format of the “Define Element Group” screen changes to the beam options. Under “Stiffness

Description”, change the “Default Material” to be steel, in this case 2. Click OK to save the element groups.

Define Element Group

Add... Delete Copy... Save Discard Set Help OK Cancel

Group Number: 3 Type: Beam

Element Sub-Type: 2D 3D Numerical Integration Order: r: 5 s: Default t: Default

Stiffness Description: Use Material (plus Cross-Section) Default Material: 2 Use Rigidity Rigidity: 1

Rigid End-Zones: None Defined by Length with Infinite Stiffness Defined by Length with Stiffness Multiplier of 1000000


Rupture Criteria: ADINA User Supplied

Calculated Element Response: Stresses/Strains Nodal Forces

Beam Option: None Bolt Force Tolerance: 0.01 Calculate Mass Properties: Default Displacements: Default Applied Initial Strains: None

Figure A28 – Element Group Definition for Conductor

Apply Load

The only loads applied for a bare conductor are gravity, which has to be defined so that the model can recognize the mass of each member. This is accomplished through the  icon, or <Model – Loading – Apply...>. This opens the “Apply Load” window (Figure A30 – at this step, this table is blank). The “Load Type” for gravitational dead loads

should be selected in the drop down box as Mass Proportional. Select “Define” to enter the values for the Mass Proportional load type. In the “Define Mass Proportional Load” window (Figure A29), select “Add...” to enter a new load definition. The “Mass Proportional Load Number” should default to 1, and the “Magnitude” should be set to 9.81. The “Direction”, given the use of Y-Z coordinates, is specified as -1 in the Z box. “Body Force” is selected by default and should remain the same. Select OK to accept the changes. To simulate ice loads, modification of the conductor density in the material properties can produce the correct loads.

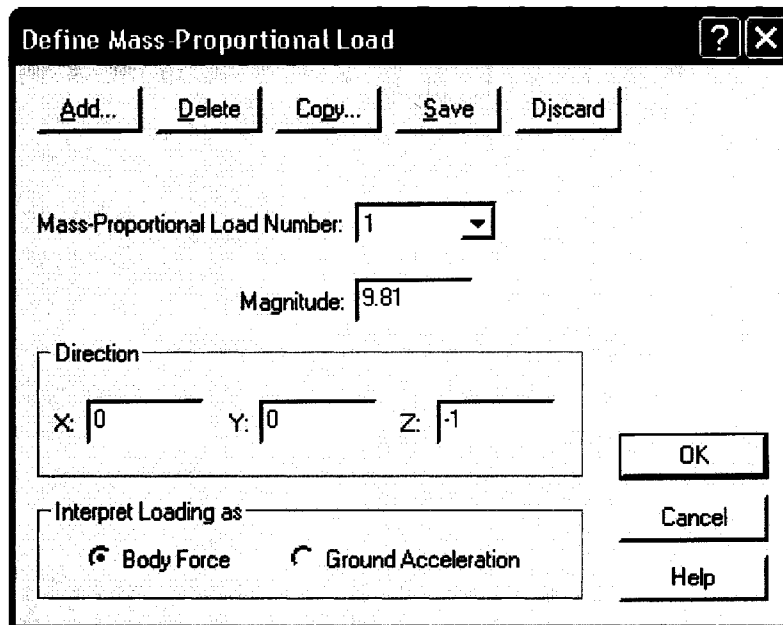


Figure A29 – Mass Proportional Load Details

Back at the “Apply Load” window (Figure A30), enter “Time Function...” 1 in the first row. Select OK. Time Function will be described later in this document.

Apply Load

Load Type: **Mass Proportional** Load Number: **1** Define...

Apply to: **Model**


Clear Del Row Ins Row

	Time Function...
1	1
2	
3	
4	
5	
6	
7	
8	
9	
10	

Apply OK Cancel Help

Figure A30 – Load Application – Mass Proportional

Define Mesh Lines

In order for analysis to be carried out, an elemental mesh has to be developed from the geometrical model now created. To start this procedure, open the mesh creation window (Figure A31) using the  icon, or from the menu bar through <Meshing – Create Mesh – Line>.

Mesh Line

Type: **Truss** Element Group: **1**

Nodal Specification

Number of Nodes per Element: **2**

Auxiliary Point: **P**

Mid-Side Nodes Placed on

☒ Curved Geometry ☐ Straight Line

Nodal Coincidence Checking

Check: **Nodes Generated at End Points**

Participating End Points

☒ End Point 1 ☒ End Point 2

Domain:

Tolerance: **1e-005**

Auto... Import... Export...

Clear Del Row Ins Row

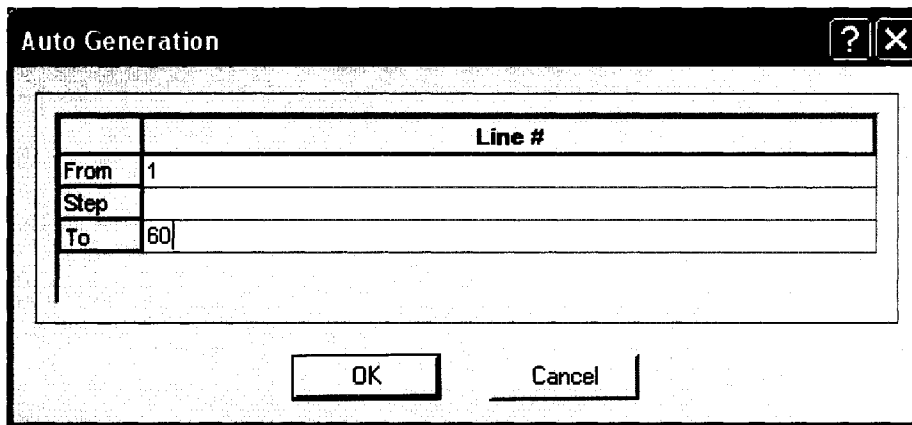
	Line #
1	
2	
3	
4	
5	
6	
7	
8	
9	
10	

Apply Cancel

OK Help

Figure A31 – Default Mesh Generation Screen

The first element mesh to be created is the conductor. The type of mesh for conductor is “Truss”, and the Element Group, as defined previously, is 1. The number of nodes per element is adequate as 2 for the conductor elements. Using the “Auto” feature, the line numbers to apply the mesh to are easily entered. Click “Auto...” to open the “Auto Generation” window (Figure A32).

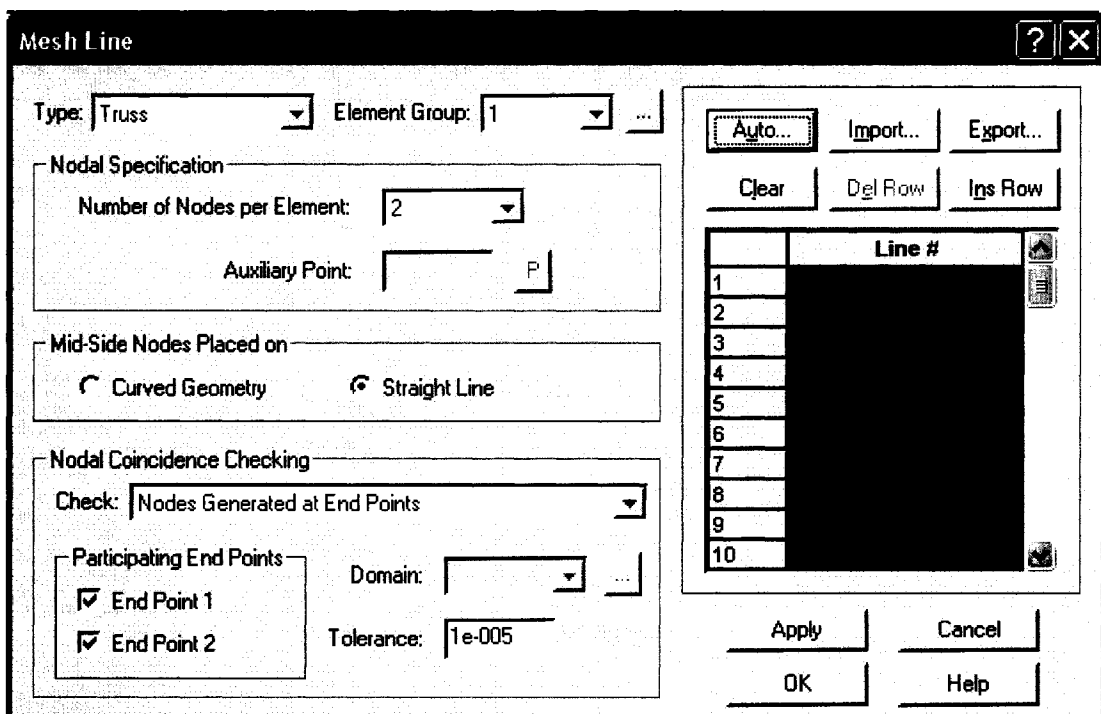


The 'Auto Generation' dialog box contains a table for defining line ranges. The table has a header row 'Line #' and three data rows: 'From' with value '1', 'Step' which is blank, and 'To' with value '60'. Below the table are 'OK' and 'Cancel' buttons.

	Line #
From	1
Step	
To	60

Figure A32 – Auto Generation of Mesh Lines

From here, enter 1 in the “From” row, and 60 in the “To” row. The “Step” default is 1 when this cell is left blank. This will generate line numbers from 1 to 60, which include all of the conductor elements. Click OK to accept the generated numbers.



The 'Mesh Line' dialog box is divided into several sections. The 'Type' is set to 'Truss' and 'Element Group' is '1'. The 'Nodal Specification' section shows 'Number of Nodes per Element' as '2' and 'Auxiliary Point' as 'P'. The 'Mid-Side Nodes Placed on' section has 'Straight Line' selected. The 'Nodal Coincidence Checking' section has 'Check' set to 'Nodes Generated at End Points', 'Participating End Points' checked for 'End Point 1' and 'End Point 2', 'Domain' is blank, and 'Tolerance' is '1e-005'. On the right, there are buttons for 'Auto...', 'Import...', 'Export...', 'Clear', 'Del Row', and 'Ins Row'. Below these is a table with 10 rows, each labeled with a line number (1-10) and a large black rectangular area. At the bottom are 'Apply', 'Cancel', 'OK', and 'Help' buttons.

	Line #
1	
2	
3	
4	
5	
6	
7	
8	
9	
10	

Figure A33 – Conductor Mesh Lines Ready to be Applied to the Model




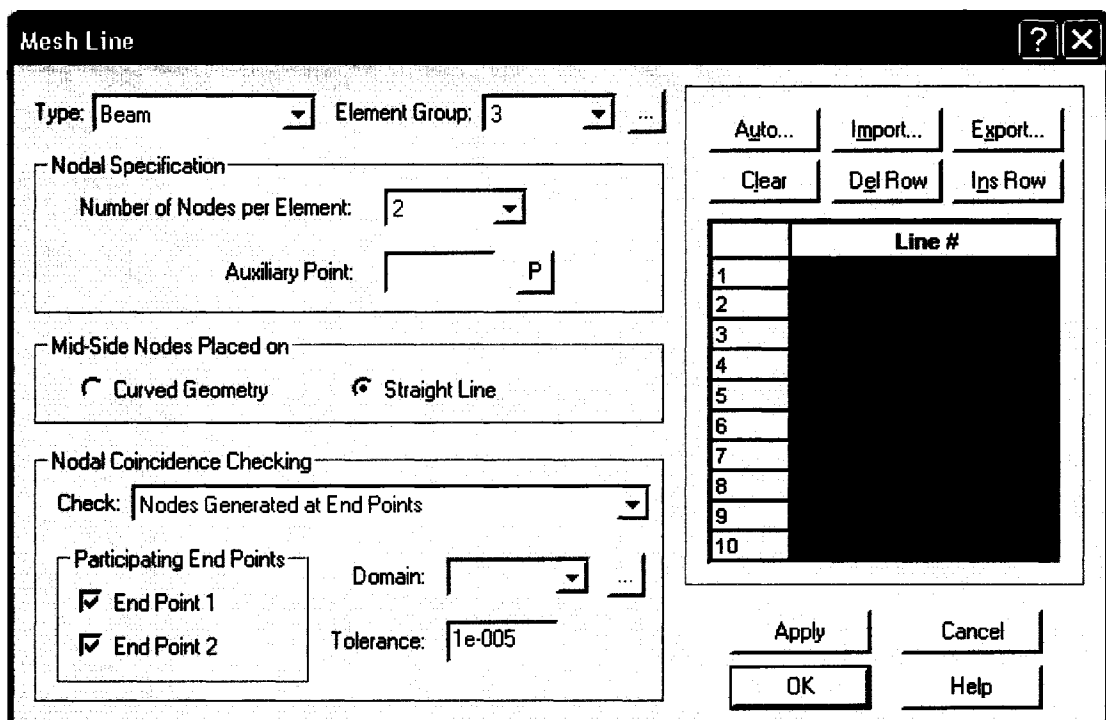
Click “Apply” to accept this mesh. You should notice that the original brown geometry lines (using the default colour set) in the main ADINA-AUI screen have now turned blue to indicate that they are now part of the mesh. Do not reapply the mesh to the lines already meshed. If something was missed, just apply the mesh definition to the neglected lines. To apply the mesh definition to the insulator, select “Clear” above the “Line #” table if required, and enter 2 in the “Element Group”. For this model, the insulator string is element 61; however, if there are more insulators, the Auto feature can be used. In this case, enter “61” in row 1. Select “Apply” to accept this mesh line. Click OK to close the “Mesh Line” window. By using “Zoom”  and turning on the “Node Labels”  and “Element Labels” , the following (Figure A34) will be displayed to show the mesh that has been applied.



Figure A34 – ADINA AUI – Zoomed to Show Applied Conductor and Insulator Mesh in Detail (Node Labels and Element Labels ON – Default colour scheme)


To define the Beam Element, change the Type to Beam, and the Element Group to 3, previously defined as beam elements (Figure A35). Line 62 was previously defined as the tower, and should be entered in the Green “Line #” section. The “Auxiliary Point” has to be defined for this model to orientate the beam in the correct axis. As it was defined as a square cross-section, node 63, just below the first conductor node is entered so that the beam is orientated with the line. Select “OK” to create this mesh element.



Fig

ure A35 – Beam Mesh Line Ready to be Applied to the Model

The mesh density of the conductor elements is defined by default as having only one subdivision. This density is adequate for the conductor, but the ground, which will later have a contact mesh applied, must have a greater mesh density due to the fact that the entire ground surface is modeled by two lines. This is defined in the <Meshing – Mesh

Density – Line> menu, or by selecting the small down box on the right side of the  icon, and selecting “Subdivide Lines”, either of which will open the “Define Line Mesh Density” window (Figure A36). For contact surfaces, the “target”, in this case the ground, must have more nodes than the “contactor”, ie the conductor. Therefore, from here, the two ground elements (#63 & #64 for this model) should have 60 elements selected. Select “Line Number” 63 from the drop box, and change the “Number of Subdivisions” to 60. Do the same for Line 64. When complete, select OK.

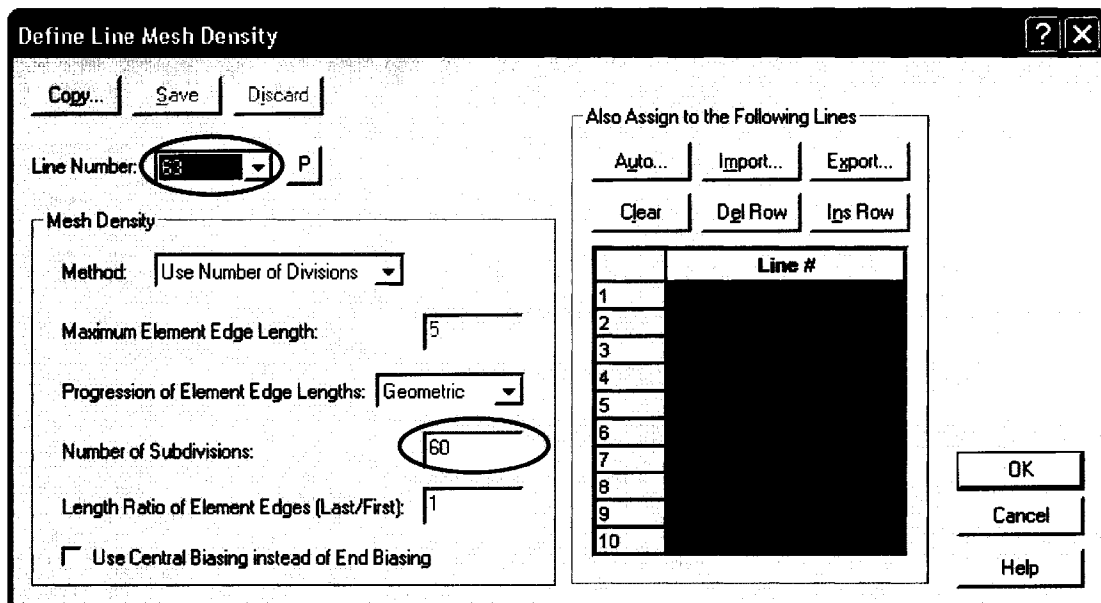


Figure A36 – Mesh Density for Ground Elements

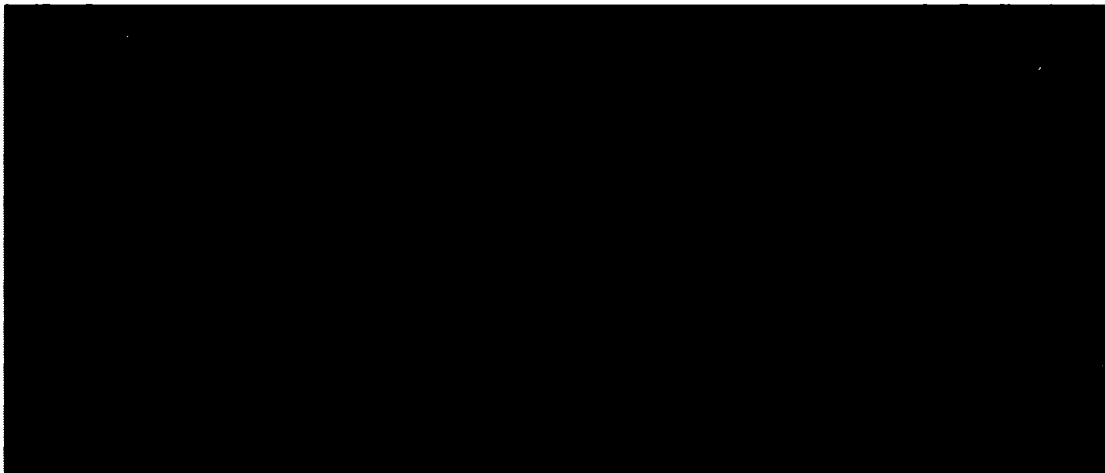



Figure A37 – Mesh Completed and Displayed

The geometrical mesh density is now displayed for the ground (Figure A37). Refresh () may have to be selected to see the line segments, as the program does not always update correctly. Note that only the mesh density has been defined, and an actual element mesh has not been applied to these lines as this mesh is only used for the contact surface definition.

Contact Surfaces

In order to provide for a contact surface between the conductor and the ground, a contact group must be defined. Through these contact surfaces, the opposing elements will not be able to pass and will be restrained against movement through these defined points. To access the contact surface definition, select <Model – Contact – Contact Group>. The “Define Contact Group” window will open (Figure A38). After selecting “Add...”, the only change required to the default selections in the window is the selection of “Planar”

in the “Contact Surface Type” menu box. The following (Figure A38) should be displayed prior to selecting the OK button.

Definition of the Contact Surfaces is now required. This is accessed through <Model – Contact – Contact Surface>. Selecting “Add...” in the “Define Contact Surface” window (Figure A39) creates contact surface 1. Contact Surface 1 will be used for the ground line as defined (in this model) as line 63 and 64. Therefore, “63” and “64” should be entered in row 1 and 2 of the table, and a brief description should be entered in the “Description” field. The window should like Figure A39.

Define Contact Group [?] [X]

Group Number:
 Type:

Contact Surface Type:
 Algorithm:
☐ Node-Node

Description:
☒ Calculate Concentrated Contact Nodal Forces

Default Coulomb Friction Coefficient:
☒ Use Continuous Contact-Segment Normal

Normal Contact w-Function Parameter:
☒ Calculate Average Contact Segment Traction

Frictional Contact v-Function Parameter:
☐ Use User-Supplied Friction

Compliance Factor:
 Use Consistent Contact Stiffness:

Contact Surface Extension Factor:
 Initial Penetration into Target:

Time to Eliminate Initial Penetration:

Contact Surface Action
☒ Single Side
 ☐ Double Side

Penetration Depth:

Contact Surface Offset
☒ Constant
 ☐ Shell Thickness
 ☐ None

Offset Distance from Defined Surface:

Tied Contact (Single-Sided and Small Displacement only)

Option:
 Tolerance:

Default Thermo-Mechanical Coupling Settings

Contact Heat Transfer Coefficient:

Fraction of Frictional Contact Heat Distributed To

Contactor:
 Target:

Default Birth/Death Time

Birth Time:
 Death Time:

Rigid Target Contact Settings

Penetration Tolerance:

Normal Contact Modulus:

Tangential Contact Modulus:

Residual Force:

Limit Force:
 Iteration Limit:

Nodal Pair Vector for Node-Node Contact

☒ Use Normal Vector Inside Target Body

☐ Use Vector Between Target and Contactor Nodes

Figure A38 - Contact Group Definition

To add the conductor as the other contact surface, select “Add...”. This brings up “Contact Surface Number” 2 (Figure A40). Enter “Conductor” in the “Description” field, and click on “Auto” to open the “Auto Generation” window. From here, similar to before, “From” 1 “to” 60 can be entered to auto generate the numbers of the conductor

elements. Select OK in the Auto Generate window to display the completed results for the “Define Contact Surfaces” task. Select OK to accept the contact surfaces.

Define Contact Surface

Buttons: Add... Delete Copy... Save Discard Help OK Cancel

Contact Surface Number: 1

Defined on:

- ☒ All Faces of Body
- ☐ ADINA-M Geometry
- ☐ All Faces of Body

Body #: [] P

Orientation Determined:

- ☒ Automatically
- ☐ from Table Input

Result Print/Save Options:

Print: [Default] Save: [Default]

Description: Ground

Line #	Orientation
1	Same as Underlying Geometry
2	Same as Underlying Geometry
3	
4	
5	
6	
7	
8	
9	
10	

Figure A39 – Contact Surface Definition – Surface 1 (Ground)

Contact Mesh For Ground

The ground contact mesh must be defined through <Model – Contact – Mesh Rigid Contact Surface> from which the “Mesh Contact Surface” window will open (Figure A41). From here, select “Contact Surface” 1 (ground – defined previously) and select OK.

Define Contact Surface [?] [X]

Contact Surface Number:

Defined on:

☒ AUI Geometry

☐ ADINA-M Geometry

☐ All Faces of Body

Body #:

Orientation Determined:

☒ Automatically

☐ from Table Input

Result Print/Save Options:

 Print:

 Save:

Description:

	Line #	Orientation
1		Same as Underlying Geometry
2		Same as Underlying Geometry
3		Same as Underlying Geometry
4		Same as Underlying Geometry
5		Same as Underlying Geometry
6		Same as Underlying Geometry
7		Same as Underlying Geometry
8		Same as Underlying Geometry
9		Same as Underlying Geometry
10		Same as Underlying Geometry

Figure A40 – Contact Surface Definition – Surface 2 (Conductor)

Mesh Contact Surface [?] [X]

Contact Surface:

Contact Group:

Nodal Specification:

 Number of Nodes per Segment:

 Pattern:

Nodal Coincidence Checking:

 Check:

 Tolerance:

Figure A41 – Ground Contact Mesh

The Model should look as shown in Figure A42. If the ground arrows are pointing up, then the ground line definition was selected from left to right and not right to left. To correct this, return to the “Define Contact Surface” window through <Model – Contact – Contact Surface>. In the “Orientation” of “Contact Surface Number” 1, select “Opposite to Underlying Geometry”, instead of “Same as Underlying Geometry” for both ground elements 63 and 64. This should reverse the direction of the contact arrows.

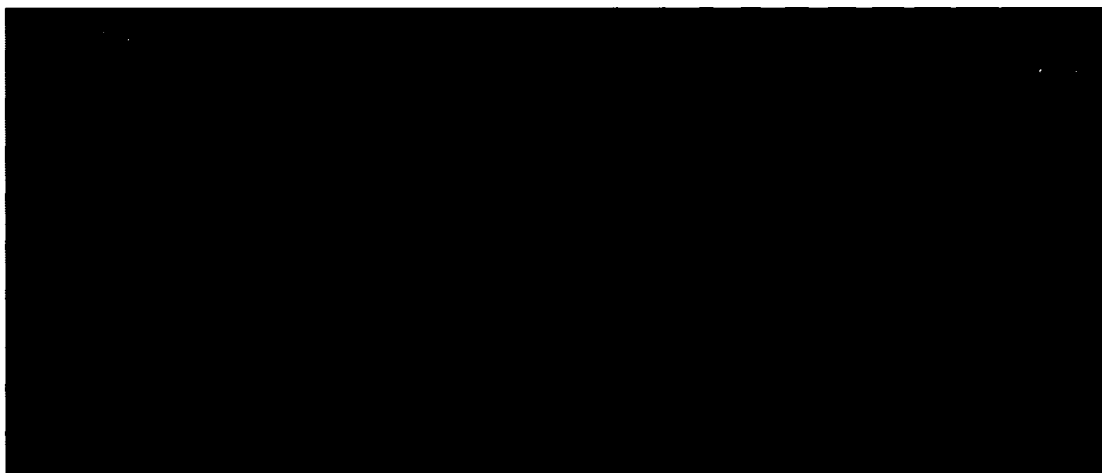


Figure A42 – ADINA AUI – Contact Surfaces and Contact Normals Displayed

Definition of the Contact Pair

With both contact surfaces defined, the relationship between the two surfaces must be established. This is through the definition of the contact pair, which can be located through <Model – Contact – Contact Pair...>. This opens the “Define Contact Pair” window (Figure A43). Click “Add...” to make a new “Contact Pair Number” 1. Using each of the two associated pick “P” buttons (Figure A43), the ADINA-AUI is displayed, from which the ground line mesh is selected as the “Target Surface” and the conductor

mesh as the “Contactor Surface”. When complete, the contact pair window should look as follows. Select OK to accept the changes. The contact definitions are now complete.

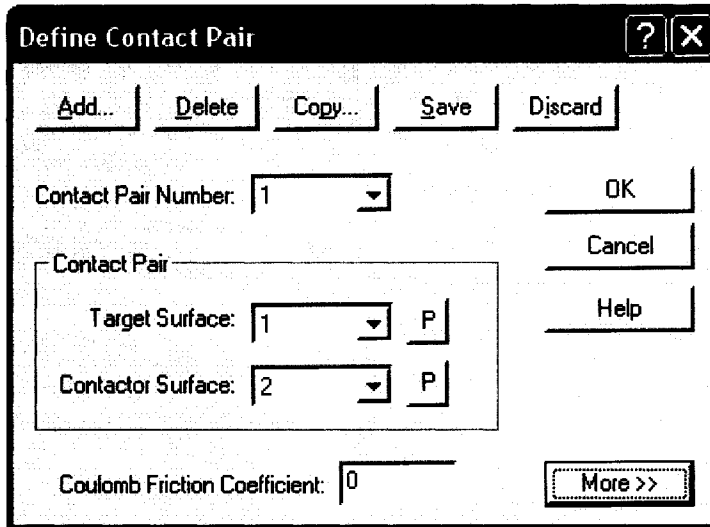


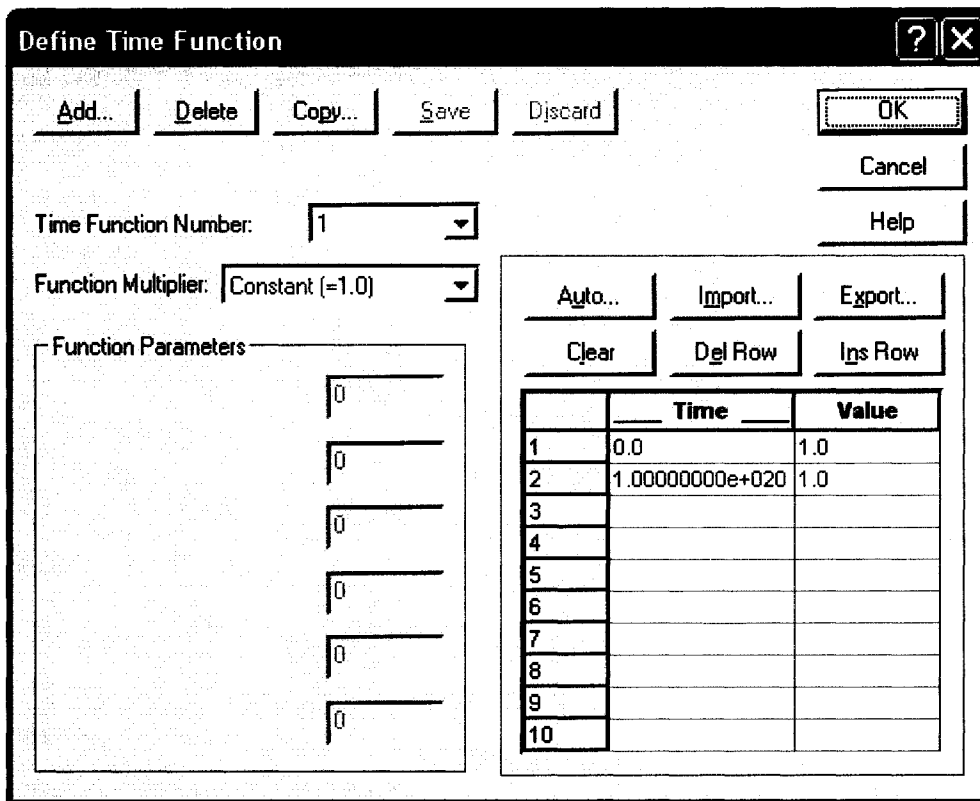
Figure A43 – Contact Pair Defined

Program Control

The final step in completion of this model is the program control exercised during execution. These details are stipulated under the <Control> menu on the menu bar. The first item is the <Control – Heading...>. This should have been completed when the model was first saved.

Time Function / Time Step

Select <Control – Time Function...> to view the “Define Time Function” window. The defaults, as shown (Figure A44), are adequate for this project. This window can be used to reduce the load level, should it be required. For example, for 50% load, the “Value” can be set as 0.5. This function is of value when studying time variable loads such as wind load, where the incremental load can be changed as a percentage of the maximum load. Select OK using the default values for this model.



Define Time Function

Add... Delete Copy... Save Discard OK Cancel Help

Time Function Number: 1

Function Multiplier: Constant (=1.0)

Function Parameters

	Time	Value
1	0.0	1.0
2	1.00000000e+020	1.0
3		
4		
5		
6		
7		
8		
9		
10		

Figure A44 – Time Function Definition

Select <Control – Time Step...> to open the “Define Time Step” window (Figure A45). From here, the number of incremental steps and their magnitude in seconds for which the model takes can be entered. For this static model, the “Number of Steps” has been set to 1; however, this number can be varied. Each of these steps has a “Constant Magnitude” of 1.0 second. Regardless of steps and increment, the overall time should equate to 1 for easy dynamic analysis described later. For static analysis, this is adequate; however, for dynamic analysis, described later, smaller increments and times greater than 1 are required. When finished, select OK.

Define Time Step

Add... Delete Copy... Save Discard Set

Time Step Name: **DEFAULT**

	Number of Steps	Constant Magnitude
1	1	1.0
2		
3		
4		
5		
6		
7		
8		
9		
10		

Auto... Import... Export... Clear Del Row Ins Row

OK Cancel Help

Figure A45 – Incremental Time Steps for Load Application

Select <Control – Analysis Assumptions – Kinematics...> to open the Kinematic assumption window (Figure A46). From here, select “Large” displacements and “Small” strains, as is required for conductor sag models. Select OK.

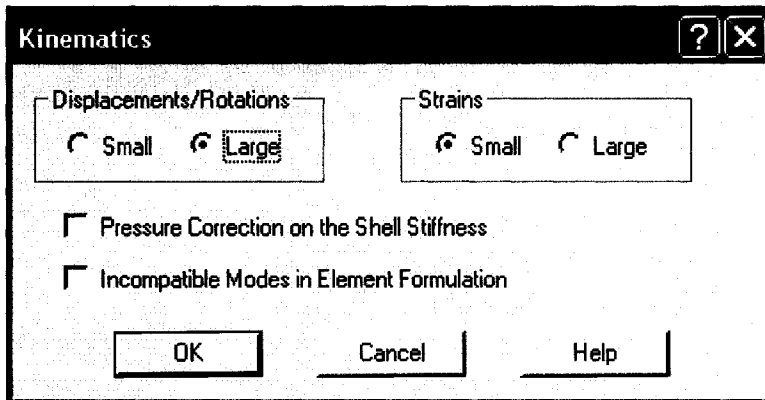


Figure A46 – Kinematics Assumption

Select <Control – Analysis Assumptions – Mass Matrix...> and select “Lumped” (Figure A47). Select OK

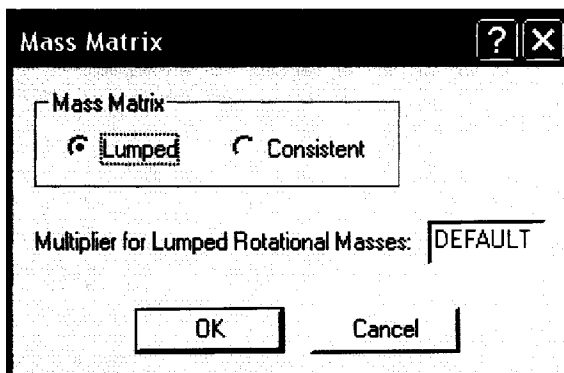




Figure A47 – Mass Matrix Assumption

The static model for two level conductor phases is now complete. Prior to executing the model, ensure that it is saved through , <File – Save>, or <File – Save As...>. To run the model, go to <Solution – Data File/Run...> or click the  icon. In the “Create the

Adina Input File” window (Figure A48), enter the same file name as the model name. This allows for easy identification of all the files created from the same model. As before, no spaces are permitted to be in the file name. Selecting “Save” runs the Adina program module and produces a solution.

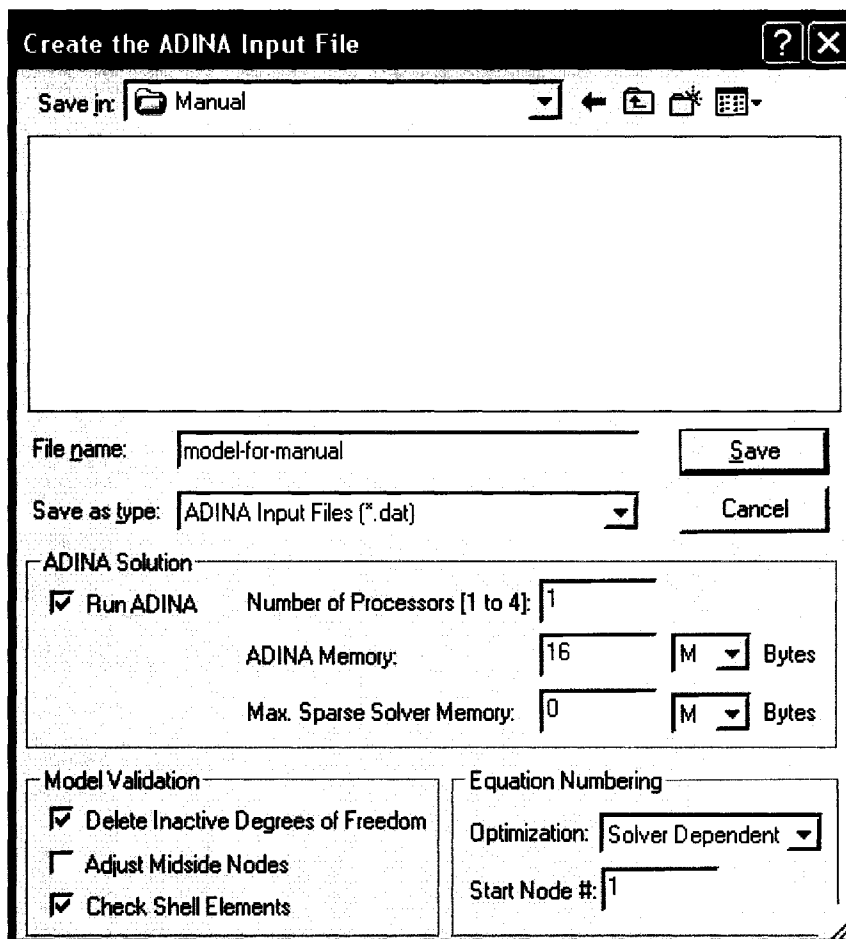


Figure A48– Generation of Adina Input File

If all goes well, the following (Figure A49 – or something like it) should be displayed.

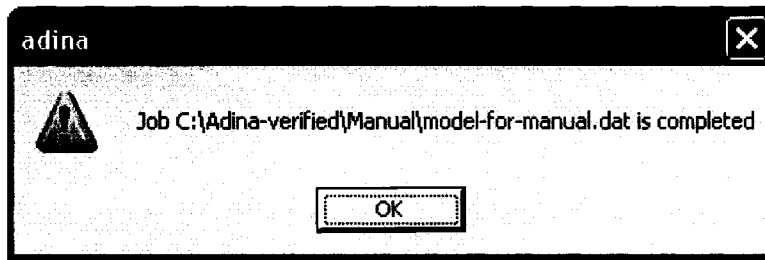


Figure A49 – Success!

If the Job Completed box displays, then the model ran successfully. Click OK to close this box and display the ADINA solution window. This window displays information on each step of the execution, from the checking of prerequisite files to the last step increment and the Job Completed text. The second last line of the text in this window should be displayed as “* Solution Successful, please check the results *”. Select “Close” to exit the ADINA solver program and return to the ADINA-AUI. The “Log Window” displays any warnings issued during execution of the model. Some warnings, such as “No element connection for node 1 directions 4, 5, 6” are normal and can be ignored.

If the Job Completed box does not display, then ADINA encountered a problem running the model. As there are too many possibilities as to what errors may have been encountered, the user should reference the ADINA manuals or the sequence in this manual for error corrections. Usually, an adequate description will be displayed in the “Log Window” to allow the user to identify the problem and go back and correct it.


Dynamic Model – Broken Insulator

When creating a dynamic model, two files are required. The first file is basically the static model created previously, which is used as the base for the second file – the dynamic model. The dynamic file uses a special restart file created during the static model run to continue the analysis. This section of the manual will address what changes are required in the static model, and what is required in the dynamic model to complete the analysis.

Creation of the Dynamic Model

Open the static model created previously. Select <File – Save As...> (not Save, as a new file has to be generated) to create the dynamic file. Add a few characters to the name to identify the dynamic part. In this manual, the static file name is {model-for-manual}, and the dynamic file name is {model-for-manual-dyn}.

Change the “Analysis Type” box from “Statics” to “Transient Dynamics” (Figure A3).

To the immediate right of this box is the “Analysis Options” icon . Selection of this icon opens the “Transient Dynamics” options (Figure A50). Select Implicit Integration and Wilson-Theta as the integration type with Theta=1.4 (default). Select OK.

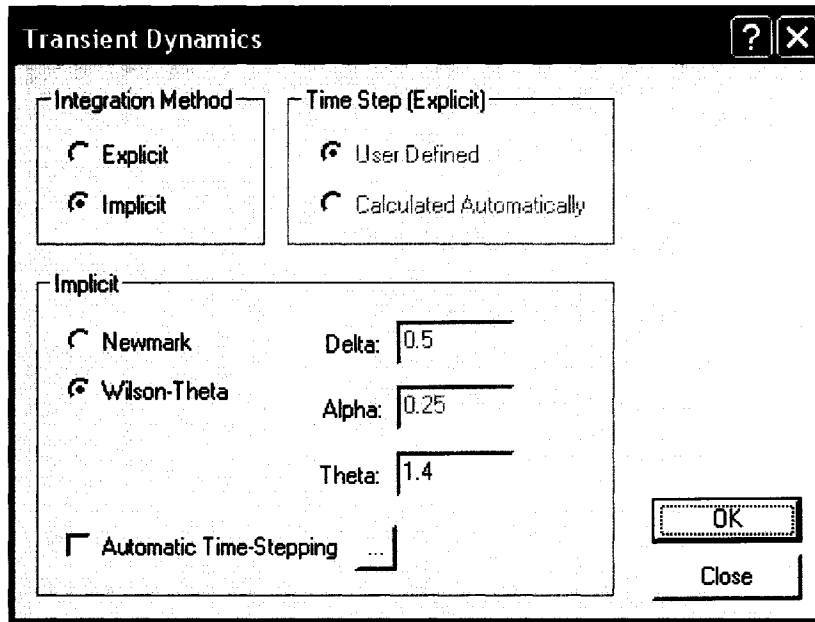


Figure A50 – Transient Dynamics Analysis Options

In order to maintain sufficient resolution in results for a proper analysis, and to have the dynamic model function correctly, a large number of steps are required for a dynamic analysis. Select <Control – Time Step...> and change the “Number of Steps” in row 1 to 3000, and the “Constant Magnitude” to 0.002 seconds (Figure A51). This will provide for an analysis of 6 seconds, in addition to the 1 second used in the static analysis for a total of 7 seconds. 4000 steps with a magnitude of 0.001 would provide a time of 4 seconds. For this analysis, all time steps after failure are one second greater than the actual failure time (failure occurs at 1 second). This is due to the static model being set as 1 second to generate the static output file, and the static restart file; and the dynamic model continues from this point. This can be modified as per user preference to a certain extent; however, sufficiently small increments are required. Automatic time stepping is

available as an option; however, setting a steady time increment makes analysis in standard spreadsheets set up for the job easier.

Define Time Step

Add... Delete Copy... Save Discard Set

Time Step Name: DEFAULT

	Number of Steps	Constant Magnitude
1	3000	0.002
2		
3		
4		
5		
6		
7		
8		
9		
10		

Auto... Import... Export... Clear Del Row Ins Row

OK Cancel Help

Figure A51 – Dynamic Analysis Time Steps

As part of the dynamic analysis, the information from the static analysis, stored in a “restart file” must be added during the analysis. This file holds the conditions of the static model so that the dynamic model can continue using the original conditions of the static model. Select <Control – Solution Process> to open the “Solution Process” window (Figure A52). Set the “Solution Start Time” to 1 (from the static analysis time of 1 second) and turn on the “Restart” box. When finished, select OK.

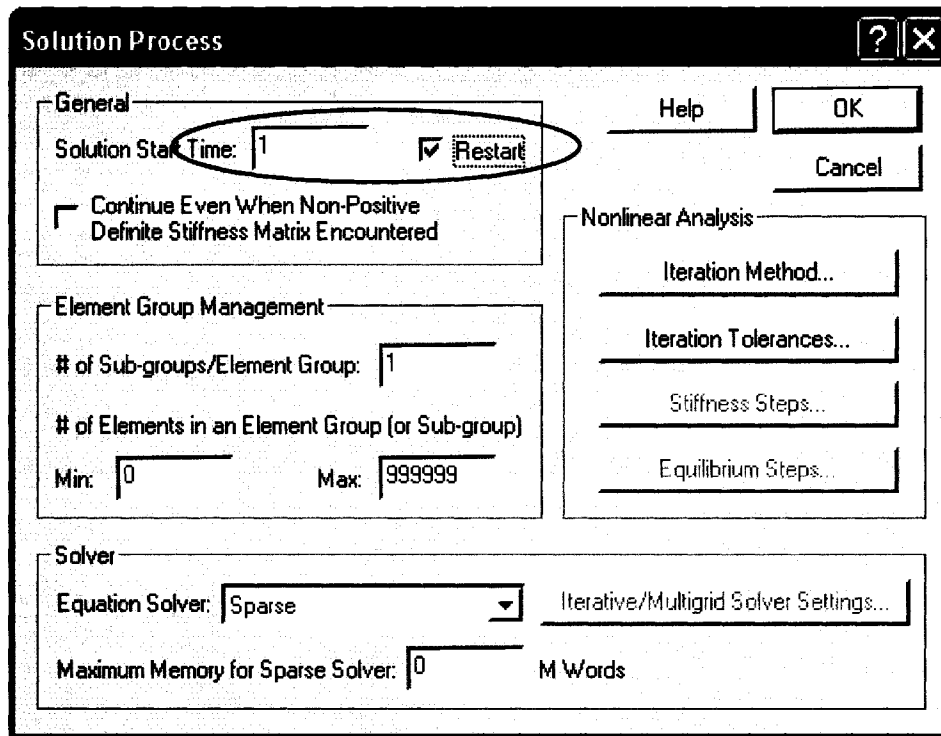


Figure A52 – Solution Process for Restart – Dynamic Analysis

For the dynamic analysis of this model, an element must be assigned a “Death” time. This will initiate the breakage and trigger the motion of the conductor. Select <Model – Geometry Attributes – Simple Geometry – Truss> to open the “Assign Truss Properties to Lines” window (Figure A53). For this model, the dynamic analysis will be a broken insulator, detailed as Line Number 61. Scroll down to line 61 and enter a “Death Time” of 1.002 seconds. This time indicates the removal of the insulator during the first time increment of the dynamic model run. If a broken conductor analysis was required, select the “Line #” corresponding to the conductor element required to be removed. Select OK.

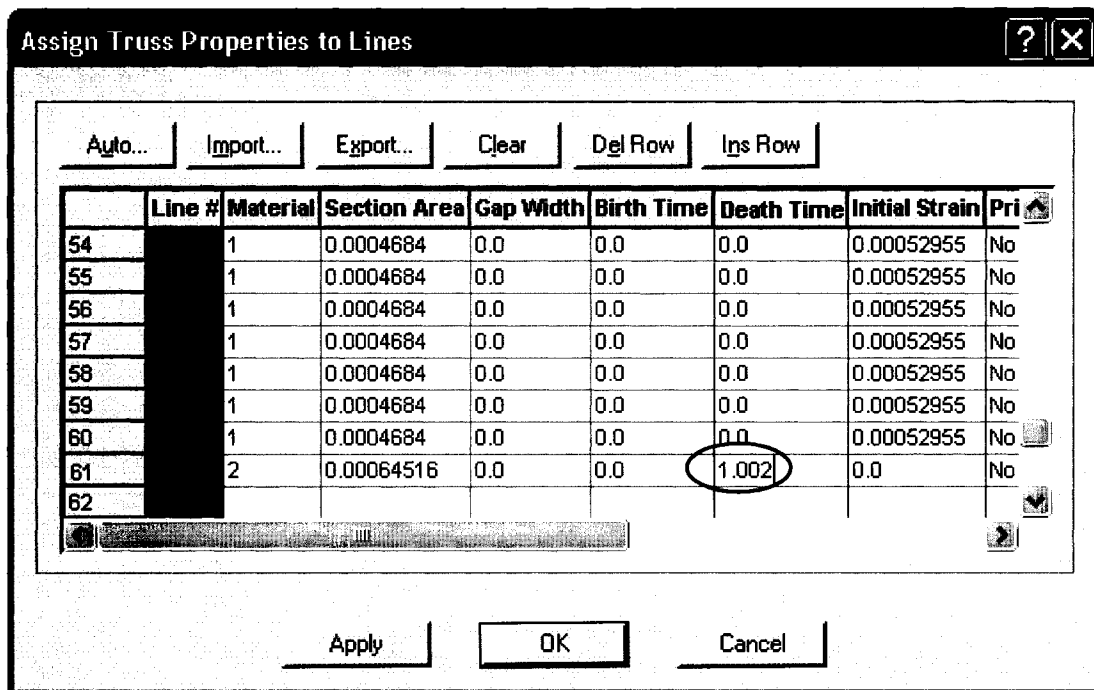



Figure A53 – Detail the Death Element for Failure

The model is now ready to run, and should be saved prior to execution. If not already performed, the static model, from which the dynamic model was developed, should be run first as per the static analysis section to generate the restart file required for the dynamic model run. To run the dynamic file, select  or <Solution – Data File/Run...> and in the “Create the Adina Input File” window provide a file name for the dynamic data file. As before, this should be the same name as the dynamic model name. After selecting “Save”, and providing that there are no errors, a new window will open titled “Specify the Restart File” (Figure A54). There should be a file available with the name of the static model and a .res extension. Depending on previous model runs, the directory containing the restart file may have to be located using standard file navigation techniques. Select the correct file so that it displays in the “File name” box and select

“Copy”. The dynamic file should now execute. Provided no errors are encountered, the “Job Completed” box should display. If a “Restart time mismatch, please check your input data” error occurs, the model has been previously run, and the dynamic model restart file was created. The dynamic model restart file will have to be deleted and the dynamic model rerun in order to complete the process. The dynamic model can only be executed once without deleting the dynamic restart file first, if it is available.

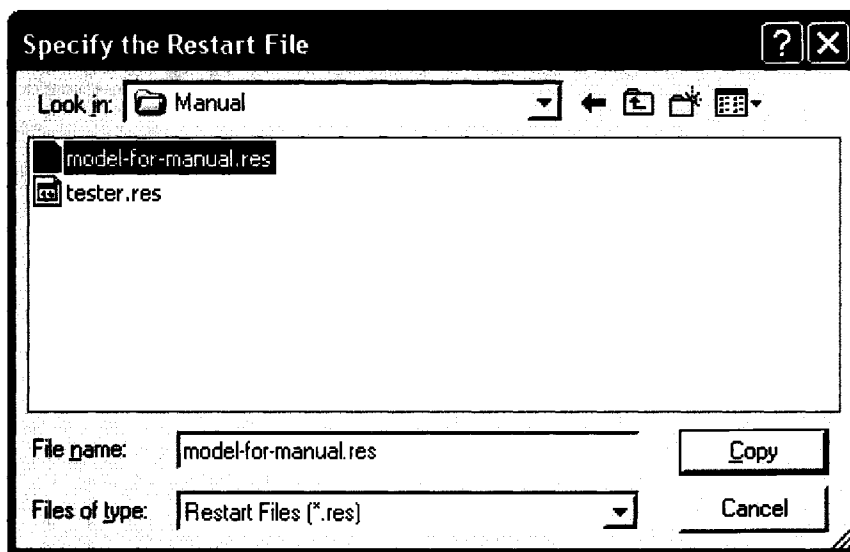


Figure A54 – Selection of Restart File

Analysis

The analysis section of this document only touches on some of the features, which can be used for analysis. For detailed analysis techniques, refer to the ADINA documentation.

After a successful model run, the “Program Module” must be changed in order to access the analysis tools. This is accomplished in the “Program Module” box (white box on lower left side of the default toolbar set – Figure A55) by setting the module to ADINA-PLOT. This sets the mode to post-processing.

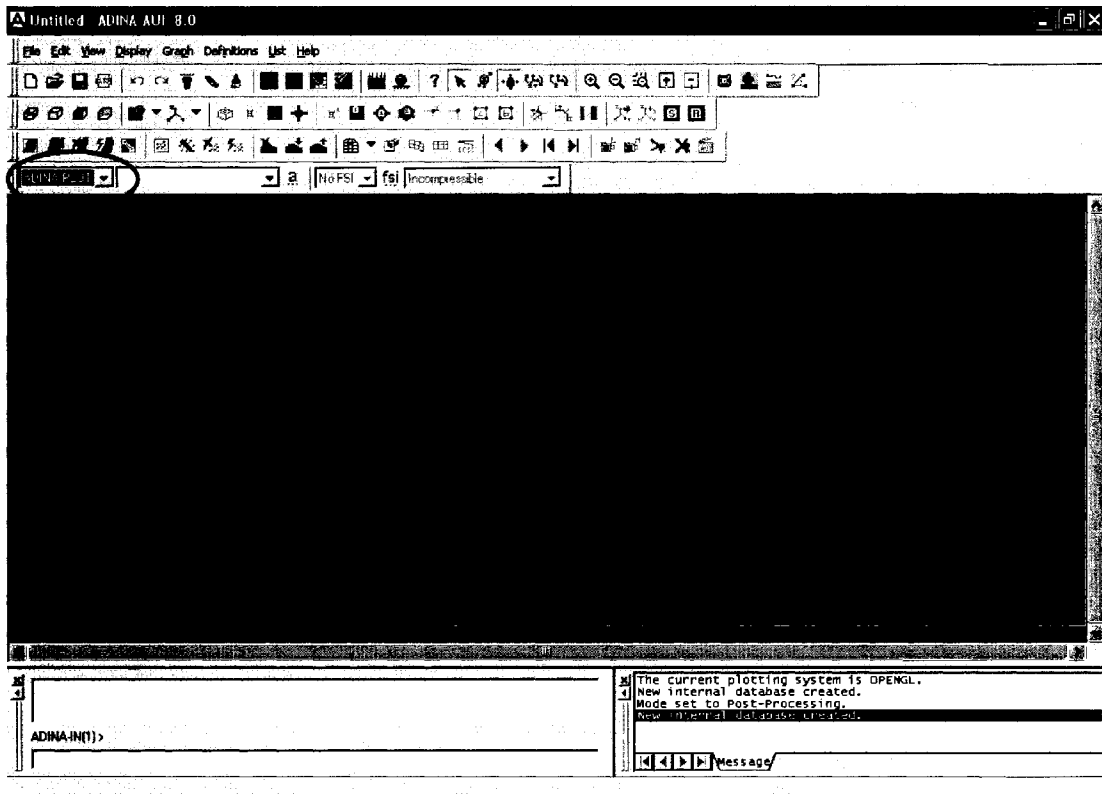



Figure A55 – Program Module Set to ADINA-PLOT

Select <File – Open> or  to retrieve the output file (porthole file - .por) generated during the model run. If only a static analysis was performed, open the porthole file for the static analysis. If a dynamic analysis was performed, then there will be a static and a dynamic porthole file. Typically, the dynamic analysis file will be of interest in this case.

Once the file opens (which may take some time depending on the size of the file), the display window will show the final position of the model after execution. The heavy green lines are the contact surfaces as defined including the contact normals (arrows). Figure A56 shows the super-span created by the failure of the insulator string.





Figure A56– ADINA-AUI View of Dynamic Model Results

To remove the contact surfaces from the view, turn off the “Show Contact Surfaces” (✱) icon, which should remove both (Figure A57). If the contact surfaces are to be shown without the normals, turn off the “Show Segment Normals” icon (↗) only. This shows the actual model elements; however, it does not show the ground elements. Note the tower still standing in the centre where the connection used to be.



Figure A57 – Dynamic Model Results Without Contact Surfaces

To view an animated sequence of the results from each load step, click on , the “Movie Load Step” icon. This shows a real time animated display of the sequence of events for the entire dynamic file.

Graphs of each element can be produced on the main screen. First, clear the graphic display by selecting the clear icon ( - this icon does not reproduce well). Select <Definitions – Model Point – Element> to open the “Define Element Point” window (Figure A58). From here, any element can be identified for individual analysis. Click “Add...” and provide an element name, such as “Mid_Span_Element” (spaces not permitted). For this case, element group 1 is the conductor, and element 30 is the conductor element just to the left of the insulator string prior to failure. Select OK to save this element definition.

Define Element Point

Buttons: Add.., Delete, Copy..., Save, Discard, OK, Cancel

Point Name: MID_SPAN_ELEMENT

Substructure: 0

Reuse: 1

Element Group: 1

Element Number: 30

Element Layer: 1

Defined by: Grid Point

Grid Point: 0

Isoparametric Coordinates: r: 0, s: 0, t: 0

Label Point: 1

Node Number: 1

Figure A58 – Define Element Point for Analysis Purposes

To produce a graph of the response of this element, select <Graph – Response Curve (Model Point)...> to open the “Display Response Curve (Model Point)” window (Figure A59). In the x-coordinate section, the default variable “Time” is ok, and the Model Point has defaulted to “Mid Span Element” as no other elements have been defined. If there are other elements, use the drop arrow to change the selection.

In the Y-Coordinate section, leave the first “variable” as “Displacement”, but change the second default variable from “A-displacement” to “Z-displacement”, and the “Model Point” to “Mid Span Element” if required. This will produce a graph of the falling of the conductor (element 30) from 1 second (failure time) to 17 seconds (total elapsed time).

In the graph attributes section, click on the down box next to “Curve Depiction” and select “Line”. Click OK to display the graph in the ADINA AUI window (Figure A60).

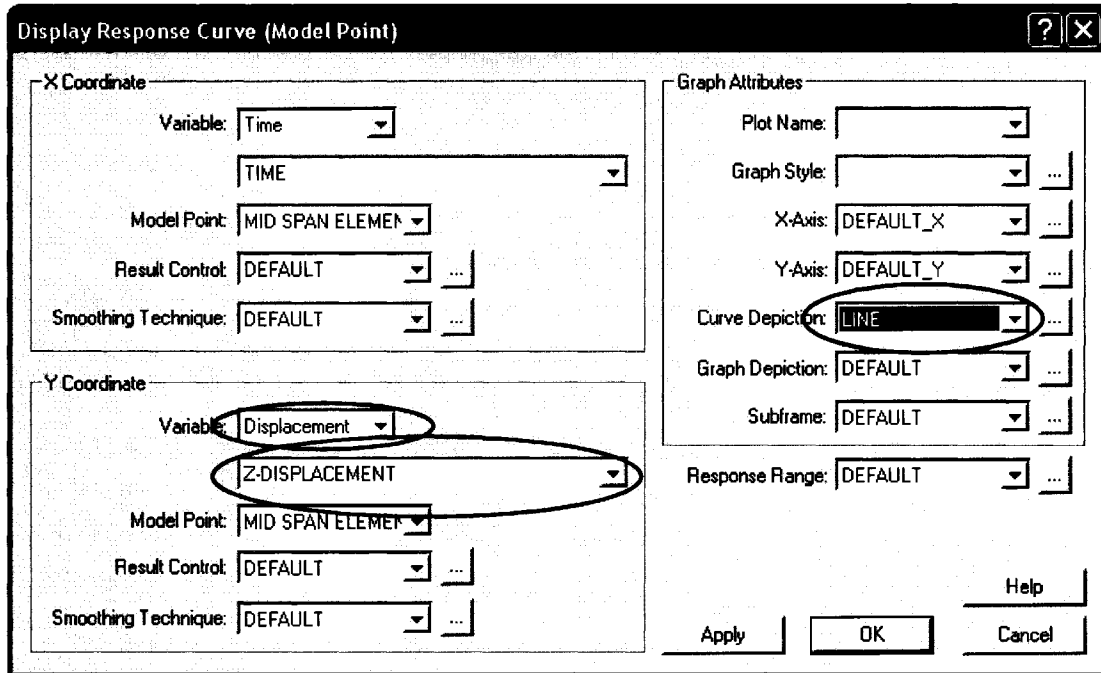


Figure A59 – Display Response Curve (Model Point)

As can be seen in Figure 60, it takes approximately 1.6 seconds (2.6 seconds, minus the one second initial time) for the conductor to hit the ground, after which it rebounds back up a couple of times at 2.8 and 4.8 seconds after failure.

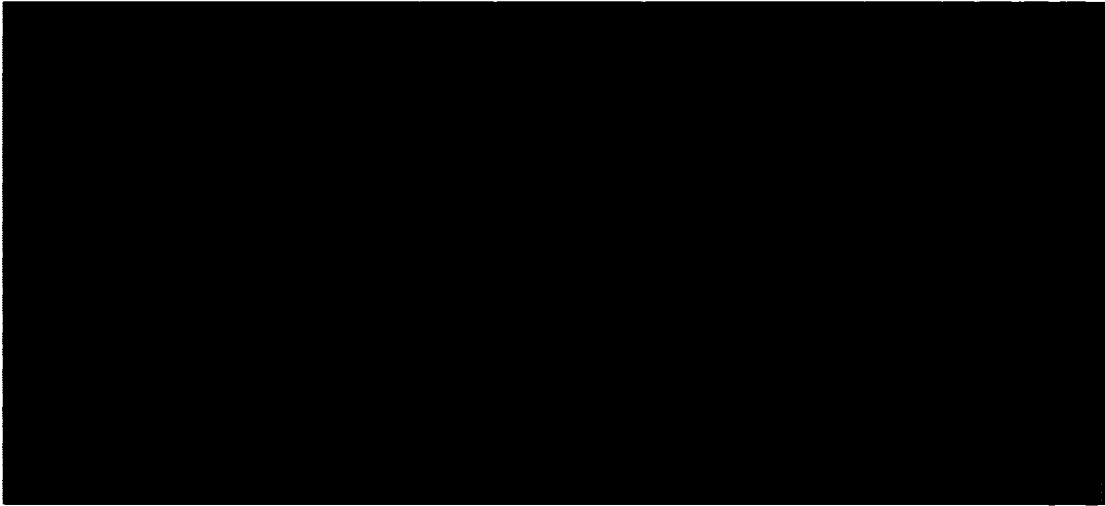


Figure A60 – Displacement of Falling Conductor

To delete the displayed curve, click clear again. To display a curve of tension for the same element, follow the same procedure as for the previous curve; however, the first Y-coordinate variable should be selected using the down box as “Force”, and the variable description should be set as “Force-R” for resultant force (Figure A61). Line is again selected as “Curve Depiction”. Select OK to plot the results.

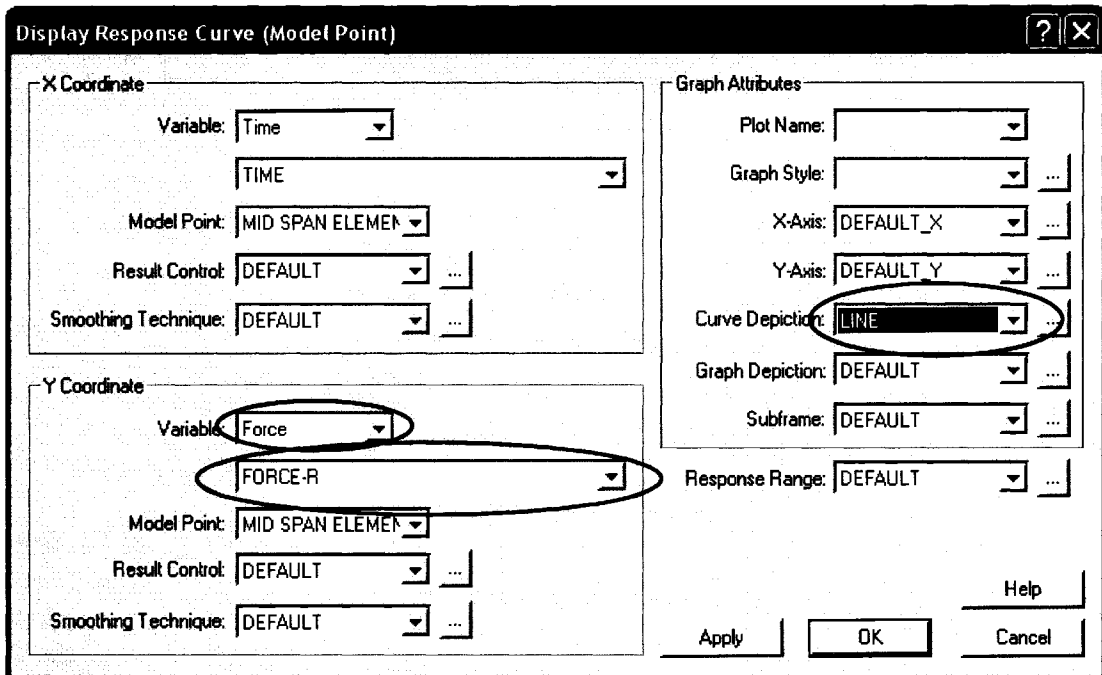


Figure A61 – Variables Changed to Produce Force Curve



Figure A62 – Plot of Conductor Force versus Time

As can be seen from this plot (Figure A62), the initial tension is approximately 18000N, with a maximum spike at 3 seconds (2 seconds after failure) of approximately 62000N.

To find out what these actual values are, select <List – Value List – Model Point> to open the “List Model Point Values” window (Figure A63). From here, select the “Model Point Name” as “Mid Span Element” if it is not the default. In the “Variables to List” section, select “Force” in the first row, left box, and “Force-R” in the Right box of the first row. Click “Apply” to view the data that was used to make the plot in Figure A62. As can be seen, the initial tension is 18612N. Using the “Export...” button, a text file can be created of this data. Scrolling down through the list will provide for the maximum force; however, there is an easier way to find the maximum. Select “Close” to close the “List Model Point Values” window.

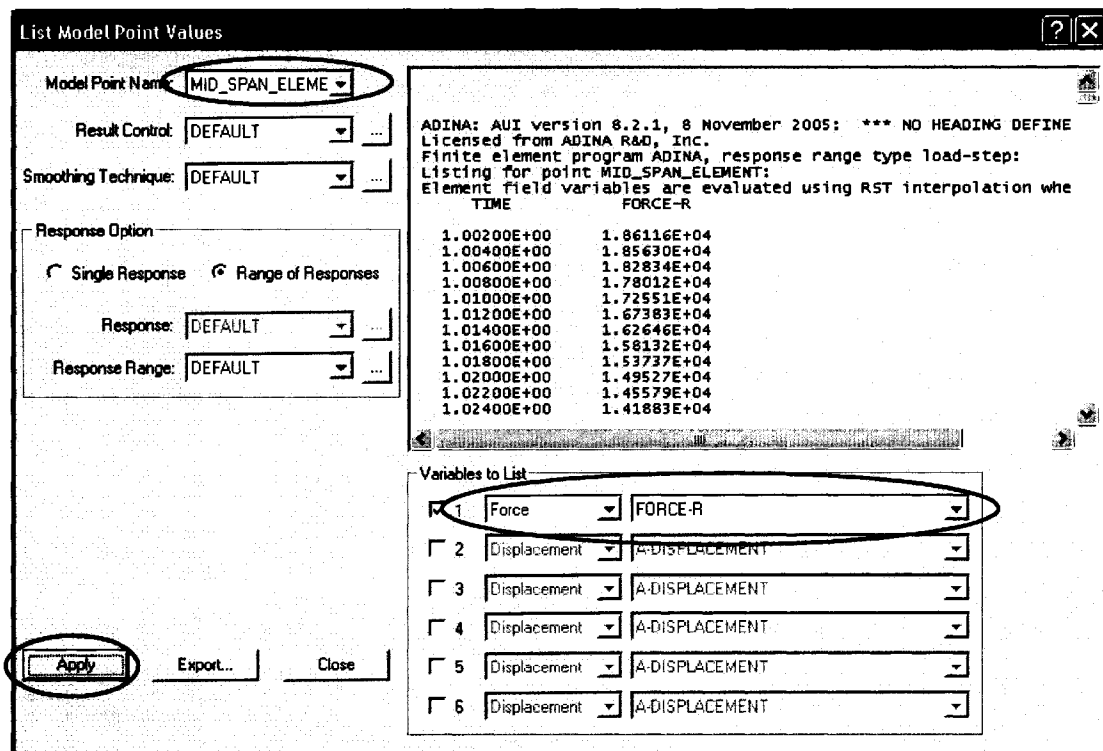


Figure A63 – All Results List Box for Model Point

Select <List – Extreme Values> to open the “List Model Point Extreme Values” window (Figure A64). Similar to the “List Model Point Values” window, select the “Model Point Name” as “Mid Span Element”, and the “Type” as “Absolute Maximum”. The variables to list are again “Force” and “Force-R”. Select “Apply”

The display provides an absolute maximum of 62997.7N at a time of 2.92 seconds (1.92 seconds after failure).

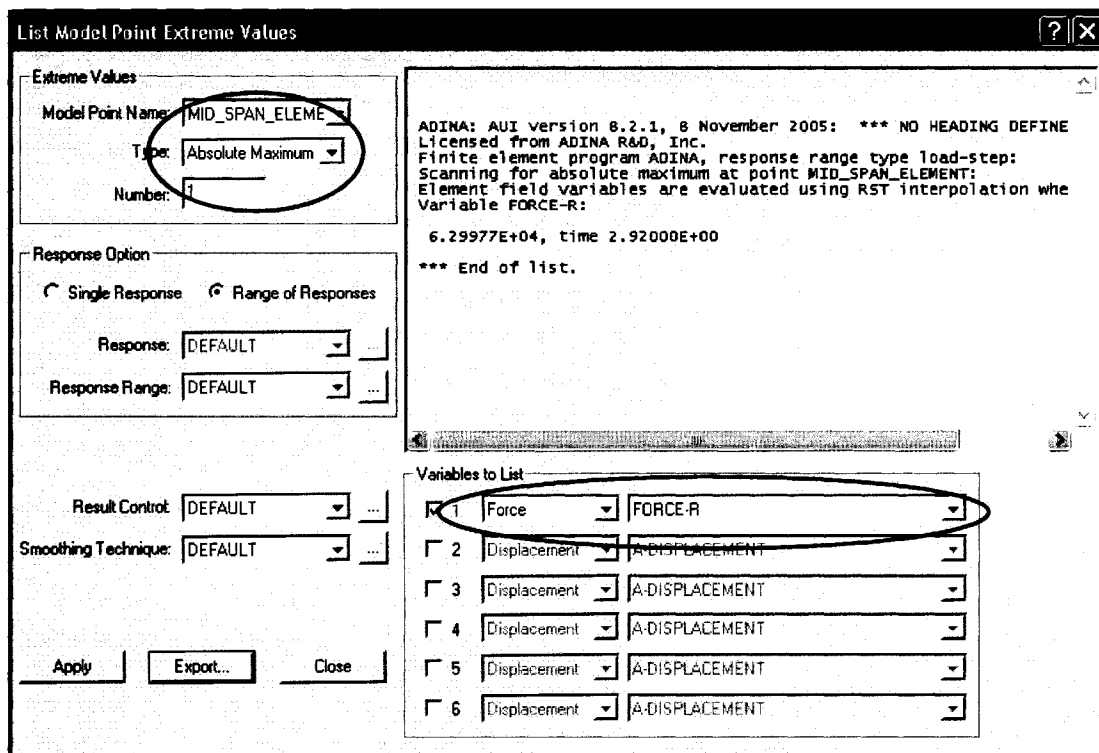


Figure A64 – Extreme Value List Box

This guide provides a method to generate a model of conductor spans, which is not covered in the ADINA documentation. Variable span lengths and elevation differences

can be easily incorporated into the modeling, with modifications in the method to generate sag nodes. Towers can also be modeled using truss elements for towers supported by additional “guy wire” truss elements carrying an initial tension. Three-dimensional beam models can also be generated allowing for cross-arm models, and multiple conductor phases.

APPENDIX 2

EPRI MODELING DATA – Model IIL1

Table A2-1 – Nodal Coordinates

Node	X1	X2	X3				
1	0	0.00000	0.00000	45	0	388.51232	-0.87409
2	0	9.30769	-0.80643	46	0	394.83462	-0.88692
3	0	18.61537	-1.55724	47	0	407.11232	-0.83857
4	0	27.92306	-2.25244	48	0	419.39001	-0.69342
5	0	37.23075	-2.89202	49	0	431.66770	-0.45150
6	0	46.53843	-3.47599	50	0	443.94539	-0.11280
7	0	55.84612	-4.00434	51	0	456.22308	0.32266
8	0	65.15381	-4.47707	52	0	468.50077	0.85490
9	0	74.46149	-4.89419	53	0	480.77847	1.48391
10	0	83.76918	-5.25569	54	0	493.05616	2.20969
11	0	93.07687	-5.56158	55	0	505.33385	3.03224
12	0	102.38455	-5.81185	56	0	517.61154	3.95156
13	0	111.69224	-6.00651	57	0	529.88923	4.96766
14	0	120.99993	-6.14555	58	0	542.16692	6.08053
15	0	130.30761	-6.22897	59	0	554.44462	7.29016
16	0	139.61530	-6.25678	60	0	566.72231	8.59657
17	0	150.30761	-6.22011	61	0	579.00000	9.99975
18	0	160.99993	-6.11003	62	0	591.71427	8.49500
19	0	171.69224	-5.92655	63	0	604.42853	7.09402
20	0	182.38455	-5.66967	64	0	617.14280	5.79682
21	0	193.07687	-5.33941	65	0	629.85706	4.60339
22	0	203.76918	-4.93575	66	0	642.57133	3.51374
23	0	214.46149	-4.45869	67	0	655.28560	2.52787
24	0	225.15381	-3.90825	68	0	667.99986	1.64577
25	0	235.84612	-3.28441	69	0	680.71413	0.86745
26	0	246.53843	-2.58717	70	0	693.42839	0.19291
27	0	257.23075	-1.81655	71	0	706.14266	-0.37786
28	0	267.92306	-0.97253	72	0	718.85693	-0.84485
29	0	278.61537	-0.05511	73	0	731.57119	-1.20807
30	0	289.30769	0.93569	74	0	744.28546	-1.46751
31	0	300.00000	1.99989	75	0	756.99972	-1.62317
32	0	306.32231	1.62781	76	0	769.71399	-1.67506
33	0	312.64462	1.28140	77	0	775.79972	-1.66318
34	0	318.96692	0.96064	78	0	781.88546	-1.62752
35	0	325.28923	0.66554	79	0	787.97119	-1.56808
36	0	331.61154	0.39611	80	0	794.05693	-1.48487
37	0	337.93385	0.15233	81	0	800.14266	-1.37787
38	0	344.25616	-0.06578	82	0	806.22839	-1.24711
39	0	350.57847	-0.25824	83	0	812.31413	-1.09256
40	0	356.90077	-0.42503	84	0	818.39986	-0.91425
41	0	363.22308	-0.56616	85	0	824.48560	-0.71215
42	0	369.54539	-0.68164	86	0	830.57133	-0.48628
43	0	375.86770	-0.77145	87	0	836.65706	-0.23663
44	0	382.19001	-0.83560	88	0	842.74280	0.03679
				89	0	848.82853	0.33399

90	0	854.91427	0.65497	144	0	1320.93728	3.82243
91	0	861.00000	0.99972	145	0	1330.94624	4.36908
92	0	867.87396	0.55987	146	0	1340.95520	4.98004
93	0	874.74791	0.15037	147	0	1350.96416	5.65531
94	0	881.62187	-0.22881	148	0	1360.97312	6.39489
95	0	888.49582	-0.57765	149	0	1370.98208	7.19879
96	0	895.36978	-0.89615	150	0	1380.99104	8.06699
97	0	902.24374	-1.18432	151	0	1391.00000	8.99951
98	0	909.11769	-1.44216	152	0	1395.78705	8.78620
99	0	915.99165	-1.66967	153	0	1400.57410	8.58760
100	0	922.86560	-1.86684	154	0	1405.36115	8.40371
101	0	929.73956	-2.03367	155	0	1410.14819	8.23453
102	0	936.61352	-2.17018	156	0	1414.93524	8.08006
103	0	943.48747	-2.27635	157	0	1419.72229	7.94030
104	0	950.36143	-2.35218	158	0	1424.50934	7.81526
105	0	957.23538	-2.39768	159	0	1429.29639	7.70492
106	0	964.10934	-2.41285	160	0	1434.08344	7.60930
107	0	974.90205	-2.37549	161	0	1438.87049	7.52839
108	0	985.69476	-2.26333	162	0	1443.65754	7.46218
109	0	996.48747	-2.07638	163	0	1448.44458	7.41070
110	0	1007.28018	-1.81466	164	0	1453.23163	7.37392
111	0	1018.07289	-1.47817	165	0	1458.01868	7.35185
112	0	1028.86560	-1.06689	166	0	1462.80573	7.34449
113	0	1039.65831	-0.58084	167	0	1474.95201	7.39181
114	0	1050.45103	-0.02000	168	0	1487.09830	7.53387
115	0	1061.24374	0.61561	169	0	1499.24458	7.77065
116	0	1072.03645	1.32599	170	0	1511.39087	8.10213
117	0	1082.82916	2.11116	171	0	1523.53715	8.52832
118	0	1093.62187	2.97111	172	0	1535.68344	9.04923
119	0	1104.41458	3.90583	173	0	1547.82972	9.66485
120	0	1115.20729	4.91533	174	0	1559.97601	10.37517
121	0	1126.00000	5.99961	175	0	1572.12229	11.18021
122	0	1133.65771	5.45375	176	0	1584.26858	12.07996
123	0	1141.31541	4.94554	177	0	1596.41486	13.07442
124	0	1148.97312	4.47497	178	0	1608.56115	14.16359
125	0	1156.63083	4.04204	179	0	1620.70743	15.34748
126	0	1164.28853	3.64677	180	0	1632.85372	16.62607
127	0	1171.94624	3.28914	181	0	1645.00000	17.99938
128	0	1179.60395	2.96915	182	0	300.00000	4.18144
129	0	1187.26166	2.68681	183	0	579.00000	12.16454
130	0	1194.91936	2.44211	184	0	861.00000	3.16000
131	0	1202.57707	2.23506	185	0	1126.00000	8.14687
132	0	1210.23478	2.06566	186	0	1391.00000	11.13545
133	0	1217.89248	1.93390	187	-3	0.00000	-24.07920
134	0	1225.55019	1.83979	188	-3	300.00000	-22.09232
135	0	1233.20790	1.78332	189	-3	579.00000	-14.10922
136	0	1240.86560	1.76450	190	-3	861.00000	-23.11376
137	0	1250.87456	1.79663	191	-3	1126.00000	-18.12689
138	0	1260.88352	1.89309	192	-3	1391.00000	-15.13831
139	0	1270.89248	2.05387	193	-3	300.00000	4.18144
140	0	1280.90144	2.27896	194	-3	579.00000	12.16454
141	0	1290.91040	2.56836	195	-3	861.00000	3.16000
142	0	1300.91936	2.92207	196	-3	1126.00000	8.14687
143	0	1310.92832	3.34009	197	-3	1391.00000	11.13545

Table A2-2 – Node Descriptions

Nodes	Description
1 – 181	Calculated Conductor Nodal Coordinates – Tension = 12464 N
182 – 186	Insulator / Crossarm attachment node
187 – 192	Tower base at ground line
193 – 197	Tower / Crossarm attachment node

Table A2-3 – Conductor Material Properties

	397 kemil ACSR	471A Anaconda Copper/Bronze
Unit Weight (N/m)	7.98	12.71
Modulus of Elasticity (N/mm²)	69627	102970
Rated Strength (N)	72500	68548
Section Area (mm²)	234	193

Table A2-4 – Tower and Insulator Material Property

Property	Value
Young's Modulus	200 GPa
Density	7850 kg/m ³

Table A2-5 – Tower member sizes

Member	Cross-sectional Area
Tower Body	0.632 m x 0.632 m
Crossarm	0.2 m x 0.2 m

Insulator cross-sectional area = 6.452E-4 m²

Conductor strain calculation

$$\epsilon = \frac{\sigma}{E} = \frac{\left(\frac{T}{A}\right)}{E} = \frac{\left(\frac{12464N}{2.34E-04m^2}\right)}{6.9627E+10Pa} = 7.65E-04$$

APPENDIX 3

KEMPNER MODELING DATA – MODEL 2

Table A3-1 – Nodal Coordinates

Node	X1	X2	X3				
1	0	0.00000	0.00000	45	0	17.24653	-0.23396
2	0	0.39197	-0.03029	46	0	17.63850	-0.23500
3	0	0.78393	-0.05849	47	0	18.03047	-0.23396
4	0	1.17590	-0.08460	48	0	18.42243	-0.23082
5	0	1.56787	-0.10862	49	0	18.81440	-0.22560
6	0	1.95983	-0.13056	50	0	19.20637	-0.21829
7	0	2.35180	-0.15040	51	0	19.59833	-0.20889
8	0	2.74377	-0.16816	52	0	19.99030	-0.19740
9	0	3.13573	-0.18382	53	0	20.38227	-0.18382
10	0	3.52770	-0.19740	54	0	20.77423	-0.16816
11	0	3.91967	-0.20889	55	0	21.16620	-0.15040
12	0	4.31163	-0.21829	56	0	21.55817	-0.13056
13	0	4.70360	-0.22560	57	0	21.95013	-0.10862
14	0	5.09557	-0.23082	58	0	22.34210	-0.08460
15	0	5.48753	-0.23396	59	0	22.73407	-0.05849
16	0	5.87950	-0.23500	60	0	23.12603	-0.03029
17	0	6.27147	-0.23396	61	0	23.51800	0.00000
18	0	6.66343	-0.23082	62	0	23.90997	-0.03029
19	0	7.05540	-0.22560	63	0	24.30193	-0.05849
20	0	7.44737	-0.21829	64	0	24.69390	-0.08460
21	0	7.83933	-0.20889	65	0	25.08587	-0.10862
22	0	8.23130	-0.19740	66	0	25.47783	-0.13056
23	0	8.62327	-0.18382	67	0	25.86980	-0.15040
24	0	9.01523	-0.16816	68	0	26.26177	-0.16816
25	0	9.40720	-0.15040	69	0	26.65373	-0.18382
26	0	9.79917	-0.13056	70	0	27.04570	-0.19740
27	0	10.19113	-0.10862	71	0	27.43767	-0.20889
28	0	10.58310	-0.08460	72	0	27.82963	-0.21829
29	0	10.97507	-0.05849	73	0	28.22160	-0.22560
30	0	11.36703	-0.03029	74	0	28.61357	-0.23082
31	0	11.75900	0.00000	75	0	29.00553	-0.23396
32	0	12.15097	-0.03029	76	0	29.39750	-0.23500
33	0	12.54293	-0.05849	77	0	29.78947	-0.23396
34	0	12.93490	-0.08460	78	0	30.18143	-0.23082
35	0	13.32687	-0.10862	79	0	30.57340	-0.22560
36	0	13.71883	-0.13056	80	0	30.96537	-0.21829
37	0	14.11080	-0.15040	81	0	31.35733	-0.20889
38	0	14.50277	-0.16816	82	0	31.74930	-0.19740
39	0	14.89473	-0.18382	83	0	32.14127	-0.18382
40	0	15.28670	-0.19740	84	0	32.53323	-0.16816
41	0	15.67867	-0.20889	85	0	32.92520	-0.15040
42	0	16.07063	-0.21829	86	0	33.31717	-0.13056
43	0	16.46260	-0.22560	87	0	33.70913	-0.10862
44	0	16.85457	-0.23082	88	0	34.10110	-0.08460
				89	0	34.49307	-0.05849

90	0	34.88503	-0.03029	132	0	51.34763	-0.21829
91	0	35.27700	0.00000	133	0	51.73960	-0.22560
92	0	35.66897	-0.03029	134	0	52.13157	-0.23082
93	0	36.06093	-0.05849	135	0	52.52353	-0.23396
94	0	36.45290	-0.08460	136	0	52.91550	-0.23500
95	0	36.84487	-0.10862	137	0	53.30747	-0.23396
96	0	37.23683	-0.13056	138	0	53.69943	-0.23082
97	0	37.62880	-0.15040	139	0	54.09140	-0.22560
98	0	38.02077	-0.16816	140	0	54.48337	-0.21829
99	0	38.41273	-0.18382	141	0	54.87533	-0.20889
100	0	38.80470	-0.19740	142	0	55.26730	-0.19740
101	0	39.19667	-0.20889	143	0	55.65927	-0.18382
102	0	39.58863	-0.21829	144	0	56.05123	-0.16816
103	0	39.98060	-0.22560	145	0	56.44320	-0.15040
104	0	40.37257	-0.23082	146	0	56.83517	-0.13056
105	0	40.76453	-0.23396	147	0	57.22713	-0.10862
106	0	41.15650	-0.23500	148	0	57.61910	-0.08460
107	0	41.54847	-0.23396	149	0	58.01107	-0.05849
108	0	41.94043	-0.23082	150	0	58.40303	-0.03029
109	0	42.33240	-0.22560	151	0	58.79500	0.00000
110	0	42.72437	-0.21829	152	0	-0.20000	0.00000
111	0	43.11633	-0.20889	153	0	0.00000	0.05880
112	0	43.50830	-0.19740	154	0	11.75900	0.05880
113	0	43.90027	-0.18382	155	0	23.51800	0.05880
114	0	44.29223	-0.16816	156	0	35.27700	0.05880
115	0	44.68420	-0.15040	157	0	47.03600	0.05880
116	0	45.07617	-0.13056	158	0	0.00000	-0.63500
117	0	45.46813	-0.10862	159	0	11.75900	-0.63500
118	0	45.86010	-0.08460	160	0	23.51800	-0.63500
119	0	46.25207	-0.05849	161	0	35.27700	-0.63500
120	0	46.64403	-0.03029	162	0	47.03600	-0.63500
121	0	47.03600	0.00000	163	0	58.79500	-0.63500
122	0	47.42797	-0.03029	164	0	-0.20000	0.05880
123	0	47.81993	-0.05849	165	0	-0.10000	0.05880
124	0	48.21190	-0.08460	166	0	11.55900	0.05880
125	0	48.60387	-0.10862	167	0	11.65900	0.05880
126	0	48.99583	-0.13056	168	0	23.31800	0.05880
127	0	49.38780	-0.15040	169	0	23.41800	0.05880
128	0	49.77977	-0.16816	170	0	35.07700	0.05880
129	0	50.17173	-0.18382	171	0	35.17700	0.05880
130	0	50.56370	-0.19740	172	0	46.83600	0.05880
131	0	50.95567	-0.20889	173	0	46.93600	0.05880

Table A3-2 – Node Descriptions

<i>Nodes</i>	<i>Description</i>
1 – 151	Calculated Conductor Nodal Coordinates – Tension = 12.813 N
152	Trigger element – conductor failure at tower 1
153 – 157	Insulator / Tower attachment node
158 – 163	Tower base at ground line
164 – 173	Spring and Fuse nodes

Table A3-3 – Conductor Material Properties

	<i>Beaded Chain</i>
<i>Unit Weight (N/m)</i>	0.1742
<i>Modulus of Elasticity (N/mm²)</i>	1623
<i>Rated Strength (N)</i>	110
<i>Section Area (mm²)</i>	8.23

Table A3-4 – Tower Material Property

<i>Young's Modulus</i>	7.03 GPa
<i>Density</i>	2705 kg/m ³

Table A3-5 – Insulator Material Property

<i>Young's Modulus</i>	200 GPa
<i>Density</i>	7850 kg/m ³

Insulator cross-sectional area = 1.0E-6 m²

Strain Calculation

$$\varepsilon = \frac{\sigma}{E} = \frac{\left(\frac{T}{A}\right)}{E} = \frac{\left(\frac{12.813N}{8.23E-06m^2}\right)}{1.623E+9Pa} = 9.602E-04$$

Table A3-6 – Structure Failure Times After Conductor Failure – Model 2

<i>Structure</i>	<i>Failure Time (s)</i>
<i>1</i>	0.080
<i>2</i>	0.113
<i>3</i>	0.216



